Universidad de Alcalá

Doctoral Thesis

Fouling and biofouling resistant membranes for water treatment processes

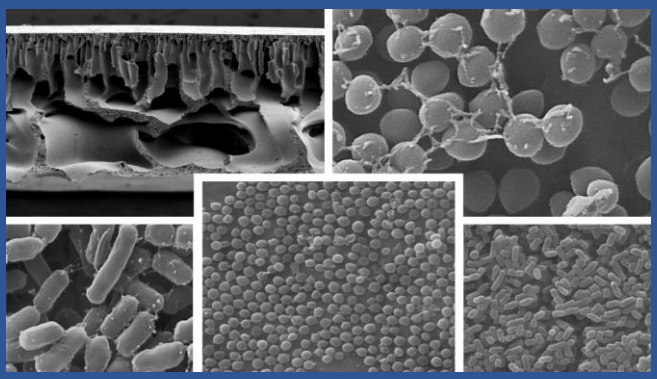

Berta Díez Odriozola

Supervisor: Roberto Rosal García

Doctoral program in

Hydrology and Water Resources Management

Doctoral Program in:

Hydrology and Water Resources Management

Fouling and biofouling resistant membranes for water treatment processes

Doctoral Thesis presented by:

Berta Díez Odriozola

Supervisor:

Dr. Roberto Rosal García

Alcalá de Henares, 2020

AGRADECIMIENTOS

Quisiera dedicar este apartado, a todas aquellas personas que han contribuido de manera profesional o personal en el desarrollo de este trabajo.

En primer lugar, quería agradecer a mi Director de Tesis, el Dr. Roberto Rosal la confianza depositada en mí durante estos años para llevar a cabo esta investigación, así como su tiempo y dedicación para que este trabajo saliera adelante.

Asimismo, agradecer a los profesores de la Universidad Rey Juan Carlos, el Dr. Arcadio Sotto, Dr. Jesús Arsuaga y Dr. Antonio Martín su ayuda, sus consejos y sus aportaciones para el desarrollo de esta tesis.

También quisiera dar las gracias a todos los profesores que me han dado la oportunidad de colaborar en sus respectivos grupos durante mis estancias de investigación. Al Dr. Süleyman Yüce de la Universidad de Aachen por su ayuda y recomendaciones, a Sarah Armbruster, por su apoyo y compañía. También, agradecer al Dr. Paul D Topham el hecho de acogerme en la Universidad de Aston, por el buen ambiente que hay en su grupo y su forma de ser, especialmente quiero dar las gracias a la Dr. Eirini Theodosiou por acogerme con los brazos abiertos y hacerme sentir como en casa, por contar conmigo en todo momento, y por su alegría y entusiasmo trabajando que siempre se contagia y te da fuerzas para continuar. Por último, gracias a la Dr. Stephanie Willerth de la Universidad de Victoria, por darme la oportunidad de vivir una experiencia única, por un verano muy interesante y muy “bio” en su grupo.

A todos mis compañeros del Departamento de Ingeniería Química de la Universidad de Alcalá, por hacer más amenos los días en el laboratorio. A los miembros de mi grupo, a Javier por los comienzos, gracias por tu ayuda. A Carlos, Sergio y Laura por crear un buen ambiente de trabajo y de

compañerismo en el grupo. En particular, quisiera agradecer a Idoia su apoyo durante todos estos años, por contar con su amistad y haber compartido con ella momentos inolvidables. Así como al grupo de Bio-e por aportar esa "chispa" de humor y buen rollo en el laboratorio.

Quisiera destacar, que todo este trabajo no hubiera sido posible sin el cariño y apoyo de mi familia, a mi hermano Ignacio, y a mis padres Mariano y Lola, muchas gracias por vuestra ayuda y comprensión. Especialmente, quisiera dar las gracias a mi madre, por haber estado siempre a mi lado, ser un pilar fundamental en mi vida y ayudarme cuando más lo he necesitado.

A Álvaro por haber sufrido esta aventura conmigo desde el principio, mil gracias por tu apoyo, por tu ayuda e infinita paciencia, pero sobre todo gracias por hacerme feliz y compartir esta vida conmigo.

Por último, pero no menos importante, gracias a todos mis amigos, en especial a mis chicas; Ángela, Lorena, Raquel y Rocío por todos estos años de amistad, por haber podido contar con vosotras en todo momento y por todos los buenos momentos que hemos vivido, tan necesarios y esenciales para poder desconectar de la rutina. A Natalia e Irene, porque la biología nos unió, gracias también por vuestro apoyo y comprensión, y por ser un ejemplo de lucha, constancia y dedicación.

FUNDINGS

This Thesis was supported by a pre-doctoral FPI contract (FPI 2015 program) from Alcalá University. This Thesis was supported by the European Union (7th Framework Programme FP7-ERA-Net Susfood, 2014/00153/001 No. 291766) by the Spanish Ministry of Economy and Competitiveness (MINECO, Programa Estatal de Investigación, Desarrollo e Innovación Orientada a los Retos de la Sociedad, CTM2013-45775-C2-1-R and CTQ2014-57858-R) and the Regional Government of Madrid through program S2013 / MAE-2716-REMTAVARES-CM.

A mi familia,

A Álvaro

TABLE OF CONTENTS:

ABSTRACT

The demand for new water resources has increased worldwide due to the rapid growth population, socio-economic development, and changing consumption patterns. This situation, coupled with rising water scarcity, generates a need for improved techniques to purify contaminated waters. Membrane technology plays an important role in water purification processes due to its efficient and versatility separation properties. However, most commercial membranes are prepared from hydrophobic materials, which makes them more susceptible to suffer the adsorption or deposition of molecules over their surface or inside their pores. This phenomenon, commonly termed as fouling, can be classified in organic, inorganic or biological fouling depending on the nature of the components. Organic fouling which is caused by the presence of organic compounds, such as polysaccharides or proteins. Inorganic fouling refers to the deposition of inorganic materials like salts or metal oxides and biofouling designates the formation of biofilms due to the attachment and growth of microorganisms on the membrane surface. Foulants can deposit within membrane pores or form a cake layer on the surface. Bacterial biofilms are complex microbial communities, embedded in a self-produced polymer matrix of extracellular polymer substances (EPS) mainly composed of water, polysaccharides, proteins and nucleic acids aimed to protect bacteria in adverse conditions. Membrane (bio)fouling is one of the major operational problems in membrane processes because it causes a decrease in permeation flux, increases energy consumption and operational costs, and reduces membrane lifespan. Due to the adverse impact of fouling, different physical and chemical cleaning processes have been proposed to prevent or reduce membrane fouling. However, these methods are not sufficiently effective and, new

strategies need to be investigated for the purpose of effectively mitigating membrane fouling.

The aim of this Doctoral Thesis was to investigate membranes modifications techniques to enhance permeability, reduce fouling and the accumulation of microorganisms on the membrane surface. To achieve this goal, membranes were prepared by the non-solvent induced phase inversion method, followed by a physical and chemical characterization and then, membranes were tested with different biofilm-forming bacterial strains to assess the anti-biofouling behaviour of the newly developed materials.

Several techniques are used for this purpose, including blending hydrophilic additives or surface coating by an electrospun nanofiber layer to produce new composite ultrafiltration membranes with enhanced anti-(bio)fouling behaviour. Blending organic or inorganic additives into the casting solution is an important approach to reduce membrane hydrophobicity and improve water filtration performance. Electrospun nanofibers are produced by the electrospinning system which is a versatile technique that utilizes a high voltage electric field to produce polymer fibres below the nanoscale from a polymer solution. Nanofibers showed several advantages such as a high surface area to volume ratio or tuneable porosity, contributing to enhance membrane fouling resistance.

The new composite ultrafiltration membranes were characterized using the following microscopy techniques: membranes morphology by Scanning Electron Microscopy (SEM), surface porosity using a Field Emission Scanning Electron Microscopy (FE-SEM), and elemental analyses using SEM combined with Energy Dispersive X-ray (SEM-EDX). The chemical composition was analysed using Attenuated Total Reflectance Fourier Transform Infrared (ATR-FTIR) spectroscopy. The hydrophilicity of membranes was determined by measuring water contact angles and surface charge by surface ζ-potential

measurements. ICP-MS analyses from metal-loaded membranes were performed to assess the possible release of nanoforms during membrane use. Membrane fouling was studied using bovine serum albumin (BSA) as a model of protein organic foulant. The intrinsic, reversible and irreversible fouling resistances, as well as the flux recovery ratio and solute rejection, were analysed to explore the effect of fouling on the membrane permeation performance. The anti-biofouling behaviour of the prepared membranes was tested against two different bacterial strains *Escherichia coli* (CECT 516, strain designation ATCC 8739) and *Staphylococcus aureus* (CECT 240, strain designation ATCC 6538P). The antimicrobial activity was assessed by counting colony-forming units. Biofilm formation was studied using SEM and confocal micrographs, biofilms were stained with FilmTracer FM 1-43 to visualize the surface of colonized membranes. Finally, bacterial viability was examined using the nucleic-acid stains SYTO 9 and propidium iodide (PI), detecting cell wall damage.

The effects of adding different hydrophilic additives were evaluated in this Thesis. Nanoparticles supported in sepiolite fibres or mesoporous silica displayed a good dispersion in casting solutions and, hence, in the polymer matrix. The results showed that the membranes functionalized with metal nanoparticles exhibited higher porosity and better pore interconnectivity. Membrane permeability was significantly enhanced with improved antifouling properties without compromising organic rejection. No leaching of metal particles was observed during use, confirming the stability of composite membranes. Metal-loaded membranes exhibited high antimicrobial activity against gram-positive and gram-negative bacteria due to the oligodynamic action of silver and copper ions.

Alternatively, the addition of hyperbranched polyamidoamine nanomaterial, Helux-3316, generate a high density of positively charged functional groups at

the membrane fluid-interface, increasing membrane hydrophilicity and water permeability. Functionalized membranes displayed antifouling behaviour revealed after filtering BSA solutions, with reduced irreversible fouling. Moreover, membranes showed an important anti-biofouling functionality due to antimicrobial activity explained by the interaction of positively charged moieties with negatively charged cell envelopes.

Other technique used in this work was the coating of membrane surface by on-top electrospinning a layer of nanofibers made by a blend of poly (acrylic acid) and poly (vinyl alcohol) onto polysulfone membranes. The results showed that electrospun layers increased membrane hydrophilicity and reduced organic fouling without affecting permeability and protein rejection performance. Moreover, the nanofibers coating showed a considerable antimicrobial activity, particularly for the bacterium *S. aureus*, attributed to the chelating effect of PAA on the divalent cations stabilizing bacterial cell envelopes.

The results are relevant to demonstrate that the previously described modification techniques effectively improve the performances of ultrafiltration membranes.

RESUMEN

La demanda de nuevos recursos hídricos ha aumentado a nivel global debido al rápido crecimiento de la población, el desarrollo socioeconómico y los cambios en los patrones de consumo. Esta situación, junto con el aumento de la escasez de agua, genera la necesidad de mejorar las técnicas para purificar las aguas contaminadas. La tecnología de membrana desempeña un papel importante en los procesos de purificación de agua debido a sus propiedades de separación eficientes y versátiles. Sin embargo, la mayoría de las membranas comerciales se fabrican a partir de materiales hidrófobos, lo que las hace más susceptibles de sufrir la adsorción o deposición de moléculas sobre su superficie o dentro de sus poros. Este fenómeno, comúnmente conocido como *fouling* o ensuciamiento, puede clasificarse en tres tipos diferentes dependiendo de la naturaleza de los mismos, así distinguimos entre ensuciamiento orgánico, inorgánico o biológico. El ensuciamiento orgánico se debe a la presencia de compuestos orgánicos, como polisacáridos o proteínas. La suciedad inorgánica se refiere a la deposición de materiales inorgánicos como sales u óxidos metálicos y la contaminación biológica o *biofouling* designa la formación de biopelículas o *biofilms* debido a la unión y crecimiento de microorganismos sobre la superficie de la membrana. Estas partículas causantes del ensuciamiento de la membrana pueden depositarse dentro de sus poros o formar una capa sobre la superficie, conocida como *cake-layer*. Las biopelículas bacterianas son comunidades microbianas complejas, revestidas por una matriz autoproducida de sustancias poliméricas extracelulares (EPS) compuestas principalmente por agua, polisacáridos, proteínas y ácidos nucleicos destinados a proteger las bacterias en condiciones adversas. El ensuciamiento de la membrana es uno de los principales problemas operativos en los procesos de membrana, ya que causa una disminución en el flujo de permeación, aumenta el consumo de energía y

el coste operativo, reduciendo la vida útil de la membrana. Debido al impacto adverso de la suciedad, se han propuesto diferentes procesos de limpieza física y química para prevenir o reducir la suciedad de la membrana. Sin embargo, estos métodos no son lo suficientemente eficaces, siendo necesario investigar nuevas estrategias para mitigar eficazmente la suciedad de la membrana. El objetivo de esta tesis doctoral fue investigar diferentes técnicas de modificación para conseguir mejorar la permeabilidad de las membranas, reduciendo la acumulación de moléculas orgánicas y microorganismos sobre su superficie.

Para lograr este objetivo, las membranas fueron preparadas por el método de inversión de fase, seguido de una caracterización fisicoquímica. Finalmente, las membranas fueron probadas con diferentes cepas bacterianas formadoras de biopelículas para evaluar el comportamiento *anti-biofouling* de los materiales recién desarrollados.

Para ello, se utilizaron varias técnicas, como la mezcla de aditivos hidrófilos o el recubrimiento superficial mediante una capa de nanofibras electrohiladas para producir nuevas membranas de ultrafiltración con un comportamiento *anti-(bio)fouling* mejorado. La combinación de aditivos orgánicos o inorgánicos en la solución polimérica es una solución importante para reducir la hidrofobicidad de la membrana y mejorar el rendimiento de la filtración de agua. Las nanofibras electrohiladas, son producidas por el sistema del electrospinning, una técnica versátil que utiliza un campo eléctrico de alta tensión para producir fibras poliméricas de tamaño nanométrico a partir de una solución polimérica. Las nanofibras muestran varias ventajas, como una alta superficie específica, contribuyendo a mejorar la resistencia a la suciedad de la membrana.

Las nuevas membranas de ultrafiltración se caracterizaron utilizando las siguientes técnicas de microscopía: La microscopía electrónica de barrido

(SEM) para estudiar la morfología de las membranas, la microscopía electrónica de barrido de emisión de campo (FE-SEM) para la porosidad superficial y el microscopio electrónico de barrido combinado con energía dispersiva de rayos X (SEM-EDX) para los análisis elementales. La composición química fue analizada utilizando la espectroscopia infrarroja (FTIR) combinada con la reflexión total atenuada (ATR-FTIR). La hidrofilicidad de las membranas se determinó midiendo los ángulos de contacto y la carga superficial por mediciones del potencial zeta de superficie (ζ). Las membranas dopadas con metales fueron analizadas por espectrometría de masas con plasma de acoplamiento inductivo (ICP-MS), evaluando la posible liberación de las nanopartículas durante su uso. La suciedad de membrana fue estudiada usando albúmina de suero bovino (BSA) como modelo de *foulant* orgánico proteico. Se analizaron las resistencias intrínsecas, reversibles e irreversibles, así como la relación de recuperación del flujo de agua y el rechazo de solutos, para explorar el efecto de la suciedad en el rendimiento de la permeación de las membranas. El comportamiento *anti-biofouling* de las membranas se comprobó utilizando dos cepas bacterianas *Escherichia coli* (CECT 516, designación de cepa ATCC 8739) y *Staphylococcus aureus* (CECT 240, designación de cepa ATCC 6538P).

La actividad antimicrobiana se evaluó contando las unidades formadoras de colonias (CFU). La formación de biopelículas se evaluó por microscopía electrónica (SEM) y microscopia confocal. Con el fin de visualizar la superficie de las membranas colonizadas, las biopelículas se tiñeron utilizando el marcador FilmTracer FM 1-43. Finalmente, la viabilidad bacteriana se examinó utilizando dos marcadores de ácidos nucleicos, el SYTO 9 y el yoduro de propidium (PI), detectando así los daños en la pared celular bacteriana.

Los efectos de la adición de diferentes aditivos hidrófilos se evaluaron en esta tesis. Las nanopartículas soportadas en fibras de sepiolita o sílice mesoporosa

mostraron una buena dispersión en la solución polimérica, y, por lo tanto, también en la matriz polimérica. Los resultados mostraron que las membranas funcionalizadas con nanopartículas metálicas presentaron una porosidad más alta y una mayor interconectividad de los poros. La permeabilidad de la membrana se mejoró significativamente, presentando propiedades anti-ensuciamiento mejoradas, todo ello sin comprometer el rechazo orgánico. No se observó lixiviación de partículas metálicas durante el uso, lo que confirma la estabilidad de las membranas. Las membranas cargadas de metal exhibieron una alta actividad antimicrobiana contra bacterias gram-positivas y gram-negativas debido a la acción oligodinámica de los iones de plata y cobre.

Alternativamente, la adición de una poliamidoamina hiperramificada comercial, el Helux-3316, genera una alta densidad de grupos funcionales cargados positivamente en la membrana, aumentando así su hidrofilicidad y la permeabilidad al agua. Las membranas funcionalizadas mostraron un comportamiento *anti-fouling*, manifestándose después de filtrar soluciones de BSA, reduciendo de forma notable la adhesión de la suciedad irreversible. Además, las membranas funcionalizadas también mostraron una importante actividad antimicrobiana, debido a la interacción de los grupos cargados positivamente con las membranas celulares cargadas negativamente, los cuales son capaces de desestabilizar la integridad celular.

Otra técnica utilizada en este trabajo consistió en el recubrimiento de la superficie de membranas de polisulfona, mediante fibras electrohiladas, compuestas por una mezcla de ácido poliacrílico (PAA) y alcohol polivinílico (PVA). Los resultados mostraron que las nanofibras, aumentaron la hidrofilicidad de las membranas y redujeron la adherencia de materia orgánica sin afectar la permeabilidad y el rechazo de proteínas.

Además, el recubrimiento de nanofibras mostró una considerable actividad antimicrobiana, particularmente para la bacteria *S. aureus*, atribuida al efecto quelante de PAA con los cationes divalentes que estabilizan la pared celular bacteriana.

Los resultados de este trabajo son relevantes para demostrar que las técnicas de modificación descritas con anterioridad mejoran eficazmente el rendimiento de las membranas de ultrafiltración, reduciendo la adhesión de materia orgánica y microorganismos sobre su superficie.

CHAPTER 1

General introduction

Chapter 1. GENERAL INTRODUCTION

1.1 Water resources and water scarcity

The demand for new water resources has been increasing worldwide due to the global growth population, socio-economic development and industrialization. In 2050 it is expected that population rises by almost 40%, increasing the demand for safe, clean and drinkable water [1]. Water resources have been assumed as abundant. However, as shown in figure 1.1 only 2.5% of global water resources are freshwater, being the rest saline. From this 2.5%, 70% is frozen in polar regions and the other 30% are in remote aquifers of difficult access. Therefore, less than 1 % of total water resources are directly available for human use. Unfortunately, most available water shows evidence of anthropogenic contamination by effluents from domestic, agricultural and industrial activities [2, 3]. Furthermore, the uneven distribution of water over the globe leads to severe water scarcity in certain regions. According to the United Nations World Water Development report, within the next 30 years, there will be 3.9 billion people living in "water-scarce" areas. Moreover, the World Health Organization estimates that at least 1.1 billion people are lacking access to clean drinking water [4, 5].

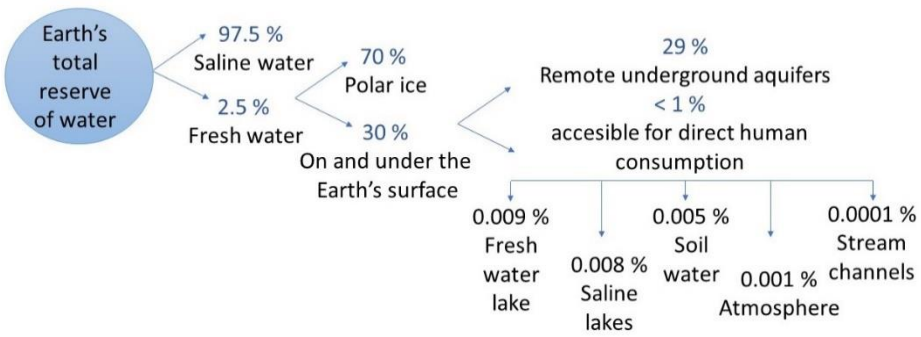

Figure 1.1. Schematic representation of the global distribution of water intended for human consumption. Adapted from reference [2].

Based on this scenario there is a need to protect the existing water resources around the world as well as design proper strategies to reduce and reuse water in order to preserve the environment and support new generations.

1.2 Membrane technology

Membrane technology contributes by almost 53% of the total world water purification volume. Water purification involves the removal of pollutants such as organic, chemical, and biological contaminants, as well as suspended solids present in the water in order to obtain sufficiently clean and satisfactory water [6, 7]. In recent years, the development of membrane technology has been widely applied in desalination and wastewater treatment in different areas such as manufacturing, biotechnology and food processing industries due to its operational simplicity and cost-efficiency [8-12].

A membrane can be defined as "*a selective physical barrier that retains unwanted materials on the surface and allows certain compounds to pass through, depending on their physical and chemical properties, when a driving force is applied across the membrane*" [13]. According to the membrane configuration, applied pressure and pore size, membranes processes are often classified into four different categories which are represented in figure 1.2.

- Microfiltration (MF) is a process in which membranes have relatively large pores, generally in the 10 to 0.1 µm range. Microfiltration membranes are useful for removing large suspended solids such as colloids, particles and some bacterial species. This process requires a relatively low operating pressure, typically below 1 bar [14].
- Ultrafiltration (UF) membranes, with a pore size range between 0.1 to 0.01 µm, are able to separate relatively large molecules such proteins, polysaccharides, humic material and all microbiological species. The operating pressure is usually in the 2-8 bar range [15].

- Nanofiltration (NF) is a separation process characterized by separating low molecular weight molecules such sugars, amino acids and some monovalent ions. These membranes have a pore size range of 0.01 µm to 0.001 µm. This technology requires high operational pressures from 5 to 15 bar [16].

- Reverse osmosis (RO) is the highest effective technology for removing inorganic contaminants, dissolved salts and chemical constituents from water. Membranes are dense with a pore size lower than 1 nm, normally used for water purification and desalination. The process requires higher operating pressure and diffusion is the dominant driving force of transport rather than pore-based on pressure difference [17].

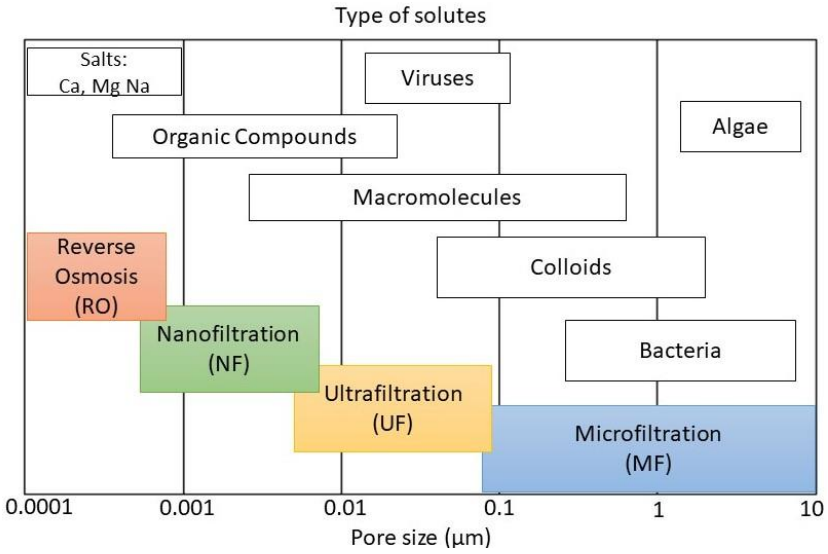

Figure.1.2. Different types of pressure-driven membrane processes. Adapted from reference [18].

1.3 Membrane preparation methods.

Membranes can be produced using several different techniques, including phase inversion, controlled stretching, interfacial polymerization, melt extrusion or electrospinning, depending of the desired membrane morphology [19, 20]. Among these techniques, phase inversion is the most commonly used to prepare both asymmetric and symmetric polymeric membranes. Generally, phase inversion is a de-mixing process whereby the homogeneous polymer solution is transformed, in a controlled manner, from liquid to solid-state. Additionally, the de-mixing process can be defined by the exchange rate between solvent and non-solvent during precipitation [21]. Therefore, phase inversion can be achieved in several ways, namely:

- Non-solvent induced phase separation (NIPS) or immersion precipitation is a process in which a polymer is dissolved in a proper solvent until a homogeneous solution is obtained, after which it is cast on a suitable support followed by immersion in a non-solvent coagulation bath, typically water. During this process solvent / non-solvent exchange takes place and polymer precipitation occurs. Finally, a solid polymer film is obtained with asymmetric structure [22, 23]. This method requires complex control of solvent exchange rate, which is strongly affected by dope composition, choice of solvent, coagulation bath composition, temperature and evaporation time. [6, 24]. NIPS is the most widely used method for membrane preparation in research and industry.

- Thermally induced phase separation (TIPS). It is a process in which a polymer is dissolved in an appropriate diluent using an elevated temperature. The solvent should have a high boiling point, low molecular weight and low volatility. Then, the hot homogeneous solution is cast into the desired shape, followed by cooling to induce

phase separation. After polymer solidification, the diluent is removed typically by solvent extraction, leaving a highly porous membrane [18, 25].

- Evaporation-induced phase separation (EIPS). A polymer is dissolved in a mixture of a volatile solvent and a less volatile non-solvent. When the polymer solution is cast on a suitable support, the solvent evaporates resulting in de-mixing. Once polymer precipitation occurs, a thin porous polymer film is formed [22]. The morphology of the casted films can be controlled by using solvent with different boiling points.

- Vapor-induced phase separation (VIPS). This method is used to prepare highly porous membranes. Once the polymer is dissolved in a specific solvent, the casting solution is exposed to an atmosphere containing a non-solvent vapour, usually water, in a vapour chamber. Upon vapour absorption, precipitation occurs, yielding the membrane structure [26].

A schematic representation of different phase inversion methods is represented in figure 1.3.

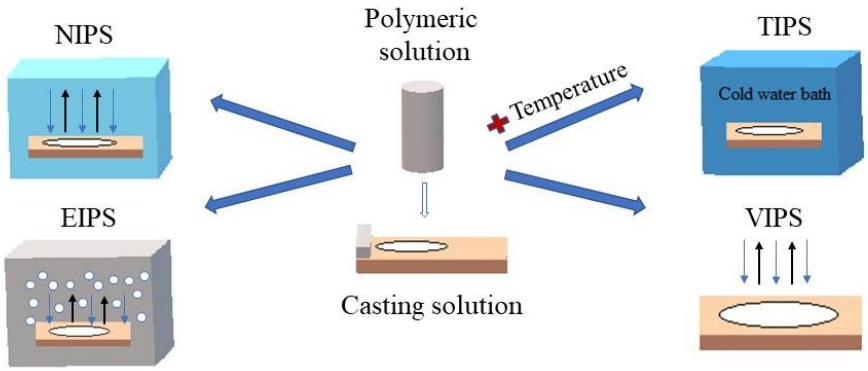

Figure.1.3. Schematic representation of different phase inversion methods

.

Taking immersion precipitation as an example, there are three components involved in phase separation, namely, polymer, solvent and non-solvent. Therefore, a ternary phase diagram can be used to describe the thermodynamic behaviour of such system, as shown in figure 1.4. The pure components are represented at the corners of the triangle while any points inside the diagram represents a mixture of the three components. The ternary phase diagram of polymer /solvent / non-solvent system is formed by a single-phase or homogeneous region and a two-phase or unstable region. In the first one, the three components are fully miscible whereas in the unstable region the solution separates in two phases, the polymer-rich phase, which forms the matrix of the membranes, and the polymer-lean phase that forms membrane pores. The binodal curve is the boundary between both regions [27].

The precipitation process is represented as a line through the phase diagram starting from point A and ending with point D. Point A represents the homogeneous casting solution made up of solvent and polymer, which is immersed in the coagulation bath (non-solvent). If the solvent is removed from the polymer solution the composition of polymer moves along A-B-C. At point B, a transition takes place from the one-phase region to the two-phase-region, a polymer-rich phase and a polymer-poor phase appear, at the upper and lower boundary of the de-mixing gap, respectively. The spinodal curve delimits the metastable region of the miscibility gap. At point C, the polymer concentration in the polymer-rich phase will be high enough to be considered solid. Further exchanges of solvent and nonsolvent lead to the final membrane composition, point D [21, 28, 29].

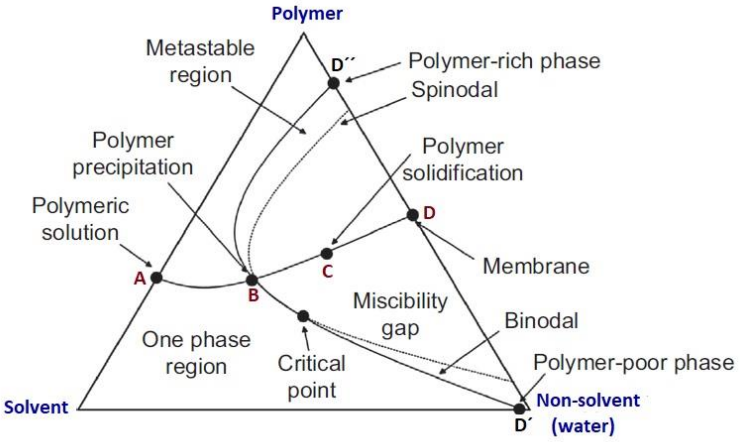

Figure 1.4. Schematic representation of three-components phase diagram during the phase inversion process. Adapted from reference [29].

1.4 Effect of additives in membrane preparation

The incorporation of some additives into the casting solution plays an important role during the membrane preparation because they can affect the solution de-mixing process during phase inversion. Commonly used additives can be classified into the following categories [30]:

- Polymer additives such as polyvinylpyrrolidone (PVP) or polyethylene glycol (PEG).
- Low-molecular-weight chemicals including salts (LiCl), inorganic acids (acetic acid and phosphoric acid), organic acids (propionic acid).
- Weak co-solvents like ethanol, propanol and acetone.
- Weak non-solvents glycerol or ethylene glycol.
- Strong non-solvents such as water.

During immersion precipitation, either instantaneous or delayed de-mixing occurs and different membranes structures can be obtained depending on the rate of polymer precipitation in the non-solvent bath (Figure 5). If the polymer precipitates quickly in the non-solvent bath, an instantaneous de-mixing takes place resulting in membranes with thin skin layer and finger-like morphology sublayer (Figure 1.5.a) [31]. However, if the composition path does not cross

the binodal curve a delayed de-mixing occurs. In this case, the membrane formation is slow, and the separation takes a longer time. These membranes show a relatively dense top layer and a characteristic sponge-like structure (Figure 1.5.b) [32, 33].

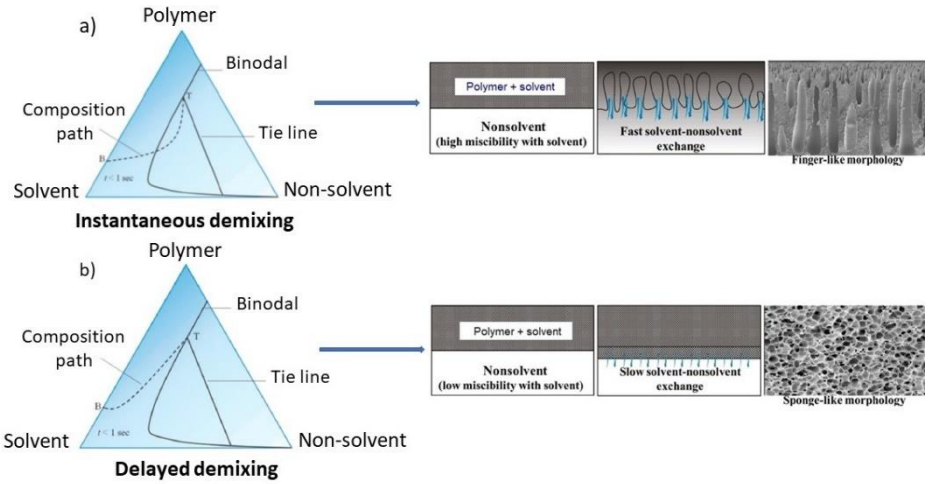

Figure.1.5. Different membrane morphologies depending on the rate of solvent-nonsolvent exchange. Adapted from reference [32, 33].

Additives significantly affect membrane structure. They can accelerate coagulation exchange, enhance pore formation, improve the interconnectivity between the pores, introduce hydrophilicity, increase viscosity or suppress macro-void formation [34].

Mansourizadeh and Ismail prepared PVDF membranes using LiCl as the nonsolvent pore-forming additive. They demonstrated that the concentration of LiCl in the dope solution affects membrane morphology [35]. At low LiCl concentration (2%) highly porous membranes with a large finger-like porous structure were obtained due to the increased phase separation rate. However, at higher concentration (4%), membranes with a sponge-like structure are found owing to the increased solution viscosity. Lan and Wang studied the influence of glycerol, butanol and PEG-400 on the morphology and performance of PES membranes when used during the membrane fabrication

[36]. They demonstrated that when butanol concentration increased for 8% to 15 % the membrane structure changed from finger-like morphology to sponge-like structure. The same effect was observed increasing glycerol concentration from 2% to 6%. At higher concentration, membrane porosity significantly decreased, which confirms that glycerol contributes to produce membranes with more compact and dense structure. Finally, at higher concentration (PEG 8%) it was observed that the viscosity of the solution increases, which delayed phase separation, thereby inhibiting finger-like pore structure.

1.5 Membrane fouling

The most common polymeric materials used for preparing microfiltration, ultrafiltration, nanofiltration and reverse osmosis membranes are: polyethersulfone (PES), polysulfone (PSF), cellulose acetate (CA), polyacrylonitrile (PAN), poly(vinylidene fluoride) (PVDF) and poly(propylene) (PP) essentially due to their high chemical stability, thermal properties and mechanical strength [33, 37]. However, one disadvantage of these polymers is that they suffer the deposition of some substances on their surface or inside their porous structure leading to a decrease in permeate flux. This phenomenon is called “fouling”, as a consequence of which expensive cleaning and periodic regeneration procedures are necessary to prevent membrane loss of performance and to mitigate the need for higher pressure and energy consumption, which would be required to maintain a constant flux. Fouling also reduces the useful service life of membranes [38, 39].

According to the International Union of pure and Applied Chemistry, fouling can be defined as follow: “*The process that results in a decrease in performance of a membrane, caused by the deposition of suspended or dissolved solids on the external membrane surface, on the membrane pores, or within the membrane pores*” [40].

Therefore, there are four different types of membrane fouling:

- Inorganic fouling: also known as a scaling or precipitation fouling, is caused by the deposition or precipitation of inorganic particles and crystallization of mineral salts, oxides and hydroxides present in the feed [41].

- Organic fouling: Natural organic matter is a primary component of organic fouling. Organic matter includes complex organic substances as a polysaccharides, proteins, nucleic acids, humic substances and fatty acids generated by the microbial decay of plants and vegetables [42, 43]. These compounds contribute to form an organic gel layer on top of the membranes and inside its pores. It is considered that adsorption is the initial precursor of such layer [44, 45].

- Particulate / colloid fouling: Colloids cover a wide size range, from a few nanometres to a few micrometres [46]. Particle matter in natural waters and wastewaters has been classified in the following categories**.** Settleable solids > 100 µm, supra-colloidal solids; 1 µm to 100 µm, colloidal solids 0.001 µm to 1 µm and dissolved solids < 0.001 µm [47]. Generally, particles close to the size of membrane pores can cause pore plugging while those much larger can accumulate on the membrane surface forming a cake layer that provides an additional hydraulic resistance to water flux [48].

Depending on the type of blocking, four fouling modes can be observed, which are represented in figure 1.6. [46, 49, 50]

- Complete pore-blocking: Meaning the complete sealing of pores by particles. This blocking requires foulant sizes larger than membrane pores.

- Standard pore-blocking: It refers to the constriction of membranes pores due to the attachment and deposition of small particles at the internal pore walls.

- Intermediate pore blocking is a combination of the preceding ones. In it, particles block membrane pores and also attach to other particles on membrane surface building up bridges between pores.

- Cake layer: Additional particles are deposited outside the external membrane surface contributing to the development of a filtration cake layer.

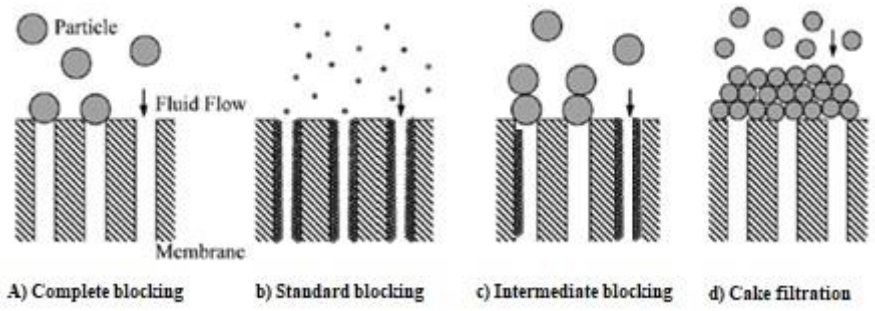

Figure.1.6. Schematic illustration for four different blocking filtration mechanisms. Adapted from reference [50].

- Microbial fouling or biofouling: Biofouling has been defined as the undesired development of biofilms on surfaces [51]. The International Union of Pure and Applied Chemistry defines biofilms as an *"Aggregate of microorganisms in which cells that are frequently embedded within a self-produced matrix of extracellular polymeric substance (EPS) adhere to each other and/or to a surface"* [52].

Biofilm formation comprises three different steps: adhesion, maturation and dispersion. The adhesion step could be categorized as a two-stage process; initial reversible attachment and irreversible attachment [53]. Figure 1.7

represents the process of biofilm formation. It begins when planktonic cells and nutrients present in the feed are transported to the surface. Initially, single cells are associated loosely with the surface via physicochemical forces. The use of fimbriae and flagella may also provide mechanical attachment to the surface [54, 55]. Then, on a time scale ranging from seconds to minutes, cells express EPS, that facilitate binding to the surface leading to the irreversible bacterial attachment to the surface. Mature biofilms present increased cell density and complexity. Within the biofilm matrix, there are channels for the circulation of water and nutrient which keep the cells interconnected. Consequently, interspecies bacterial can interact among themselves, sharing different metabolic substrates. Finally, some bacteria and biofilm aggregates can be released from the matrix, allowing the biofilm to expand on the surface and colonize new niches [56]. EPS can be defined as a *"Polymeric conglomeration generally composed of extracellular biopolymers such as polysaccharides and proteins, in various structural forms"* [42]. EPS production offers several advantages for biofilm-forming microorganisms, as they provide mechanical support for the bacterial community and protection against several environmental conditions such as dehydration or salinity [57].

Biofilm formation and bacterial quorum sensing (QS) are closely interconnected processes. Quorum sensing can be defined as "*A cell-cell communication mechanism that synchronizes gene expression in response to population cell density*" [58]. This process is coordinated by small diffusible molecules called; autoinducers. The concentration of these signalling molecules regulates the expression of a series of genes, allowing cells to modulate surface adhesion, EPS production, maturation and/or the dissolution of the biofilm [59, 60]. QS is a complex communication system able to detect cell density in a specific bacterial community, and as a function of it and environmental factors, regulate gene transcription to create adaptive responses [61].

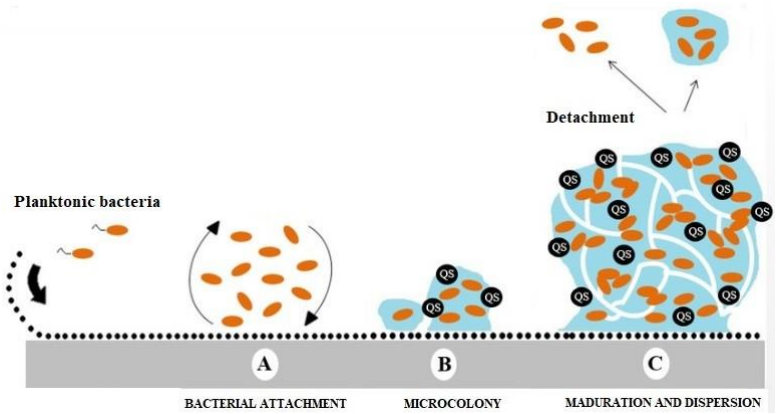

Figure 1.7: Biofilm formation steps (A) bacterial attachment to a surface (B) microcolony formation (C) biofilm maturation and bacterial dispersion. Quorum sensing (QS) are molecules responsible for cell-to-cell communication into the biofilm. Adapted from reference [62].

1.6 Strategies to mitigate fouling and biofouling.

Membrane modifications can be achieved through various techniques in order to mitigate the negative effects of fouling and biofouling.

1.6.1 Surface grafting

Refers to the addition of hydrophilic chains, functional moieties or electrostatically charged groups onto the membrane surface. Surface grafting creates permanent surface changes by covalent bonding between grafted chains and membrane [63, 64]. This technique presents some advantages such as being an easy modification process allowing relatively higher chemical stability with high spatial control of grafting onto the desired surface [65]. However, it has the disadvantage of requiring energy-intensive methods, resulting in an increase in membrane cost and the difficulty to scale-up this technique on the large-scale. Table 1.1 shows a summary of recent studies using surface grafting. Membrane surface can be activated for grafting using different methods:

1.6.1.A Plasma-induced grafting

Plasma can be defined as the fourth state of matter which consists on an electrically quasi-neutral gas partially ionized. Plasma is typically achieved when gases are excited into energetic states using microwaves or radio frequency waves [66]. When a polymeric material is exposed to the plasma, different functional groups can be created on its surface that can be used for subsequent grafting or crosslinking reactions. In this way, plasma treatment can be classified into two categories. A schematic representation of these mechanisms is represented in figure 1.8.

- Plasma functionalization or plasma activation: The substrate is struck with electrons and ions from the plasma-phase to generate surface radicals. The attachment of functional groups depends on the plasma gas used which may be either inert or reactive. Plasma activation using reactive gases such as oxygen results in the introduction of carboxylic acid, hydroxyl or peroxide functional groups. Jahel et al. activated the surface of polypropylene (PP) membranes used oxygen plasma treatment, which allow the introduction of oxygen-containing functional groups, facilitating the deposition of TiO_2 nanoparticles (NPs) on the surface by the dip-coating method [67]. Plasma sustained in carbon dioxide or carbon monoxide gases results in the introduction of carboxyl acid groups and also generate hydroxyl, aldehydes, ester and ketones groups [68]. Nitrogen and ammonia plasmas generate surface primary, secondary and tertiary amines and amides. Although treatment with inert gas plasma such as helium or argon does not result in the production of surface functional groups, it tends to be less aggressive rendering more stable membranes. Inert plasma can be used in combination with other gases or monomer precursors to produce homogeneous plasma discharge [69]. The addition of polar

groups mainly occurred after treatment, when the polymer was exposed to oxygen from air [66].

- Plasma polymerization or plasma deposition involves monomer fragmentation and radical site formation on the membrane surface using a plasma discharge. Reactive fragments can recombine forming polymers in the gas phase, so creating a plasma-deposited polymer coating on the substrate [70]. Therefore, instead of the attachment of functional groups, free radicals on the surface are able to initiate graft polymerization [71].

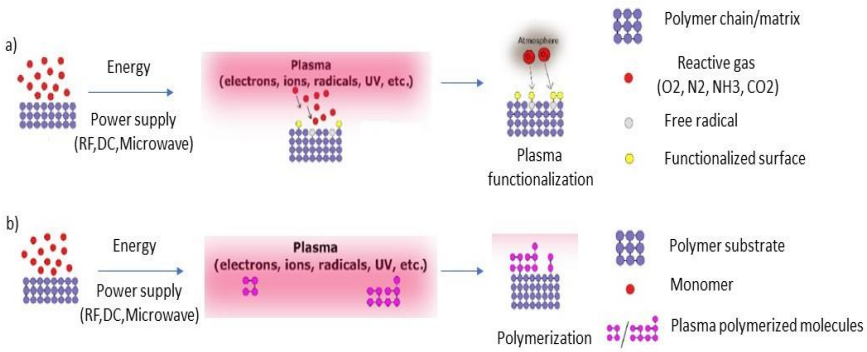

Figure 1.8. Schematic representation of plasma functionalization (a) and plasma polymerization (b) mechanism. Adapted from reference [71].

1.6.1.B UV-induce grafting.

Photochemical-initiated graft polymerization, especially UV grafting is one of the most common techniques for membrane surface modifications due to its simplicity, versatility and low-cost. This method modifies the membrane surface by introducing functional groups without substantially affecting the bulk properties [72]. The photo-initiated graft polymerization can be performed with or without photoinitiator.

Polyarylsulfone membranes are intrinsically photosensitive, which means that they are able to produce active sites or free radicals upon irradiation without the presence of any photoinitiators. It has been reported that UV-light absorption takes place in the backbone of the polyethersulfone polymeric chains due to the phenoxyl-phenyl chromophores present in its structure, resulting in a homolytic cleavage of C-S bonds at the position of a sulfonic group. This process gives rise to the formation of two radical positions, an aryl radical and the sulfonyl radical that later lose its sulfonyl group producing an additional aryl radical that induces the grafting process [73]. Abdul Rahman et al. prepared polyacrylic-polyethersulfone membrane modified via UV photo-grafting. Membranes were immersed in a solution containing acrylic acid monomers and UV irradiated. The resultant membranes showed higher water permeability and lower salt diffusion [74]. Igbinigun et al. grafted allylamine monomers on the active surface of PES membranes using UV light followed by the binding of graphene oxide nanosheets. Functionalized membranes showed smooth surfaces, higher hydrophilicity, lower fouling attachment and higher water flux [75].

Nevertheless, other polymeric membranes require the addition of a photo-initiator or photosensitizer and an additional step, known as photo-activation phase in order to initiate the grafting process. Kaneda et al. modified polyvinyl fluoride (PVDF) membranes by irreversibly grafting graphene oxide (GO) nanosheets via benzophenone-initiated crosslinking reaction under UV irradiation. The resulting membranes showed higher antibacterial activity against *Escherichia coli* without compromising solute retention properties or membrane permeability [76]. Yang et al. grafted monomer of acrylic acid on the surface of PP hollow fibre membranes using benzophenone as a photo initiator under UV irradiation to obtain membranes with higher flux and better rejection rate [77].

1.6.2 Membrane surface coating

Is a simple, economical and environmentally friendly method for surface modification involving the deposition of a coated layer on membrane surface [78]. This technique aims at reinforcing surface properties causing minimal effects on the composition of the bulk material. The major disadvantage of this method is that the coated layer can be unstable. In this way, surface coatings created with strong covalent bonding at the substrate-coating interface offer enhanced performance and long-term stability [84]. Moreover, high molecular weight polymers are used to avoid the penetration of the coated-layer into membrane pores [79]. Table 1.2. shows a summary of recent studies of different surface coating membrane modifications.

- Polydopamine coating. Polydopamine is a bio-polymer, inspired by the strong adhesion property of mussels, that can easily self-polymerize under alkaline conditions (pH typically between 7.5-8.5) using oxygen as an oxidant, to yield a very thin layer onto many substrates [80, 81].

  Polydopamine coating imparts high surface hydrophilicity and anti-organic fouling properties. Furthermore, polydopamine presents multiple functional groups that are able to interact with a wide range of molecules, providing an important platform to form covalently grafted functional layers over a substrate [82].

- Electrospun nanofiber layer is a method that offers some unique benefits due to the superior properties of the nanofibers, which exhibit high interconnectivity, tunable porosity, ease of surface functionalization and high surface area to volume ratio [83]. Electrospun layers can also incorporate different antimicrobial agents such as metallic NPs, carbon nanomaterials or antimicrobial biopolymers, thereby contributing to reduce the biofilm formation [84]. Electrospinning is the only technique generally available to

produce fibres with extremely small diameters. As shown in figure 1.9, an electrospinning system consists of three different components: a high voltage power supply, a spinneret and a collecting plate usually a metal screen plate, or rotating device. This technique utilizes a high voltage source to inject charge of a certain polarity into a polymer solution, which is then accelerated towards a collector of opposite polarity [85].

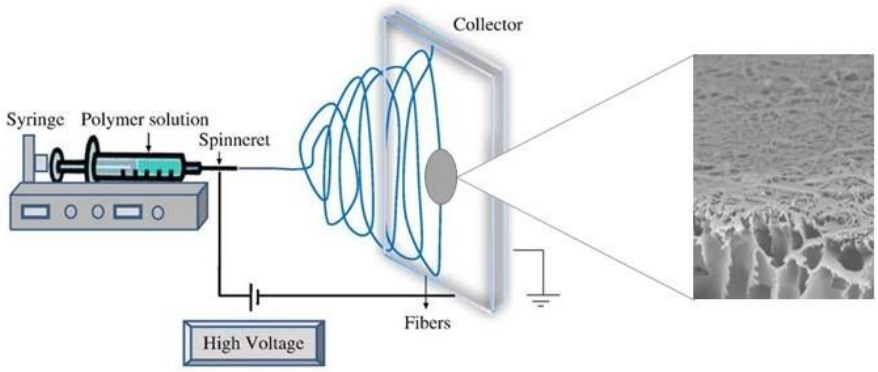

Figure.1.9. Scheme of the electrospinning system with major components. Adapted from reference [86].

Table 1.1: Summary of selected recent studies using surface-grafting modification techniques.

Base membrane	Modification	Main results	Reference
Polyvinylidene fluoride (PVDF)	Argon-plasma treatment + Polystyrene sulfonate deposition	-Average pore radius decreased -Selective to divalent anions -Good removal of Cr (VI) and stability	[87]
Polysulfone (PsU)	Argon-oxygen plasma treatment + Natural seed basil gum NPs	-Increased pure water permeability -Reduced membrane fouling -Higher BSA (bovine serum albumin) rejection rate	[88]
Polypropylene (PP)	O_2 plasma treatment + Deposition of TiO_2 NPs	-Significant improvement of the membrane hydrophilicity	[67]
Polysulfone (PsU)	NH_3-O_2 plasma treatment	-Higher hydrophilicity and permeability -Enhancement of membrane antifouling properties using BSA (bovine serum albumin)	[89]
Polyethylene terephthalate (PET)	Plasma- induced graft polymerization	-Higher hydrophilicity -Decreased effective pore radius	[90]
Polyvinylidene fluoride (PVDF)	Plasma induced self-polymerization of PAA+Self-assembly of ZnO NPs	-Higher membrane hydrophilicity and water flux -Self- cleaning and antifouling properties under UV light	[91]
Polyethersulfone (PES)	UV-grafting of acrylic acid monomers	-Higher water permeability -Lower salt diffusion	[74]
Polyethersulfone (PES)	Grafted allylamine monomers using UV-light	-Higher hydrophilicity, surface ζ-potential and water flux and lower fouling with humic acid	[75]
Polyvinylidene fluoride (PVDF)	UV-grafting of graphene oxide via benzophenone-initiated crosslinking	-Strong antibacterial activity -No effect on membrane permeability or solute rejection properties	[76]
Polypropylene (PP)	UV-grafting polyacrylic acid (PAA) using benzophenone as photo initiator	Higher water flux and rejection rate	[77]

Table 1.2. Summary of recent studies of membranes modified using different surface coatings.

Base membrane	Modification	Main results	Reference
Polysulfone (PsU)	Polydopamine (PD)-layer	- Increased membrane surface hydrophilicity -Excessive deposition decreases membrane permeability, due to pore blocking and reduced pore size -Optimal concentration 2 mg/mL- 15 min deposition time	[92]
Polysulfone (PsU)	Silver (Ag) - PD layer	- "in situ" immobilization of AgNPs - Increased pure water flux, maintaining BSA rejection and enhanced protein-fouling resistance -Good antibacterial activity	[93]
Poly(vinylidene fluoride) (PVDF) **+** Polysulfone (PsU)	PD-layer	-Restored the properties and performances of aged membranes -Low water flux reduction, higher retention -Lower protein adsorption and polysaccharide accumulation	[94]
Poly(ether imide) (PEI)	PD layer + immobilized AgNPs	-Improved permeation and separation -Anti-biofouling against gram-positive and gram-negative bacteria	[95]
Poly(vinylidene fluoride) (PVDF)	Dopamine coating + in situ immobilized CuNPs	-Increased surface hydrophilicity -Enhanced antibacterial activity against the gram-negative bacteria *E. coli*	[96]
Poly(vinylidene fluoride) (PVDF)	TiO_2 electrospun nanofiber coating	-Higher hydrophilicity and glucose rejection rate. -Enhanced antifouling behaviour	[97]
Polysulfone (PsU)	Poly(acrylic acid) (PAA) -poly(vinyl alcohol) (PVA) electrospun layer	-Increased membrane hydrophilicity -Reduced organic fouling (BSA) -Antimicrobial activity against *E. coli* and *S. aureus*	[98]
Poly(vinylidene fluoride) (PVDF)	Electrospun PVDF nanofibers containing SiO_2 NPS	-Superhydrophobic membranes -More stable flux than uncoated membranes	[99]

1.6.3 Blending technique

Polymer blending is a process in which two or more compounds are physically mixed into the casting solution using the same solvent. Polymer material or inorganic nanofillers are frequently used as additives in the phase separation process to manipulate membrane surface properties. Since most of these additives are hydrophilic in nature, this method is considered the simplest way to enhance membrane hydrophilicity thus reducing fouling. The limiting factor associated with this technique is the poor compatibility between hydrophilic additives and hydrophobic polymers as well as inevitable leaching of the blended materials after long-term use [73, 100]. Table 1.3. shows a summary of the recent studies of blending polymeric membranes using inorganic and organic compounds.

1.6.3.A Blending inorganic materials.

1.6.3.A.a Inorganic nanoparticles

Nanoparticles are a promising additive, which may improve membrane performance and properties. Many types of inorganic materials have been directly incorporated into the polymer solution during the membrane preparation, including titanium dioxide, graphene oxide, alumina or silver and copper NPs [101].

TiO_2 is as attractive choice due to its characteristic properties such as good chemical and thermal stability, low toxicity, photo-catalytic activity, super-hydrophilicity and self-cleaning capacity that can be used to mitigate fouling [102, 103]. Anvari et al. incorporated TiO_2 NPs in the PVDF/PAN casting solution to prepare ultrafiltration composite membranes by phase inversion. Blended membranes exhibited higher hydrophilicity, improved pure water flux and enhanced antifouling properties [104]. Furthermore, AgNPs received a great deal of attention due to their broad-spectrum antibacterial properties and low cost. AgNPs serve as a local supply of Ag^+ ions, which can prevent

bacterial colonization and reduce solute adhesion the membrane surface. Rehan et al. prepared polyethersulfone (PES) membranes blended with AgNPs using the immersion precipitation technique to obtain outstanding antibacterial and anti-biofouling properties [105].

However, the incorporation of inorganic materials has two important drawbacks. On the one hand, nanoparticles are prone to aggregate during dope preparation. On the other hand, there is a risk that nanoparticles can be released to the environment [106]. To overcome these problems, a variety of porous materials such as mesoporous silica nanoparticles, nano-minerals materials (halloysite nanotubes, sepiolite, zeolite) or metal-organic frameworks (MOFs) have been proposed as supports to control the nanoparticle stability.

1.6.3.A.b Mesoporous silica particles (MSPs)

MSPs have gained popularity over the last years due to their useful characteristics such as a high specific surface area, uniform pore size between 2-50 nm and easy functionalization. Mesoporous silica can be synthesized in basic and acidic environments and normally relies on a surfactant template to generate its porous structure [107]. The most common types of mesoporous nanoparticles are Mobil crystalline material (MCM-41) and Santa Barbara Amorphous type material (SBA-15). Guo et al. prepared PES membranes using functionalized SBA-15 material with titanium and zirconium nanoparticles to improve membrane hydrophilicity and permeability. Anti-fouling behaviour was obtained using a concentration as low as 0.6% of SBA-15 materials [108]. Martín et al functionalized SBA-15 with amine and carboxylic groups by co-condensation method thereby enhancing the surface porosity, hydrophilicity and permeability of PES membranes. The antifouling properties of composite membranes was improved, especially against irreversible fouling [109].

1.6.3.A.c Nanomineral materials

- Halloysite nanotubes (HNT) is an aluminosilicate nanoclay mineral with a chemical formula $Al_2Si_2O_5(OH)_4 \cdot 2\ H_2O$ [110]. Its crystalline configuration consists of a 1:1 multi-walled inorganic nanotube formed by tetrahedral (SiO) and octahedral (Al-OH) sheets with a hollow tubular structure and regular open-ending pores [101, 111]. It is commonly used as a filler in polymeric matrixes due to its large surface area, tubular shape, well-crystallized structure and excellent dispersity [112]. Chen et al. prepared PES ultrafiltration membranes via phase inversion method containing HNTs loaded with copper ions (Cu^{2+}) as an antibacterial agent. Cu^{2+}-HNTs/PES membranes were more hydrophilic, and presented enhanced permeability [113].

- Sepiolite is a hydrated magnesium silicate with the theoretical formula $Mg_8Si_{12}O_{30}(OH)_4(H_2O)_4 \cdot 8\ H_2O$ [114]. Its structure can be defined as a quincunx arrangement of blocks separated by parallel channels. This configuration induces a needle-like particle shape, which possesses excellent sorptive properties and large specific surface-area [115]. Sepiolite has been employed as support to incorporate metallic nanoparticles into the silicate matrix after magnesium lixiviation in acid conditions [116]. Díez et al. prepared composite PSU-PVP ultrafiltration membranes by phase inversion including sepiolite supported nanometals. Nanoparticle stability was confirmed as no nanomaterials migrated to the filtrate. The antimicrobial behaviour prevented bacterial colonization for either gram-positive and gram-negative bacteria [117].

- Zeolites are microporous, hydrated aluminosilicates minerals with a general formula of $M_{x/m}\ [(AlO_2)_x(SiO_2)_y]$, where $M_{x/m}$ refers an ion-exchangeable cation [118]. It has been demonstrated that the

incorporation of zeolites into a polymer matrix contributed to increase membrane permeability, additionally enhancing mechanical strength, thermal resistance and chemical stability [119]. Moreover, nanoparticles can be loaded inside zeolites for antibacterial applications [120]. Yurekli et al. prepared polysulfone membrane impregnated by a zeolite nanoparticle in order to remove heavy metals (nickel cations) from water due to their excellent sorption capacity [121]. Furthermore, Shi et al. prepared PVDF ultrafiltration membranes containing Ag-loaded zeolite nanoparticles with longer-term antibacterial capacity [122].

1.6.3.A.d Metal-organic frameworks (MOFs)

MOFs are crystalline microporous materials that consist of a regular network of metal ions interrelated by multifunctional organic molecules [123]. They show some special features such as a large surface area, high pore volumes, tuneable pore size and high metal content that offer valuable active sites [124]. Firouzjaei et al. explored the synergetic effect of graphene oxide nanoparticles incorporated in a silver-based MOF into a thin-film nanocomposite (TFN) membrane to improved anti-biofouling and anti-fouling properties [125]. Mohammadnezhad et al. prepared PES nanofiltration membranes by the phase inversion method, modified with nanocrystalline Ce (III) MOFs. Composite membranes showed higher permeability, hydrophilicity, dye rejection capacity and good antifouling behaviour during waste water treatment [126]. Yang et al. fabricated composite CA ultrafiltration membranes by blending graphene oxide (GO) and MOF-GO in the matrix. Modified CA/MOF-GO hybrid membranes showed larger pores size and smoother surfaces. The hydrophilicity and water flux were also improved, exhibiting satisfactory performance in water purification process [127].

1.6.3.B Blending organic materials.

1.6.3.B.a Polymer additives

Hydrophilic polymer additives such as PVP or PEG are common additives used to improve membrane performance or to facilitate membrane fabrication.

- Polyvinyl pyrrolidone is an excellent pore forming agent due to its hydrophilicity. Thermodynamically, it works as a de-mixing enhancer that accelerates the phase inversion process, contributing to form a uniform finger-like porous structure, which results in improved membrane flux [128]. Incidentally, it has been observed that increased PVP concentration, suppresses macrovoid formation leading to a decrease in water permeability [129].

- Polyethylene glycol is a promising hydrophilic additive used to promote pore formation and to enhance permeation properties in polymeric membranes [130]. PEG is available in a variety of molecular weights with a general formula of $H(OCH_2CH_2)_n$-OH, where *n* is the average of repeating oxyethylene groups [131]. PEG also reduce the thermodynamic stability of the casting solution leading to the formation of finger-like porous structures. Xu et al. found that increasing the PEG molecular weight from 200 to 10,000 Da in the casting solutions, membrane morphology changed from finger-like porous structure to spheres or ellipsoids with poorer mechanical properties [132].

1.6.3.B.b Dendritic polymers

Dendritic polymers constitute a family that includes dendrimers and random hyperbranched polymers, which has received considerable attention to develop a variety of nanoscale materials [133].

- A dendrimer is a polymer that contains numerous terminal functional groups and a highly branched topological structured [134]. Dendrimers are produced step-by-step in a controlled and iterative manufacturing process, growing off a central core, each subsequent step representing a new “generation” of dendrimer. Their properties can vary depending on the size (generation) and the number or density of terminal functional groups [135]. Among the various classes of dendrimers, primary-amine terminated polyamidoamine (PAMAM) was the first family to be commercialized [136]. Bharali et al. prepared polysulfone composite membranes by phase inversion using different non-solvent additives. PAMAM-dendrimers (G0) were directly incorporated into the polymeric solution, providing a selective layer for CO_2 absorption in gas separation processes [137]. Furthermore, dendrimers can be used as a template to encapsulate different compounds in their inner void spaces or attached to their surface. Kotte et al. demonstrated an easy route to prepare catalytic PVDF membranes with in-situ synthesized PAMAM (G1) dendrimers that were used as hosts and containers for platinum nanoparticles [138]. Li et al. used PAMAM dendrimers for preparing dendrimer encapsulated silver nanoparticles which were grafting on the surface of PVDF membranes via interfacial reaction, showing good solubility, permeability and antibacterial properties [139].

- Hyperbranched polymers (HBPs) are a class of highly branched polymers, which similar to dendrimers, contain numerous end functional groups, spatial cavities and some unique physical and chemical properties [140]. In contrast to dendrimers, HBPs are easily synthesized in one-step polymerization processes, made them preferred candidates for large-scale applications, being the cheap analogue of dendrimers [135].

Zhao et al. prepared PVDF membranes via phase inversion process using the hyperbranched polyglycerol as additive. Membranes with higher hydrophilic character, and surface pore size were obtained with increased water flux [141]. Ji et al. developed a novel amphiphilic hyperbranched poly(ether amine) (hPEA) by introducing epoxy-containing coumarin moieties (EC) and fluorinated carbon chains (CF6) through epoxy/amine click chemistry. The blended solution was prepared by dissolving PVDF and the resulting copolymer (hPEA-EC-CF6), and membranes prepared by phase inversion showed good adsorption properties to hydrophilic dyes in aqueous solutions [142].

Table 1.3. Recent studies of blended and composite polymeric membranes.

Base membrane	Blending modification	Main results	Reference
PES (Polyethersulfone)	TiO_2 NPs	- Mitigated membrane fouling - Increased macrovoid porous structure - Improvement of membrane permeation flux.	[143]
PVDF/PAN (Poly(vinylidene fluoride) (Polyacrylonitrile)	TiO_2 NPs	- Enhanced membrane hydrophilicity - Improvement pure water flux and antifouling properties	[104]
PsF (Polysulfone)	Graphene Oxide (GO)	- Enhanced hydrophilicity, porosity, permeability and pure water flux - Improved on mechanical properties at low GO concentration and higher ion rejection properties	[144]
PES (Polyehtersulfone)	Ag-NPs	-Antibacterial and anti-biofouling properties -Enhanced permeability	[105]
PsF (Polysulfone)	Silver-GO NPs	-Antimicrobial activity against gram negative (*E. coli)* and gram-positive *(S. aureus)* bacteria. - BSA-fouling reduction	[145]
Polyethersulfone (PES)	Ti, Zr NPs embedded in SBA-15 mesoporous silica	-Improved membrane permeability and hydrophilicity -Lower BSA membrane absorption	[108]
Polyethersulfone (PES)	Amine and carboxylic functionalized SBA-15 particles	-Enhanced surface porosity, hydrophilicity and water permeation flux. -Reduced fouling adhesion, especially irreversible fouling.	[109]
Polyethersulfone (PES)	Halloysite nanotubes loaded with copper ions (Cu^{2+}-HNTs)	-Higher membrane hydrophilicity and permeability -Enhanced mechanical strength -Good antibacterial activity against *E.coli* and *S.aureus*	[113]
Polysulfone (PsU)	Sepiolite-loaded silver and copper nanoparticles	-Enhanced surface hydrophilicity-Higher nanoparticle stability -Effective antimicrobial activity preventing bacterial colonization	[117]

Table 1.3. Recent studies of blended and composite polymeric membranes – continuation -.

Base membrane	Blending modification	Main results	Reference
PVDF Poly(vinylidene fluoride)	Blending Ag^{+}-Zeolite particles	-Improved hydrophilicity -Higher thermal stability -Enhanced mechanical properties -Long term antifouling capability and excellent antimicrobial activity against *E. coli*	[122]
Thin-film composite (TFC)	Graphene oxide (GO) + (Ag-MOF)	-Higher hydrophilicity and water permeability -Improved anti-biofouling and antifouling properties	[125]
Polysulfone (PsU)	Polyvinylpyrrolidone (PVP)	-Improved pure water flux and membrane hydrophilicity and higher anti-fouling behaviour	[146]
PVDF Poly(vinylidene fluoride)	Polyethylene glycol (PEG)	-Enhanced pore formation -Higher molecular weight leads to higher permeability	[147]
Cellulose acetate (CA)	Polyethylene glycol (PEG)	-Enhanced pure water flux and better pore distribution -Enhanced hydrophilicity	[148]
(PsU) Polysulfone	PAMAM-Dendrimers (G0) – PEG	-Higher permeability - Effective for CO_2 permeation	[137]
PVDF Poly(vinylidene fluoride)	PAMAM (G1)-dendrimer encapsulated Pt(O) NPs	-Highly active and reusable catalyst for the hydrogenation of alkenes and alkynes to the corresponding alkanes	[138]
PVDF Poly(vinylidene fluoride)	Hyperbranched polyglycerol (HPG)	-Pore forming agent, enhanced pore size -Higher hydrophilicity -Increased pure water flux	[141]
PVDF Poly(vinylidene fluoride)	Amphiphilic hyperbranched poly (ether amine) (hPEA)	-Selective adsorption of hydrophilic dyes -Enhanced hydrophilicity	[142]

1.7 References

1. WWAP, *(UNESCO World Water Assessment Programme). The United Nations World Water Development report: Leaving No one Behind Paris, UNESCO*. 2019.
2. Le, N.L. and S.P. Nunes, *Materials and membrane technologies for water and energy sustainability.* Sustainable Materials and Technologies, 2016. **7**: p. 1-28.
3. Nqombolo, A., et al., *Wastewater Treatment Using Membrane Technology*. 2018.
4. *Urban Urgency. Water caucus summary. World Water Council (WWC), Marseille, France. 2007*
5. WHO, *Millennium development goals: Progress on sanitation and drinking-water.* WHO/UNICEF joint monitoring programme for water supply. 2010.
6. Zahid, M., et al., *A Comprehensive Review on Polymeric Nano-Composite Membranes for Water Treatment.* Journal of Membrane Science & Technology, 2018. **08**.
7. Madaeni, S.S., Ghaemi, N., & Rajabi, H., *Advances in polymeric membranes for water treatment.* Advances in Membrane Technologies for Water Treatment, 2015. **3-41**.
8. Van Der Bruggen, B., et al., *A review of pressure-driven membrane processes in wastewater treatment and drinking water production.* Environmental Progress, 2003. **22**(1): p. 46-56.
9. Charcosset, C., *Membrane processes in biotechnology: An overview.* Biotechnology Advances, 2006. **24**(5): p. 482-492.
10. Ciardelli, G., L. Corsi, and M. Marcucci, *Membrane separation for wastewater reuse in the textile industry.* Resources, Conservation and Recycling, 2001. **31**(2): p. 189-197.
11. Bernardo, P., Drioli, E., Golemme, G., *(2009) Membrane Gas Separation: A Review/State of the Art.* Industrial & Engineering Chemistry Research. **48**(10): p. 4638-4663.
12. Daufin, G., Escudier, J. P.,Carrère, H., Bérot, S., Fillaudeau, L., Decloux, M., *Recent and Emerging Applications of Membrane Processes in the Food and Dairy Industry.* Food and Bioproducts Processing, 2001. **79**(2): p. 89-102.
13. Judd, S., *Chapter 2 - Membrane technology*, in *Membranes for Industrial Wastewater Recovery and Re-use*, S. Judd and B. Jefferson, Editors. 2003, Elsevier Science: Amsterdam. p. 13-74.
14. Reif, O., *Microfiltration Membranes: Characteristics and Manufacturing.* Advances in biochemical engineering/biotechnology, 2006. **98**: p. 73-103.

15. Garba, M., et al., *Complexing agents for metal removal using ultrafiltration membranes: a review.* Environmental Chemistry Letters, 2019.
16. Ahsan, A. and M. Imteaz, *(2019) Nanofiltration Membrane Technology Providing Quality Drinking Water*, in *Nanotechnology in Water and Wastewater Treatment*, A. Ahsan and A.F. Ismail, Editors., Elsevier. p. 291-295.
17. Warsinger, D., et al., *A review of polymeric membranes and processes for potable water reuse.* Progress in Polymer Science, 2018. **81**.
18. Kim, J.F., et al., *Thermally induced phase separation and electrospinning methods for emerging membrane applications: A review.* AIChE Journal, 2016. **62**(2): p. 461-490.
19. Baker, R.W., *(2004) Membrane Technology and Applications.* Wiley, West Sussex, United Kingdom.
20. Mulder, M., *Basic Principles of Membrane Technology: Springer Science & Business Media, Berlin, Germany. 079234247X.* 1996.
21. Purkait, M.K., Sinha,M.K.,Mondal,P,.Singh,R., *Introduction to membranes, In M. K. Purkait, M. K. Sinha, P. Mondal, and R. Singh (Eds), Interface Science and Technology, Elsevier, Volume 25, 2018, Pages 1-37*. 2018.
22. Lalia, B.S., et al., *A review on membrane fabrication: Structure, properties and performance relationship.* Desalination, 2013. **326**: p. 77-95.
23. Bassyouni, M., Abdel-Aziz, M. H., Zoromba, M. Sh., Abdel-Hamid, S. M. S., Drioli, E. *A review of polymeric nanocomposite membranes for water purification.* Journal of Industrial and Engineering Chemistry. 2019. **73**: p. 19-46.
24. Simone, S., *Coagulation Bath*, in *Encyclopedia of Membranes*, E. Drioli and L. Giorno, Editors. 2015, Springer Berlin Heidelberg: Berlin, Heidelberg. p. 1-2.
25. Li, K., et al., *Membrane formation via thermally induced phase separation (TIPS): Model development and validation.* Journal of Membrane Science, 2006. **279**: p. 50-60.
26. Venault, A., et al., *A Review on Polymeric Membranes and Hydrogels Prepared by Vapor-Induced Phase Separation Process.* Polymer Reviews, 2013. **53**(4): p. 568-626.
27. Barzin, J., Sadatnia, B., *(2008) Correlation between macrovoid formation and the ternary phase diagram for polyethersulfone membranes prepared from two nearly similar solvents.* Journal of Membrane Science. **325**(1): p. 92-97.
28. El-Gendi, A., H. Abdallah, and S. Ali, *Construction of Ternary Phase Diagram and Membrane Morphology Evaluation for*

Polyamide/Formic acid/Water System. Australian Journal of Basic and Applied Sciences, 2012. **6**: p. 62-68.

29. Figoli, A., T. Marino, and F. Galiano, *Polymeric membranes in biorefinery*, in *Membrane Technologies for Biorefining*, A. Figoli, A. Cassano, and A. Basile, Editors. 2016, Woodhead Publishing. p. 29-59.
30. Aroon, M.A., Ismail, A. F., Montazer-Rahmati, M. M.,Matsuura, T., *(2010) Morphology and permeation properties of polysulfone membranes for gas separation: Effects of non-solvent additives and co-solvent.* Separation and Purification Technology. **72**(2): p. 194-202.
31. Idris, A., et al., *Effects of Phase Separation Behavior on Morphology and Performance of Polycarbonate Membranes.* Membranes (Basel), 2017. **7**(2).
32. Tan, X. and D. Rodrigue, *A Review on Porous Polymeric Membrane Preparation. Part I: Production Techniques with Polysulfone and Poly (Vinylidene Fluoride).* Polymers, 2019. **11**(7): p. 1160.
33. Guillen, G.R., et al., *Preparation and Characterization of Membranes Formed by Nonsolvent Induced Phase Separation: A Review.* Industrial & Engineering Chemistry Research, 2011. **50**(7): p. 3798-3817.
34. Urkiaga, A., D. Iturbe, and J. Etxebarria, *Effect of different additives on the fabrication of hydrophilic polysulfone ultrafiltration membranes.* Desalination and water treatment, 2015. **56**: p. 1-12.
35. Mansourizadeh, A. and A.F. Ismail, *Effect of LiCl concentration in the polymer dope on the structure and performance of hydrophobic PVDF hollow fiber membranes for CO_2 absorption.* Chemical Engineering Journal, 2010. **165**(3): p. 980-988.
36. Lan, P. and W. Wang, *Structure Morphology of Polyethersulfone Hollow Fiber Membrane via Immersion Precipitation Phase Inversion Process.* Applied Mechanics and Materials, 2012. **152-154**: p. 574-578.
37. Padaki, M., et al., *Membrane technology enhancement in oil–water separation. A review.* Desalination, 2015. **357**: p. 197-207.
38. Lee, S. and C.-H. Lee, *Effect of operating conditions on $CaSO_4$ scale formation mechanism in nanofiltration for water softening.* Water Research, 2000. **34**(15): p. 3854-3866.
39. Seidel, A. and M. Elimelech, *Coupling between chemical and physical interactions in natural organic matter (NOM) fouling of nanofiltration membranes: implications for fouling control.* Journal of Membrane Science, 2002. **203**(1): p. 245-255.
40. Koros, W.J., Y.H. Ma, and T. Shimidzu, *Terminology for membranes and membrane processes (IUPAC Recommendations 1996)*, in *Pure and Applied Chemistry*. 1996. p. 1479.
41. Saleh, T.A., Gupta, V.K., , *Membrane fouling and strategies for cleaning and fouling control, in T. A. Saleh and V. K. Gupta (Eds.)*

Nanomaterial and Polymer Membranes, Elsevier, 2016, Pages 25-53. 2016.

42. Alvarado, C., Farris, K., Kilduff, J., *(2016) Membrane fouling, modelling and recent developments for mitigation, In Nicholas P. Hankins and Rajindar Singh (Eds.) Emerging Membrane Technology for Sustainable Water Treatment, Elsevier, Pages 433-462*.
43. Amy, G. *Fundamental understanding of organic matter fouling of membranes.* Desalination, 2008. **231**(1): p. 44-51.
44. Ly, Q.V., et al., *Characteristics and influencing factors of organic fouling in forward osmosis operation for wastewater applications: A comprehensive review.* Environment International, 2019. **129**: p. 164-184.
45. Cui, X. and K.-H. Choo, *Natural Organic Matter Removal and Fouling Control in Low-Pressure Membrane Filtration for Water Treatment.* Environmental Engineering Research, 2014. **19**(1): p. 1-8.
46. Guo, W., H.-H. Ngo, and J. Li, *A mini-review on membrane fouling.* Bioresource Technology, 2012. **122**: p. 27-34.
47. Rudolfs, W. and J.L. Balmat, *Colloids in Sewage: I. Separation of Sewage Colloids with the Aid of the Electron Microscope.* Sewage and Industrial Wastes, 1952. **24**(3): p. 247-256.
48. Huang, H., R. Spinette, and C. O'Melia, *Direct-flow microfiltration of aquasols: I. Impacts of particle stabilities and size.* Journal of Membrane Science, 2008. **314** (1-2): p. 90-100.
49. Amosa, M.K. *Towards sustainable membrane filtration of palm oil mill effluent: analysis of fouling phenomena from a hybrid PAC-UF process.* Applied Water Science. 2017. **7**(6): p. 3365-3375.
50. Iritani, E., *A Review on Modeling of Pore-Blocking Behaviors of Membranes During Pressurized Membrane Filtration.* Drying Technology, 2013, **31**(2): p. 146-162.
51. Matin, A., et al., *Biofouling in reverse osmosis membranes for seawater desalination: Phenomena and prevention.* Desalination, 2011. **281**: p. 1-16.
52. Vert, M., Doi, Y., Hellwich, K., Hess, M., Hodge, P., Kubisa, P., Rinaudo, M., Schué, F., *Terminology for biorelated polymers and applications (IUPAC Recommendations 2012)*, in *Pure and Applied Chemistry, 2012, 84*. p. 377-410.
53. Renner, L.D. and D.B. Weibel, *Physicochemical regulation of biofilm formation.* MRS bulletin, 2011. **36**(5): p. 347-355.
54. Bixler, G.D., Bhushan, B. *Biofouling: lessons from nature.* Philos Trans A Math Phys Eng Sci, 2012. **370**(1967): p. 2381-417.
55. Crouzet, M., Le Senechal, C.,Brozel, V. S.,Costaglioli, P.,Barthe, C.,Bonneu, M.,Garbay, B.,Vilain, S., *Exploring early steps in biofilm*

formation: set-up of an experimental system for molecular studies. BMC Microbiol, 2014. **14**: p. 253.

56. Rabin, N., Zheng, Y., Opoku-Temeng, C., Du, Y., Bonsu, E., Sintim, H. O., *Biofilm formation mechanisms and targets for developing antibiofilm agents.* Future Med Chem, 2015. **7**(4): p. 493-512.
57. Flemming, H.C., *Biofouling in water systems-cases, causes and countermeasures.* Appl Microbiol Biotechnol, 2002. **59**(6): p. 629-40.
58. Solano, C., M. Echeverz, and I. Lasa, *Biofilm dispersion and quorum sensing.* Curr Opin Microbiol, 2014. **18**: p. 96-104.
59. Lazar, V., *Quorum sensing in biofilms-how to destroy the bacterial citadels or their cohesion/power?* Anaerobe, 2011. **17**(6): p. 280-5.
60. Nadell, C., J. Xavier, and K. Foster, *The sociobiology of biofilms. .* FEMS microbiology reviews, 2009. **33**: p. 206-24.
61. Bassler, B.L., Losick, R., *Bacterially speaking.* Cell, 2006 **125**(2): p. 237-46.
62. Moura, M.C., Napoleão, T. H., Paiva M.G.P, Coelho, L.C.B.B, *Bacterial biofilms: The structure, development and potential of plant compounds for alternative control, In Leon V. Berhard (Ed.) Advances in Medicine and Biology, Nova Publishers, 2017, **143** pp. 1-13*.
63. Kumar, R. and A.F. Ismail, *Fouling control on microfiltration/ultrafiltration membranes: Effects of morphology, hydrophilicity, and charge.* Journal of Applied Polymer Science, 2015. **132**(21).
64. Zare, S. and A. Kargari. *Membrane properties in membrane distillation*, in *Emerging Technologies for Sustainable Desalination Handbook*, V.G. Gude, Editor. 2018, Butterworth-Heinemann. p. 107-156.
65. Lee, X.J., et al., *Surface grafting techniques on the improvement of membrane bioreactor: State-of-the-art advances.* Bioresource Technology, 2018. **269**: p. 489-502.
66. De Geyter, N. and R. Morent. *Cold plasma surface modification of biodegradable polymer biomaterials*, in *Biomaterials for Bone Regeneration*, P. Dubruel and S. Van Vlierberghe, Editors. 2014, Woodhead Publishing. p. 202-224.
67. Jaleh, B., Etivand, E. S., Mohazzab, B. F., Nasrollahzadeh, M., Varma, R.S., *Improving Wettability: Deposition of TiO_2 Nanoparticles on the O_2 Plasma Activated Polypropylene Membrane.* International journal of molecular sciences, 2019. **20**(13): p. 3309.
68. Siow, K.S., et al., *Plasma Methods for the Generation of Chemically Reactive Surfaces for Biomolecule Immobilization and Cell Colonization - A Review.* Plasma Processes and Polymers, 2006. **3**(6-7): p. 392-418.

69. Wang, J. and X. Chen, *Plasma Modification and Synthesis of Membrane Materials-A Mechanistic Review.* 2018. **8**(3).
70. Desmet, T., et al., *Nonthermal Plasma Technology as a Versatile Strategy for Polymeric Biomaterials Surface Modification: A Review.* Biomacromolecules, 2009. **10**(9): p. 2351-2378.
71. Nageswaran, G., L. Jothi, and S. Jagannathan. *Chapter 4 - Plasma Assisted Polymer Modifications*, in *Non-Thermal Plasma Technology for Polymeric Materials*, S. Thomas, et al., Editors. 2019, Elsevier. p. 95-127.
72. Garcia-Ivars, J., et al., *Surface photomodification of flat-sheet PES membranes with improved antifouling properties by varying UV irradiation time and additive solution pH.* Chemical Engineering Journal, 2016. **283**: p. 231-242.
73. Van der Bruggen, B., *Chemical modification of polyethersulfone nanofiltration membranes: A review.* Journal of Applied Polymer Science, 2009. **114**(1): p. 630-642.
74. Abdul Rahman, A.F.H.B. and M.N.B. Abu Seman, *(2018) Polyacrylic-polyethersulfone membrane modified via UV photografting for forward osmosis application.* Journal of Environmental Chemical Engineering. **6**(4): p. 4368-4379.
75. Igbinigun, E., et al., *Graphene oxide functionalized polyethersulfone membrane to reduce organic fouling.* Journal of Membrane Science, 2016. **514**: p. 518-526.
76. Kaneda, M., et al., *Photografting Graphene Oxide to Inert Membrane Materials to Impart Antibacterial Activity.* Environmental Science & Technology Letters, 2019. **6**(3): p. 141-147.
77. Yang, S. J., et al., *Preparation of hydrophilic polypropylene hollow fiber membranes by UV modification.* Integrated Ferroelectrics, 2016. **169**(1): p. 83-89.
78. Li, F., et al., *Surface modification of PES ultrafiltration membrane by polydopamine coating and poly(ethylene glycol) grafting: Morphology, stability, and anti-fouling.* Desalination, 2014. **344**: p. 422-430.
79. Choudhury, N.R., A.G. Kannan, and N. Dutta. *Chapter 21 - Novel nanocomposites and hybrids for high-temperature lubricating coating applications*, in *Tribology of Polymeric Nanocomposites (Second Edition)*, K. Friedrich and A.K. Schlarb, Editors. 2013, Butterworth-Heinemann: Oxford. p. 717-778.
80. Kim, K.-Y., et al., *Polydopamine coating effects on ultrafiltration membrane to enhance power density and mitigate biofouling of ultrafiltration microbial fuel cells (UF-MFCs).* Water Research, 2014. **54**: p. 62-68.

81. Capozzi, L.C., et al., *Ultrafiltration Membranes Functionalized with Polydopamine with Enhanced Contaminant Removal by Adsorption.* Macromolecular Materials and Engineering, 2017. **302**(5): p. 1600481.
82. Ding, Y.H., M. Floren, and W. Tan, *Mussel-inspired polydopamine for bio-surface functionalization.* Biosurface and Biotribology, 2016. **2**(4): p. 121-136.
83. Mishra, R., J. Militky, and M. Venkataraman. *Electrospun nanofibers*, in *Nanotechnology in Textiles*, R. Mishra and J. Militky, Editors. 2019, Woodhead Publishing. p. 35-161.
84. Afshari, M., *Introduction*, in *Electrospun Nanofibers*, M. Afshari, Editor. 2017, Woodhead Publishing. p. 1-8.
85. Hamrang A, B.D., *Applied Methodologies in Polymer Research and Technology.* CRC Press, 2014: p. 18-20.
86. Bhardwaj, N., Kundu, S.C. *Electrospinning: A fascinating fiber fabrication technique.* Biotechnology Advances. 2010. **28**(3): p. 325-347.
87. Sandoval-Olvera, I.G., et al., *Ultrafiltration membranes modified by PSS deposition and plasma treatment for Cr(VI) removal.* Separation and Purification Technology, 2019. **210**: p. 371-381.
88. Tafreshi, J. and H. Fashandi, *Environmentally Friendly modification of polysulfone ultrafiltration membrane using organic plant-derived nanoparticles prepared from basil seed gum (BSG) and Ar/O_2 low-pressure plasma.* Journal of Environmental Chemical Engineering, 2019. **7**(4): p. 103245.
89. Zhang, X., et al., *Polysulfone membrane treated with NH_3-O_2 plasma and its property.* High Performance Polymers, 2017. **30**(9): p. 1139-1144.
90. Trachevskiy, V., Vakuliuk, P., Kartel, M., & Bo, W., *Surface polymerization of monomers on the polyethylene terephthalate membrane in low temperature plasma for water treatment.* Surface, 2017. **9** (24): p. 111-117.
91. Laohaprapanon, S., et al., *Self-cleaning and antifouling properties of plasma-grafted poly(vinylidene fluoride) membrane coated with ZnO for water treatment.* Journal of the Taiwan Institute of Chemical Engineers, 2017. **70**: p. 15-22.
92. Kasemset, S., et al., *Effect of polydopamine deposition conditions on polysulfone ultrafiltration membrane properties and threshold flux during oil/water emulsion filtration.* Polymer, 2016. **97**: p. 247-257.
93. Wu, H., et al., *Preparation and characterization of antifouling and antibacterial polysulfone ultrafiltration membranes incorporated with a silver-polydopamine nanohybrid.* Journal of Applied Polymer Science, 2018. **135**(27): p. 46430.

94. Gao, F., et al., *Aged PVDF and PSF ultrafiltration membranes restored by functional polydopamine for adjustable pore sizes and fouling control.* Journal of Membrane Science, 2019. **570-571**: p. 156-167.
95. Saraswathi, M.S.S.A., et al., *Polydopamine layered poly (ether imide) ultrafiltration membranes tailored with silver nanoparticles designed for better permeability, selectivity and antifouling.* Journal of Industrial and Engineering Chemistry, 2019. **76**: p. 141-149.
96. Li, R., et al., *A novel strategy to develop antifouling and antibacterial conductive Cu/polydopamine/polyvinylidene fluoride membranes for water treatment.* Journal of Colloid and Interface Science, 2018. **531**: p. 493-501.
97. Kumar, M. and J. Jaafar, *Preparation and characterization of TiO_2 nanofiber coated PVDF membrane for softdrink wastewater treatement.* Environment & Ecosystem Science, 2018. **2**: p. 35-38.
98. Díez, B., G. Amariei, and R. Rosal, *Electrospun Composite Membranes for Fouling and Biofouling Control.* Industrial & Engineering Chemistry Research, 2018. **57**: p. 14561–14570.
99. Efome, J.E., Rana, D., Matsuura, T.,Lan, C. Q., *Enhanced performance of PVDF nanocomposite membrane by nanofiber coating: A membrane for sustainable desalination through MD.* Water Research, 2016. **89**: p. 39-49.
100. Alenazi, N.A., Hussein, Mahmoud A., Alamry, Khalid A., Asiri, Abdullah M., *Modified polyether-sulfone membrane: a mini review.* Designed Monomers and Polymers. 2017. **20**(1): p. 532-546.
101. Otitoju, T.A., A.L. Ahmad, and B.S. Ooi, *Recent advances in hydrophilic modification and performance of polyethersulfone (PES) membrane via additive blending.* RSC Advances, 2018. **8**(40): p. 22710-22728.
102. Yu, J.C., Yu, J., Ho, W., Zhao, J., *Light-induced super-hydrophilicity and photocatalytic activity of mesoporous TiO_2 thin films.* Journal of Photochemistry and Photobiology A: Chemistry, 2002. **148**(1): p. 331-339.
103. Shi, H., Magaye, R., Castranova, V., Zhao, J., *Titanium dioxide nanoparticles: a review of current toxicological data.* Particle and Fibre Toxicology, 2013. **10**: p. 15.
104. Anvari, A., Azimi Yancheshme, A., Tavakolmoghadam, M., Rekabdar, F., Safekordi, A., *Effect of TiO_2 nanoparticles on antifouling and separation properties of PVDF/PAN blend membrane.* Desalination and water treatment. 2019. **154**: p. 92-100.
105. Rehan, Z.A., Gzara, L., Khan, S. B., Alamry, K. A., El-Shahawi, M. S., Albeirutty, M. H., Figoli, A., Drioli, E., Asiri, A. M., *Synthesis and Characterization of Silver Nanoparticles-Filled Polyethersulfone Membranes for Antibacterial and Anti-Biofouling Application.* Recent Patents on Nanotechnology, 2016. **10**(3): p. 231-251.

106. Ng, L.Y., Mohammad, Abdul., Leo, Choe., Hilal, Nidal, *Polymeric membranes incorporated with metal/metal oxide nanoparticles: A comprehensive review.* Desalination, 2010. **308**.
107. Morsi, R.E., Mohamed, R. S., *Nanostructured mesoporous silica: influence of the preparation conditions on the physical-surface properties for efficient organic dye uptake.* Royal Society Open Science, 2018. **5**(3): p. 172021.
108. Guo, J., Sotto, A., Martín, A., Kim, J., *Preparation and characterization of polyethersulfone mixed matrix membranes embedded with Ti- or Zr-incorporated SBA-15 materials.* Journal of Industrial and Engineering Chemistry, 2017. **45**: p. 257-265.
109. Martín, A., Arsuaga, Jesús M., Roldán, Nuria., de Abajo, Javier., Martínez, Ana., Sotto, A., *Enhanced ultrafiltration PES membranes doped with mesostructured functionalized silica particles.* Desalination, 2015. **357**: p. 16-25.
110. Saif, M., H. Asif, and M. Saeed, *Properties and modification methods of halloysite nanotubes: A state-of-The-art review.* Journal of the Chilean Chemical Society, 2018. **63**: p. 4109-4125.
111. Kamal, N.K., V.; Zekri, A.; Ahzi, S, *Polysulfone Membranes Embedded with Halloysites Nanotubes: Preparation and Properties.* Membranes (Basel), 2020. **10**(2).
112. Joussein, E., Petit, S., Churchman, J., Theng, B., Righi, D., Delvaux, B., *Halloysite clay minerals - A review.* Clay Minerals, 2005. **40**: p. 383-426.
113. Chen, Y., Zhang, Y., Liu, J., Zhang, H., Wang, K., *Preparation and antibacterial property of polyethersulfone ultrafiltration hybrid membrane containing halloysite nanotubes loaded with copper ions.* Chemical Engineering Journal, 2012. **210**: p. 298-308.
114. Portela, R., Rubio-Marcos, F., Leret, P., Fernández, J., Banares, M., Avila, P., *Nanostructured ZnO/Sepiolite Monolithic Sorbents for H_2S Removal.* Journal of Materials Chemistry A, 2014.
115. Esteban-Cubillo, A., Pina-Zapardiel, R., Moya, J. S., Barba, M. F., Pecharromán, C., *The role of magnesium on the stability of crystalline sepiolite structure.* Journal of the European Ceramic Society, 2008. **28**(9): p. 1763-1768.
116. Esteban-Cubillo, A., Pecharromán, C., Aguilar, E., Santarén, J., Moya, José S., *Antibacterial activity of copper monodispersed nanoparticles into sepiolite.* Journal of Materials Science, 2006. **41**(16): p. 5208-5212.
117. Díez, B., Santiago-Morales, J., Martínez-Bueno, M.J., Fernández-Alba, A. R., Rosal, R., *Antimicrobial organic–inorganic composite membranes including sepiolite-supported nanometals.* RSC Advances, 2017. **7**(4): p. 2323-2332.

118. Kulikova, S.A. and S.E. Vinokurov, *The Influence of Zeolite (Sokyrnytsya Deposit) on the Physical and Chemical Resistance of a Magnesium Potassium Phosphate Compound for the Immobilization of High-Level Waste.* Molecules, 2019. **24**(19).
119. Maghami, M., Abdelrasoul,A., *Zeolites-Mixed-Matrix Nanofiltration Membranes for the Next Generation of Water Purification.* IntechOpen, 2018.
120. Azizi-Lalabadi, M., Ehsani, A., Divband, B., Alizadeh-Sani, M. *Antimicrobial activity of Titanium dioxide and Zinc oxide nanoparticles supported in 4A zeolite and evaluation the morphological characteristic.* Scientific Reports. 2019. **9**(1): p. 17439.
121. Yurekli, Y., *Removal of heavy metals in wastewater by using zeolite nano-particles impregnated polysulfone membranes.* Journal of Hazardous Materials, 2016. **309**: p. 53-64.
122. Shi, H., Xue, L., Gao, A., Zhou, Q., *Dual layer hollow fiber PVDF ultra-filtration membranes containing Ag nano-particle loaded zeolite with longer term anti-bacterial capacity in salt water.* Water Science & Technology, 2016. **73**(9): p. 2159-67.
123. Leus, K., et al., *A coordinative saturated vanadium containing metal organic framework that shows a remarkable catalytic activity*, in *Studies in Surface Science and Catalysis*, E.M. Gaigneaux, et al., Editors. 2010, Elsevier. p. 329-332.
124. Singh, R. and Geetanjali, *Metal organic frameworks for drug delivery*, in *Applications of Nanocomposite Materials in Drug Delivery*, Inamuddin, A.M. Asiri, and A. Mohammad, Editors. 2018, Woodhead Publishing. p. 605-617.
125. Firouzjaei, M.D., et al., *Exploiting Synergetic Effects of Graphene Oxide and a Silver-Based Metal–Organic Framework To Enhance Antifouling and Anti-Biofouling Properties of Thin-Film Nanocomposite Membranes.* ACS Applied Materials & Interfaces, 2018. **10**(49): p. 42967-42978.
126. Mohammadnezhad, F., M. Feyzi, and S. Zinadini, *A novel Ce-MOF/PES mixed matrix membrane; synthesis, characterization and antifouling evaluation.* Journal of Industrial and Engineering Chemistry, 2019. **71**: p. 99-111.
127. Yang, S., et al., *Effects of GO and MOF@GO on the permeation and antifouling properties of cellulose acetate ultrafiltration membrane.* Journal of Membrane Science, 2019. **569**: p. 48-59.
128. Amin, P., Bhanushali, V., Joshi, S., *(2018) Role of Polyvinlyppyrrolidone in Membrane Technologies.* International Journal of ChemTech Research. **11**: p. 247-259.
129. Chakrabarty, B., A.K. Ghoshal, and M.K. Purkait, *Preparation, characterization and performance studies of polysulfone membranes*

using PVP as an additive. Journal of Membrane Science, 2008. **315**(1): p. 36-47.
130. Wongchitphimon, S., et al., *Effect of polyethylene glycol (PEG) as an additive on the fabrication of polyvinylidene fluoride-co-hexafluropropylene (PVDF-HFP) asymmetric microporous hollow fiber membranes.* Journal of Membrane Science, 2011. **369**(1): p. 329-338.
131. David W. Grainger, C.J.K., *Comprehensive Biomaterials II.* Elsevier. , 2017: p. 434-435.
132. Xu, Z.-L. and F.A. Qusay, *Effect of polyethylene glycol molecular weights and concentrations on polyethersulfone hollow fiber ultrafiltration membranes.* Journal of Applied Polymer Science, 2004. **91**(5): p. 3398-3407.
133. Diallo, M.S., et al., *Dendrimer Enhanced Ultrafiltration. Recovery of Cu(II) from Aqueous Solutions Using PAMAM Dendrimers with Ethylene Diamine Core and Terminal NH_2 Groups.* Environmental Science & Technology, 2005. **39**(5): p. 1366-1377.
134. Abbasi, E., Aval, S. F., Akbarzadeh, A., Milani, M., Nasrabadi, H. T., Joo, S. W., Hanifehpour, Y., Nejati-Koshki, K., Pashaei-Asl, R. , *(2014) Dendrimers: synthesis, applications, and properties.* Nanoscale Research Letters. **9**(1): p. 247-247.
135. Caminade, A.M., Yan, D., Smith, D. K., *(2015) Dendrimers and hyperbranched polymers.* Chemical Society Reviews. **44**(12): p. 3870-3873.
136. Bojaran, M., Akbari, A., Yunessnia lehi, A., *Novel ultrafiltration membranes with the least fouling properties for the treatment of veterinary antibiotics in the pharmaceutical wastewater.* Polymers for Advanced Technologies. 2019, **30**(7): p. 1716-1723.
137. Panchali Bharali, S.B., Swapnali Hazarika, *Effect of Additives on Morphology and Permeability of Dendrimer Membrane for CO_2 Separation.* International Research Journal of Engineering and Technology (IRJET), 2018. **5**: p. 418-424.
138. Kotte, M.R., et al., *A Facile and Scalable Route to the Preparation of Catalytic Membranes with in Situ Synthesized Supramolecular Dendrimer Particle Hosts for Pt(0) Nanoparticles Using a Low-Generation PAMAM Dendrimer (G1-NH_2) as Precursor.* ACS Applied Materials & Interfaces, 2018. **10**(39): p. 33238-33251.
139. Li, G., et al., *The effect of silver-PAMAM dendrimer nanocomposites on the performance of PVDF membranes.* Desalination, 2014. **338**: p. 115-120.
140. Sun, Z., *Hyperbranched Polymers in Modifying Natural Plant Fibers and Their Applications in Polymer Matrix Composites—A Review.* Journal of Agricultural and Food Chemistry, 2019. **67**(32): p. 8715-8724.

141. Zhao, Y.-H., et al., *Porous membranes modified by hyperbranched polymers: I. Preparation and characterization of PVDF membrane using hyperbranched polyglycerol as additive.* Journal of Membrane Science, 2007. **290**(1): p. 222-229.
142. Ji, K., et al., *Hyperbranched Poly(ether amine)@Poly(vinylidene fluoride) Hybrid Membrane with Oriented Nanostructures for Fast Molecular Filtration.* Langmuir, 2018. **34**(13): p. 3787-3796.
143. Shahruddin, M., et al., *Study of the Effectiveness of Titanium Dioxide (TiO_2) nanoparticle in Polyethersulfone (PES) Composite Membrane for Removal of Oil in Oily Wastewater.* Journal of Applied Membrane Science & Technology, 2017. **19**.
144. Ravishankar, H., J. Christy, and V. Jegatheesan, *Graphene Oxide (GO)-Blended Polysulfone (PSf) Ultrafiltration Membranes for Lead Ion Rejection.* Membranes (Basel), 2018. **8**(3).
145. Ali, F., Alam, J., Shukla, A. K., Alhoshan, M., Ansari, M., Al-Masry, W., Rehman, S., Alam, M. , *Evaluation of antibacterial and antifouling properties of silver-loaded GO polysulfone nanocomposite membrane against Escherichia coli, Staphylococcus aureus, and BSA protein.* Reactive and Functional Polymers. 2019, **140**.
146. Tiron, L.G., M. Vlad, and Ş. Baltă, *Research on Hydrophilic Nature of Polyvinylpyrrolidone on Polysulfone Membrane Filtration.* IOP Conference Series: Materials Science and Engineering, 2018. **374**: p. 012059.
147. Syawaliah, et al., *Effects of PEG Molecular Weights on PVDF Membrane for Humic Acid-fed Ultrafiltration Process.* IOP Conference Series: Materials Science and Engineering, 2017. **180**: p. 012129.
148. Mulyati, S., et al., *The effect of poly ethylene glycol additive on the characteristics and performance of cellulose acetate ultrafiltration membrane for removal of Cr(III) from aqueous solution.* IOP Conference Series: Materials Science and Engineering, 2018. **352**: p. 012051.

OBJECTIVES

OBJECTIVES

Most commercial membranes are prepared from hydrophobic materials, which makes them more susceptible to suffer the absorption of fouling substances and microorganisms over their surface. Fouling and biofouling increase energy costs, decrease membrane permeability and compromise permeate quality during water filtration processes.

The overall aim of this Doctoral Thesis is the development and/or modification of membrane to minimise their tendency to fouling and biofouling and, therefore, improve their performance in water purification processes. To achieve this goal newly functionalized membranes will be prepared by phase inversion method, followed by physical and chemical characterization and testing using model microorganisms as bioassays.

Specific objectives:

- To investigate membrane modification techniques including blending organic and inorganic hydrophilic additives, UV-irradiation and surface coating to create ultrafiltration membranes with increased resistance to the adsorption of organic foulants and the attachment of microorganisms.
- To analyse the physicochemical properties of modified membranes and the influence of fillers and functionalizing chemicals in altering membrane morphology and water permeability and filtration performance.
- To assess the mechanisms by which the newly developed materials avoid the colonization by microbial cells and the formation of biofouling using different biofilm-forming bacterial strains.

CHAPTER 2

Antimicrobial organic-inorganic composite membranes including sepiolite-supported nanometal

Chapter 2. ANTIMICROBIAL ORGANIC–INORGANIC COMPOSITE MEMBRANES INCLUDING SEPIOLITE-SUPPORTED NANOMETALS

2.1 Abstract

In this study, composite polysulfone–polyvinylpyrrolidone (PSU–PVP) membranes were prepared using silver and copper loaded sepiolite as a filler. Metal-loaded sepiolite was evenly dispersed within the membranes. No leaching of metal particles was observed during use and only dissolved metals were responsible for membrane antimicrobial activity. The membranes displayed high antibacterial activity showing surfaces free of bacterial colonisation (<20 CFU cm^2). *Escherichia coli* was inactivated at a higher rate (below detection limit in less than 60 min for silver sepiolite loaded membranes) than *Staphylococcus aureus*. All membranes could be successfully reused after daily inoculations and subsequent washing allowing up to 20 cycles with <99.999% CFU removal. The silver leached daily represented ± 0.2-0.4% of the total initial silver content of membranes (0.8-1.0% for copper in copper-containing membranes). Despite its initial lower rate of inactivation, the resistance to *S. aureus* colonisation lasted longer than that to *E. coli* in an assay consisting of daily inoculations on the same membranes.

2.2 Introduction

The demand for new water resources has become increasingly urgent worldwide due to a fast-growing global population and an increasing water demand. Global warming is expected to lead to a severe decrease in freshwater resources even doubling the effect of population growth alone [1]. Membranes play a central role in water and wastewater treatment with continuous technology improvements, new uses and cost reductions [2].

Ultrafiltration is the established technology for reclaiming wastewater and for the pre-treatment of seawater prior to reverse osmosis, the two major processes aiming to expand water resources [3, 4]. Polysulfone and polyethersulfone are the most common materials for preparing ultrafiltration membranes due to their good mechanical and chemical properties, easy processing and wide availability [5]. However, a major problem of polysulfone or polyethersulfone membranes is that their hydrophobic nature favours a relatively rapid loss of permeate flow due to fouling and biofouling, which are the main factors determining membrane performance in practical applications [6]. Fouling is a consequence of the adsorption and deposition of solutes, while biofouling refers to the growth of microorganisms on membrane surface. Both cause loss of permeability, increased transmembrane pressure and shorten membrane life. The formation of biofilm layers also supposes a serious risk of pathogen proliferation [7]. Several strategies have been developed for controlling membrane biofouling in order to prevent or reduce bacterial attachment. They include disinfection using biocidal treatments, nutrient limitation and the modification of the physicochemical properties of membranes [6]. Membrane materials, particularly membrane surface, can be modified in order to render membranes with improved resistance to bacterial attachment. For example, modifying hydrophobicity and roughness, which have been associated to higher biofouling potential due to stronger membrane-bacteria interactions [8]. The increase of membrane hydrophilicity has been widely explored with the added value that it is an approach also valid for mitigating non-biological fouling and to increase membrane permeability [9]. Surface modifications and the use of additives have been reported by several researchers in order to prepare hydrophilic membranes [10, 11]. A commonly additive used for this purpose is polyvinylpyrrolidone (PVP) [12, 13]. Besides being highly hydrophilic, PVP reduces the miscibility of casting solutions with non-solvent water, which enhances phase separation during

membrane fabrication [14]. Another approach is to provide antimicrobial properties by loading materials able to inhibit microbial growth. The use of metal-loaded antimicrobial materials exploits the well-known oligodynamic action of some metals, notably silver and copper, which strongly inhibit microbial growth [15, 16]. Accordingly, silver and copper-loaded membranes have been used to prevent bacterial attachment and reduce biofilm formation [17, 18]. The mechanism of action of metals in their nanoforms has been debated in the scientific literature, particularly for the case of silver [19]. The discussion tried to determine whether the release of ion metals is the only reason for their antimicrobial action or nano-bio interactions play a significant role. It has been recently shown that silver nanoparticles exert a biological effect only in aerobic conditions, which are the only that make it possible the release of silver ions, which suggests that specific nanoparticle interactions are probably not relevant [20]. The advantage of using metals in nanoparticle form would be to exploit their role as nanocarriers based on the higher rate of dissolution of particles with large surface area. However, nanoforms must tackle the problem of their possible release into the environment, which is a major concern in view of the potential risk of nanoparticles [21]. The attachment of nanometals to supports, rather than the direct dispersion of nanoparticles into the polymeric solution, is a possibility to overcome this problem by making migration more difficult or impossible [22].

The objective of this study was to prepare composite polysulfone ultrafiltration membranes including a source of silver and copper ions using sepiolite fibres as metal reservoir. Sepiolite acts as a vehicle for introducing silver nanoforms and copper salts into the polymeric solution avoiding the problems derived from nanoparticle aggregation or chemical incompatibility with casting solvents. Moreover, the fact that the metals were attached to a silicate was expected to impart stability and minimize the risk of nanoparticle dissemination into the environment. Membranes were produced using a

conventional phase inversion process and were tested using strains of the Gram-negative bacterium *Escherichia coli* and the Gram-positive *Staphylococcus aureus*. Special attention has been paid to assess the release of metal nanoparticles and membrane durability.

2.3 Material and methods

2.3.1 Materials

Polysulfone (PSU, 60 kDa) and 1-methyl-2-pyrrolidone (NMP) were purchased from Across Organic. Polyvinylpyrrolidone (PVP,40 kDa) was obtained from Sigma-Aldrich. The components of culture media were biological grade acquired from Conda-Pronadisa (Spain). Ultrapure water was generated from a Direct-Q™ 5 Ultrapure Water Systems from Millipore (Bedford, MA, USA) with a specific resistance of 18.2 MΩ cm.

Sepiolite is a porous hydrated magnesium silicate with a large specific surface area and a needle-like morphology with high surface area and exceptional sorptive properties. Silver, copper and silver/copper-loaded sepiolites were produced by Tolsa S.A, Spain using a procedure described elsewhere [23]. Briefly, a mechanically dispersed sepiolite was put in contact with the precursor salts at low pH in order to favour magnesium lixiviation and the introduction of metallic cations. The addition of NaOH induced the precipitation of silver hydroxide or hydrated copper nitrate. The materials were then washed and dried at a minimum temperature of 150 °C yielding nanoparticles of silver and a mixture of copper compounds depending on the drying conditions. In this case copper-containing sepiolite was not reduced and, therefore, copper was not forming metallic nanoparticles, but amorphous copper hydroxide, with minor contribution of copper oxide. As a result of the thermal treatment, sepiolite channel structure collapsed and nanoparticles got embedded into the silicate structure as well as attached to

their surface. The advantage of this process is that the metals or metal compounds became supported on particles with a non-nanodimension, which makes them easier to handle and limits the risk of their release into the environment. It also allows a high weight load of active metals. The explanation on how sepiolite can be used as a host for different metallic cations upon magnesium leaching and the material acting as scaffold for the growth of metal nanoparticles can be found elsewhere [24]. Sepiolite composition was determined by ICP-MS using a NexION 300XX Perkin-Elmer apparatus after microwave digestion according to the prescriptions of EPA Method 3052 in a Mileston Ultra-WAVE equipment, which allowed to close the balance with a global error <5%.

2.3.2 Membrane preparation

Control PSU and composite membranes with metal-loaded sepiolite were prepared via phase inversion. The casting solution was prepared by dissolving PVP in NMP followed by stirring until suspension. The required amount of metal-loaded sepiolite was added to the aforementioned solution and dispersed in an ice water bath. Control materials were also prepared without PVP. PSU was then added, and the mixture magnetically stirred for another 2h at 70 °C. Table 2.1 shows the chemical composition of casting solutions and the nomenclature used in what follows. The casting solution was degassed for 10 min and casted on the glass plate of an automatic film applicator AB3120 (TQC, The Netherlands) adjusted to a thickness of 200 µm. Immediately after, the membrane was immersed into a distilled water bath at 16 °C for 1 min. After the immersion, the membrane was removed, and its surface was cleaned with water and kept in distilled water for 24 h to remove residual solvent. Prior to storage, the membranes were dried at 50°C and then vacuum-dried at 90°C (-0.9 bar) during 24 h. Some membranes were irradiated with ultraviolet (UV) radiation at room temperature for using a Vilber-Lourmat Bio-Lin BLX-254

Crosslinker equipped with 5 x 8 W 254 nm T-8C lamps. The irradiance was 820 μW cm^2.

Table 2.1 Composition of casting solutions [a]

Membrane	Identifier	PSU (wt%)	PVP (wt%)	NMP (wt%)	Filler (wt%)
PSU (Control)	M(0)	15.0	-	85.0	-
SpAg-1@PSU	M(1)	15.0	-	84.9	0.15
SpAg-5@PSU	M(2)	14.9	-	84.3	0.78
PSU-PVP-5	M(3)	15.0	0.79	84.2	-
PSU-PVP-10	M(4)	15.0	1.67	93.3	-
PSU-PVP-15	M(5)	15.0	2.65	82.3	-
PSU-PVP-25	M(6)	15.0	5.01	80.0	-
SpAg@PSU-PVP-5	M(7)	14.9	0.78	83.4	0.99
SpAg@PSU-PVP-10	M(8)	14.9	1.65	82.5	0.99
SpAg@PSU-PVP-15	M(9)	14.9	2.62	81.5	0.99
SpAg@PSU-PVP-25	M(10)	14.9	4.96	79.2	0.99
SpAgCu@PSU-PVP-5	M(11)	14.9	0.78	83.4	0.99
SpCu@PSU-PVP-5	M(12)	14.9	0.78	83.4	0.99

PSU–PVP-x means x wt% PVP with respect to the total amount of PSU + PVP. The filler was sepiolite and represented 1 and 5 wt% respectively in SpAg-1@PSU and SpAg-5@PSU specimens. For the rest of sepiolite-loaded materials, the amount of sepiolite was ~5 wt%.

2.3.3 Membrane characterization

The morphology of membrane cross-section was observed using Scanning Electron Microscopy (SEM) in a XL-30 Philips apparatus. Surface porosity was observed using a Field Emission Scanning Electron Microscope (FE-SEM) in a Hitachi SU8000 equipment operating at 1 kV on non-metalized samples coated with graphite. Elemental analyses of the membranes were carried out using SEM combined with energy dispersive X-ray spectroscopy (EDS) JEOL JSM 6400 operating at an acceleration voltage of 20 kV.

The hydrophilicity of membranes was determined by measuring water contact angles of vacuum-dried specimens (90°C, 2 hours). Each measurement was conducted in triplicate using the sessile drop technique using an optical

contact angle meter (Krüss DSA25 Drop Shape Analysis System) operating at room temperature.

Surface ζ-potential was measured via electrophoretic light scattering (DLS, Malvern Zetasizer Nano ZS) and using a Surface Zeta Potential Cell (ZEN 1020) from Malvern. A rectangular section of the membrane was taped on the sample holder using Araldite adhesive. The cell was inserted into a disposable 10 mm square cuvette containing 10 mM KCl, pH 7.0, aqueous solution with of 0.5% (w/w) polyacrylic acid (450 kDa) used as a tracer (a negatively charged tracer is required for negatively charged surfaces). Measurements were conducted at 25 °C at six different displacements from the sample surface in order to calculate the surface ζ-potential.

Attenuated total reflectance Fourier transform infrared (ATR-FTIR) spectra were recorded using a Thermo-Scientific Nicolet iS10 apparatus with a Smart iTR-Diamond ATR module. XRD spectra of PSU–PVP-5 membranes, metal loaded sepiolites and the composite membranes were recorded using an X-ray diffractometer PolycrystalX'pert Pro PANalytical which employed Ni-filtered Cu Kα (k = 1.5406 nm) radiation and operated at 0.02 min^{-1}, 45 kV and 40 mA.

2.3.4 Membrane filtration studies

Membrane permeability was measured in a Millipore filtration cell with an effective membrane area of 28.7 cm^2 and a total cell volume of 100 mL using membranes preconditioned in distilled water. Membrane permeability was determined from the pure water flux, J, per unit transmembrane pressure (TMP):

$$P = \frac{J}{\Delta P} \qquad (1)$$

The average surface pore radius of the membranes, r_m, was estimated using the filtration velocity method according to the Guerout–Elford–Ferry equation:

$$r_m = \sqrt{\frac{(2.9-1.7\varepsilon)8L\eta}{\varepsilon \Delta P}} \qquad (2)$$

The mean radius obtained is considered a cross-sectional average of all the pores involved in permeate flow. η is the water viscosity: 8.9 x 10^{-4} Pa s. Membrane porosity, ε, was determined by water uptake using the weights of wet and dry membranes. All measurements were performed in triplicate using a TMP pressure difference of 0.20 MPa at 20 °C.

2.3.5 Metal and nanoparticle release studies

ICP-MS analyses of metal released from membranes were performed on an ICP-MS model X Series 2 system apparatus from Thermo Scientific. The calibration curve was prepared by using standards in ultrapure water 1% HNO_3 (v/v). Dynamic and static tests for metal release were carried out in order to assess the rate of liberation/migration of active metals from membranes. In static tests, membranes were submerged in ultrapure water with or without 150 mg L^{-1} of NaCl, which was based on the parametric values established for chloride (250 mg L^{-1}) and sodium (200 mg L^{-1}) by the European Drinking Water Directive, Council Directive 98/83/EC, for water intended for human consumption. The experiments were performed at 20 °C using 50 mL of water in opaque glass bottles for a contact time of up to 4 days in static runs.

In order to quantify the release of metals under flow conditions and to assess the possible release of nanoforms during membrane use, a dynamic experiment was performed that consisted of taking samples at different cumulative volumes representing a total filtration time of approx. 6 h. The samples were further ultrafiltrated using Vivaspin 20, 5 kDa, polyethersulfone

ultrafiltration centrifuge tubes. A 5 kDa membrane would retain particles over 2 nm, larger than the smaller silver nanoparticles found attached to sepiolite [25]. The samples were then analysed for metals using ICP-MS. In case of nanoparticle release, the amount detected in the 5 kDa ultrafiltrate would be significantly lower than that coming directly from membrane permeate. TMP was set at 2 bar and at least two replicates of each assay were performed.

2.3.6 Antimicrobial bioassays

The bioassays were performed using two bacteria, *E. coli* (CETC 516) and *S. aureus* (CETC 240), which are the strains suggested by the ISO 22196 concerning the measurement of antibacterial activity on plastic surfaces. The bacteria were preserved at -80 °C in glycerol (20% v/v) until use. Reactivation was performed by culture in nutrient broth (10 g L^{-1} peptone, 5 g L^{-1} sodium chloride, 5 g L^{-1} meat extract and, in case of solid medium, 15 g L^{-1} powder agar). pH was adjusted to 7.0 ± 0.1 using NaOH or HCl. Bacterial growth was measured by optical density (OD) at 600 nm.

The membranes to be tested for antimicrobial behaviour were placed in sterile 24 well microplates and exposed to cultures containing an initial concentration of 10^6 cells per ml. The volume of test inoculum was fixed at 0.15 mL mg^{-1} of membrane. Incubation took place at 36 °C during 20 h. After incubation, the viable bacteria were measured both in cultures in contact with membranes and on membrane surface. For cultures, 10-fold serial dilutions were performed in phosphate buffered physiological saline (PBS) and 10 mL of the dilution was spot-plated on solid agar and incubated at 36 °C for 24 h, after which, the number of colonies were counted. The number of viable bacteria on membrane surface was determined after detaching them by means of the following procedure. First, the membranes kept in contact with microorganisms were recovered and transferred to sterile 24-well microplates and washed with PBS for 25 min in an orbital shaker. Then, PBS was replaced

with 2mL of SCDLP broth (soybean casein digest broth with lecithin and polysorbate according to ISO 22196) in order to remove bacteria from membrane. Microplates were kept under mechanical agitation for 30 min. SCDLP liquid was serially diluted in PBS and 10 mL of each dilution was spot plated on agar. All samples were measured in triplicate.

SEM images of membranes exposed to bacterial colonisation were obtained in a ZEISS DSM-950 instrument operating at 25 kV. For it, clean membranes were inoculated with 0.15 mL mg^{-1} of nutrient broth (NB), pH 7.0±0.1 with 10^6 cells per mL and incubated for 20 h at 36°C, after which membranes were cleaned with phosphate buffered saline (PBS), fixed and dehydrated with ethanol and acetone prior to SEM imaging.

The durability of the antimicrobial effect of membranes with metal-loaded sepiolites was assessed by performing successive inoculation of *E.coli* or *S.aureus* on the same membrane specimens after removing the preceding culture by careful washing. The membranes were placed in 24-well microplates and exposed to 10^6 cells per mL (0.15 mL mg^{-1} of membrane) using a 500-fold diluted nutrient broth (1/500 NB) at 36 °C for 20 h. After the prescribed time, samples from the culture in contact with membranes were serially diluted in order to count viable bacteria according to the procedure described before. The minimum number of colonies assessed was 10 CFU mL^1. The used membranes were transferred to new sterile wells and incubated with the same inoculum (10^6 cells per mL in 1/500 NB). The same procedure was repeated as many times as required until bacterial colonies appeared in the liquid. The number of cycles of inoculation and washing without microbial growth was considered an indicator of the service life of membranes. Finally, the biocidal activity of metal-loaded membranes was evaluated from the rate of decay of viable cells during the period immediately after inoculation with

10^6 cells per mL in 1/500 NB. Supernatant broth was sampled at different times and viable bacteria were counted as described before.

2.4 Results and discussion

2.4.1 Membrane properties and performance

Sepiolite composition was determined by ICP-MS. The composition of the three sepiolites used was, expressed as metal, 17.6 ± 0.5 wt% Ag for silver–sepiolite (SpAg), 12.8 ± 0.8 wt% Cu for copper-sepiolite (SpCu) and 7.9 ± 0.4 wt% Ag and 9.5 ± 0.7 wt% Cu for the mixed silver/copper-sepiolite (SpAgCu). Fig.2.1 shows TEM images of sepiolite loaded with silver, silver-copper and copper. Silver nanoparticles displayed a relatively broad nanoparticle size distribution, approximately ranging from 5-50 nm, enclosed or supported on the sepiolite fibrillar structure. It is important to note that copper hydroxide was not visible in TEM images and only silver nanoparticles do as black dots. Sepiolite fibres had an average length of 1-2 mm, and ~20 nm width.

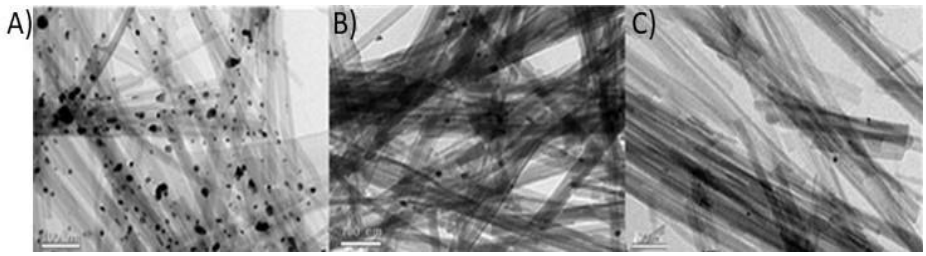

Figure.2.1. TEM micrographs of sepiolites loaded with silver (A: SpAg), silver-copper (B: SpAgCu) and copper (C: SpCu).

The surface morphology of membranes is shown in Fig. 2.2 for three representative specimens. Sepiolite loaded and non-loaded membranes exhibited a porous surface with a relatively thin skin layer and internal sponge-wall asymmetric morphology showing large, finger-like macrovoids. PSU-PVP and composite specimens did not display any significant evident differences in macrovoid structure or skin layer thickness.

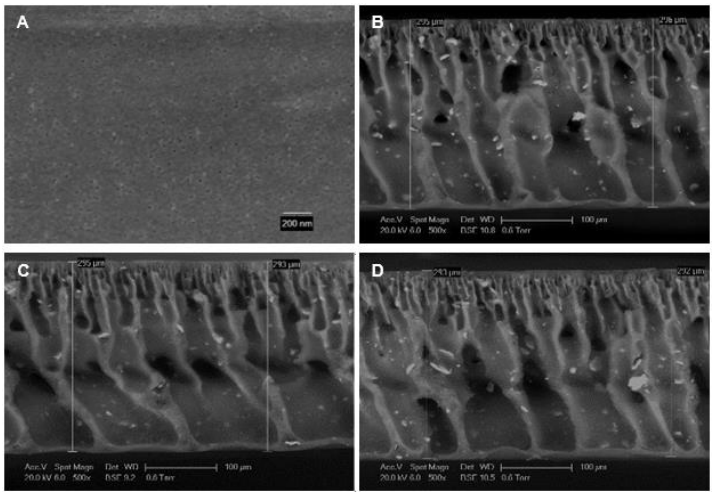

Figure.2.2. Representative SEM images of composites membranes. Upper view of M(11) (SpAgCu@PSU-PVP-5, A) and cross-sectional SEM micrographs of M(3) (PSU-PVP-5, B), M(7) (SpAg@PSU-PVP-5, C) and M(11) (SpAgCu@PSU-PVP-5, D).

This result was in agreement with the porosity measurements shown in Fig.2.3 which reveals a trend towards higher porosity for membranes containing sepiolite materials, M(7) to M(10) compared to PSU-PVP. The increase of membrane porosity with hydrophilic fillers is a well-known fact explained as a consequence of the faster interdiffusion process resulting from their addition to the ternary thermodynamic system [26].

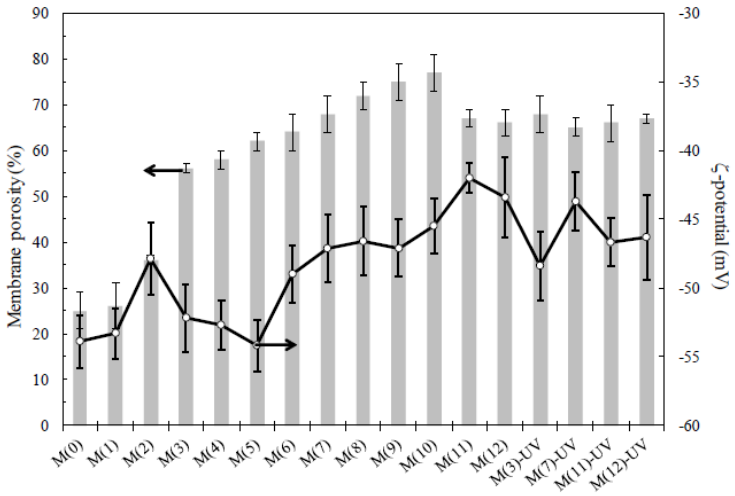

Figure. 2.3. Membrane porosity and surface ζ-potential for all tested specimens

Fig. 2.4 shows membrane permeability and pore sizes calculated from equation (1) and (2). Our results showed that the introduction of PVP resulted in larger water permeability and increased surface pore sizes, but the differences were only clearly observed for membranes with up to 10 wt% PVP.

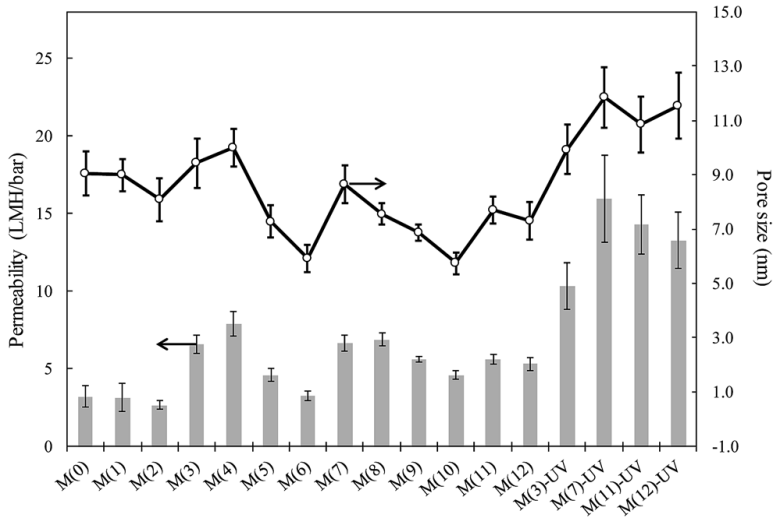

Figure. 2.4. Water permeability (bars, left scale) and surface pore sizes calculated according to the Guerout–Elford–Ferry equation (lines and circles, right scale)

The use of the non-solvent hydrophilic additive PVP, reduces the miscibility of casting solutions with water and has been shown to enhance phase separation up to a certain concentration. Accelerating de-mixing contributes to the enlargement of membrane surface pores with a parallel increase in permeability [27]. The results agreed with previous findings and showed a trade-off between thermodynamic and kinetic factors controlling the de-mixing process during phase separation. The permeability increases with PVP concentration due to the enhanced phase separation but drops for higher concentrations due to the delayed de-mixing and the kinetic hindrance derived from the viscosity increase of the casting solution [14, 28]. The introduction of sepiolite particles did not significantly alter water permeability or surface pore size with similar values for the SpAg@PSU-PVP membranes,

M(7)-M(10), with respect to their counterparts without sepiolite, M(3)-M(6). Pore sizes were quite similar in all cases and always in the 5-12 nm range. UV irradiated membranes displayed higher permeabilities than non-irradiated specimens. The functionalization of PSU membranes using techniques such as irradiation, plasma treatment or chemical agents is a well-known way of increasing the hydrophilicity of PSU membranes and, consequently, to increase membrane flux without using chemical additives [29, 30]. The formation of carboxylic and sulfonic acid groups on membranes is supposed to create internal repulsion forces within the pores, which causes their enlargement and, therefore, an increase in permeability.

We obtained surface ζ-potential values slightly less negative for composite membranes with respect to the neat PSU membrane (-53.9 ± 3.2 mV). The results are shown in Fig. 2.3 and could be attributed to the relatively lower negative charge of sepiolite particles, the ζ-potential of which was, at pH 7.0, -38.8 ± 7.2 for SpAg, -37.6 ± 5.2 mV for SpAgCu and -28.1 ± 4.8 mV for SpCu (measured in 10 mM KCl). The small difference in surface change for composite membranes including sepiolite particles suggests that the particles became completely entrapped into the polymeric matrix. Water contact angle measurements also support this assumption. PSU membranes were hydrophobic according to their water contact angle, which was 81° (± 3). The introduction of the hydrophilic PVP only slightly reduced contact angles, with a value of 73° (± 2) for 5 wt% PVP membranes. The addition of metal-loaded sepiolite did not significantly change surface hydrophilicity, but irradiated membranes were clearly more hydrophilic with an average contact angle of 43° (± 2) for the irradiated specimens.

The changes in membrane surface were tracked by ATR-FTIR as shown in Fig.2.5. ATR-FTIR measurements on PSU and PSU-PVP specimens gave information on chemical changes on membrane surface. The addition of PVP

to PSU membrane led to a new band at 1674 cm^{-1}, which corresponds to amide I carbonyl peak [31]. PSU irradiated membranes show a new broad band around 1721 cm^{-1} linked to C=O stretching, which can be attributed to carboxyl groups and is compatible with the oxidative photolysis of aromatic groups from the outer membrane layer [32]. The band was clearly observed for PSU-UV membranes in which the PVP signal at 1674 cm^{-1} was absent. This was confirmed by a decrease in peaks at 1323 and 1236 cm^{-1} corresponding to sulfone and ether stretching respectively. It can also be observed that amide I peak shifted to 1666 cm^{-1}, what could correspond to formation of hydrogen bonds between carbonyl and hydroxyl groups from oxidized species of PVP or PSU [33].

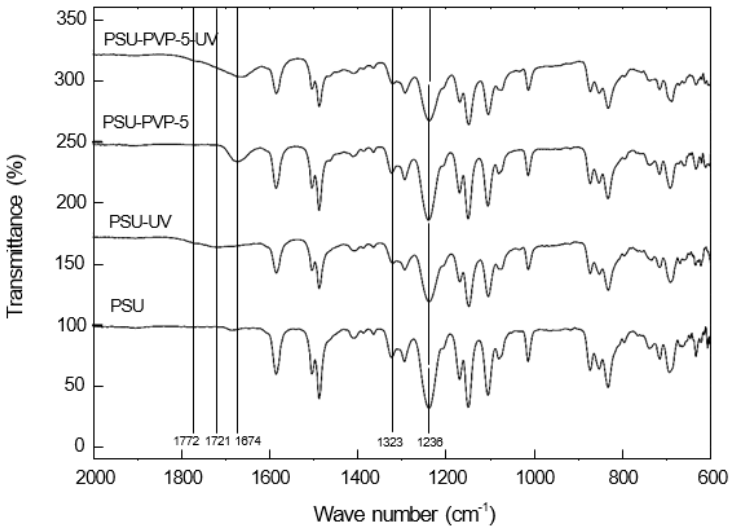

Figure. 2.5. ATR-FTIR spectra of PSU, PSU-PVP and irradiated membranes

The presence of metals in membrane samples has been assessed by means of SEM-EDS (Fig. 2.6), which shows the presence of silver and copper in composite membranes. It is interesting to note that the corresponding to metal appear frequently aligned in a row, corresponding to the direction of sepiolite fibres. (This alignment was highlighted in the inset of Fig. 2.6.A.).

The images show a good dispersion within membrane specimens without visible particle aggregation.

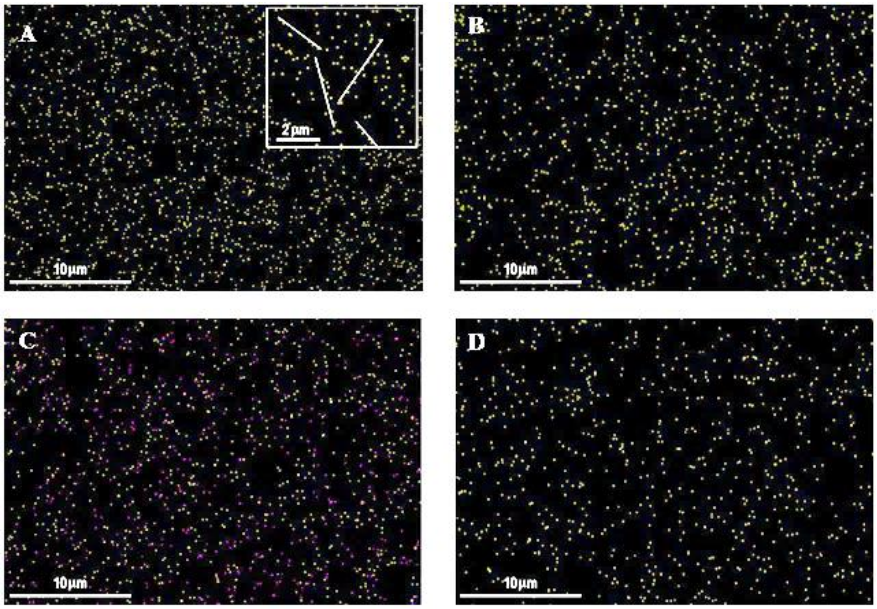

Figure.2. 6. SEM-EDS micrographs of metal-loaded membranes. **A**: SpAg-5@PSU (Ag yellow)**B**: SpAg@PSU-PVP-5 (Ag yellow) **C**: SpAgCu@PSU-PVP-5 (Ag yellow, Cu pink) **D**: SpCu@PSU-PVP-5 (Cu yellow).The inset in Fig 6-A highlights the alignment of spots.

The XRD spectra of PsU-PVP-5 membranes, metal loaded sepiolites and the composite membranes are shown in Fig. 2.7. Silver loaded materials (SpAg and SpAgCu) show the typical XRD patterns of metallic silver with four sharp diffraction peaks at 2θ values of 38.0, 44.1, 64.3 and 77.3°, which corresponded to Bragg's reflections from the (111), (200) (220) and (311) planes of Ag and in good agreement with the reported data [34]. We got no peaks corresponding the cubic structure of silver oxide indicating that all the silver was in reduced form [35]. XRD of copper sepiolite shows less peaks, probably because of the amorphous nature of copper hydroxide. The small peaks appearing could be attributed to the (-111) and (111) planes of monoclinic copper oxide at 2θ 35.7 and 39.0°, although a precise assignment is difficult [36].

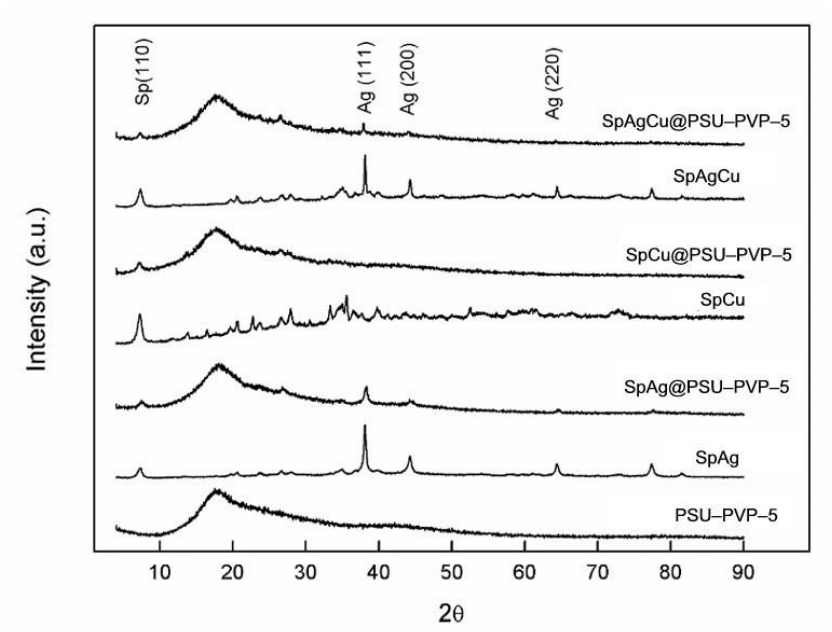

Figure. 2.7. XRD spectra of SpAgCu@PSU-PVP-5, SpAg@PSU-PVP-5, SpCu@PSU-PVP-5 and PSU-PVP-5 membranes, and metal loaded sepiolites SpAg, SpCu and SpAgCu.

2.4.2 Metal release and nanomaterial stability

The two reasons for using sepiolite as metal support were to ensure a good dispersion of nanoparticles in the polymeric solution and to avoid their release into the environment. In order to assess the possible migration of nanometals, a series of successive filtration runs were performed using the same membranes, the filtrates being analysed by ICP-MS before and after 5 kDa ultrafiltration. The results are shown in Fig. 2.8. The upper limit of the bars is the amount of silver or copper in the permeate of composite membranes, whereas the lower correspond to the same values in the 5 kDa ultrafiltrate of an aliquot of the first permeate. Significant differences between the upper and lower bar boundaries were only found for silver during the first batch, indicating that no nanoparticles were released except for silver during the first ultrafiltration period. These nanoparticles probably corresponded to the less tightly bound in the more accessible sepiolite fibres. Afterwards, the results

showed that silver and copper could not migrate in nanoparticle form to the filtrate. A further evidence supporting this claim is that no significant amounts of silicon were found in ICP-MS analyses beyond the solubility limit of sepiolite itself, showing that sepiolite fibres did not detach from the polymer.

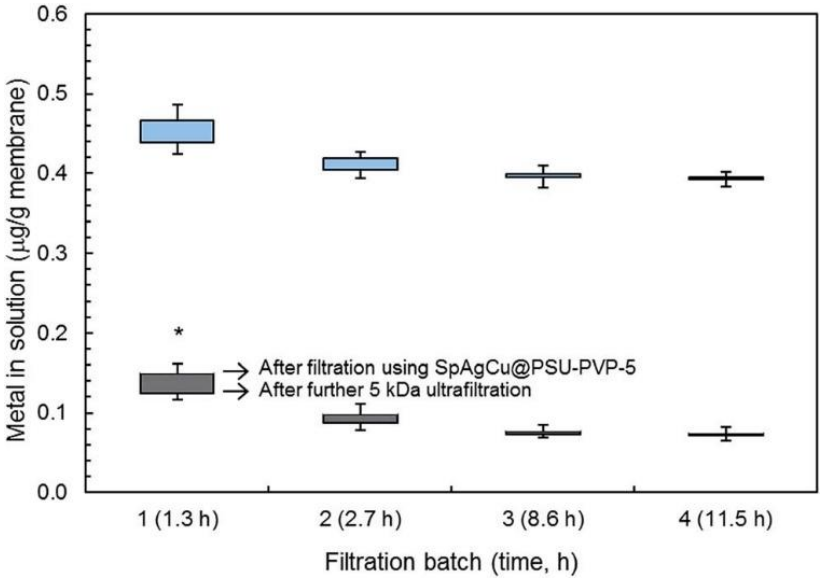

Figure. 2.8. ICP-MS analyses of silver (below, grey) and copper (upper, blue) measured in successive filtrations using SpAgCu@PSU-PVP-5 membranes and 5 kDa ultrafiltration of membrane permeate. Significant differences between the upper and lower limits were only found for silver in the first batch (asterisk). (Only the upper and lower parts of error bars are shown for clarity.)

The same experiment combining filtration-ultrafiltration was performed with metal-loaded sepiolite materials kept in water suspension for one hour. ICP-MS analyses showing the amount of metals passing to the solution yielded 4.3 ± 0.3 µg g^{-1} of sepiolite for silver and 17.8 ± 1.5 µg g^{-1} of sepiolite for copper, which, considering the concentration of sepiolite filler in membranes (5 wt%) are figures comparable to those shown in Fig. 2.8. The amount of nanomaterials detached from sepiolite fibres (retained for 5 kDa UF) were 1.7 ± 0.5 µg g^{-1} of sepiolite for silver and 2.2 ± 0.6 µg g^{-1} of sepiolite for copper

somewhat higher (after correcting for the 5 wt% concentration in membranes) than the values obtained for sepiolite loaded membranes most probably due to the stabilizing role of polymer for the less tightly attached metal particles.

Fig. 2.9 shows the amounts of copper and silver released by different membranes containing SpAg, SpAgCu and SpCu, (SpAg@PSU-PVP-5, SpAgCu@PSU-PVP-5 and SpCu@PSU-PVP-5) indicated as M(7), M(11) and M(12) respectively. Membrane specimens were kept for 4 days in water (and in water containing 150 mg L^{-1} NaCl). M(7) released more silver than M(11) as expected from its higher silver content. The percentage of silver leached could be estimated in both cases as approx. ~ 0.2-0.4% of their total initial silver content for every 24 h period (0.8-1.0% for copper in copper-containing membranes). Using these figures, a rough estimation of the time on service for membranes is provided below.

Metal release was higher for UV-irradiated membranes, probably due to their higher surface hydrophilicity, which would favour the access of water molecules and the migration of solvated cations (Ag^+, $Cu^{2+)}$ or the hydroxylated species that dominate the speciation of copper, $Cu_2(OH)_2^{2+}$ and $Cu_3(OH)_4^{2+}$ according to visual MINTEQ (version 3.1, KTH, Stockholm, Sweden). In the presence of chloride, the amount of silver released was considerably lower due to the formation of insoluble AgCl (according to visual MINTEQ 150mg L^{-1} NaCl yielded saturated solutions of AgCl for >50 μg Ag^+ per L and in all cases the concentration of AgCl(aq) was one order of magnitude higher than that of the free ion Ag^+). For copper, the results run in parallel, with higher metal release in irradiated membranes or in membranes with higher copper content (SpCu@PsU-PVP-5). The rate of release of copper was higher than that of silver because copper was already in the $Cu_{(II)}$ oxidation state in the sepiolite material, whereas silver required an additional oxidation step from Ag(0) to Ag^+. We preferred this material over sepiolite with Cu(0) or CuO because the

amount of copper required for a biocidal effect is larger than that of silver due to its role as essential metal [37].

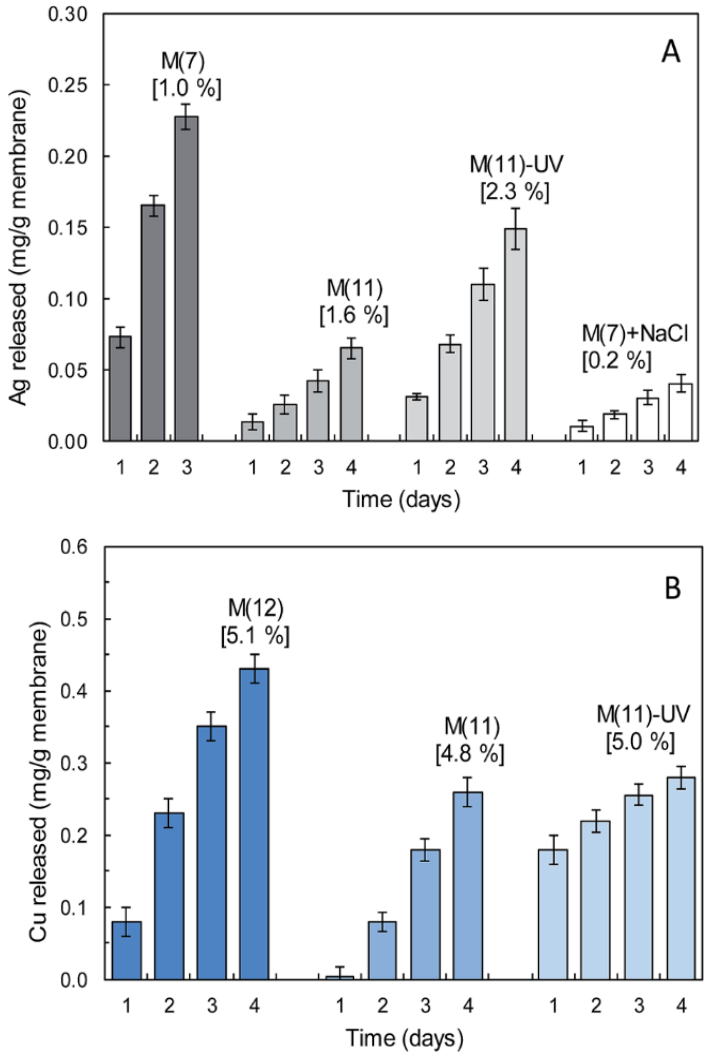

Figure.2.9. Silver (A) and copper (B) released from M(7) (SpAg@PSU–PVP-5), M(11) (SpAgCu@PSU–PVP-5), M(12) (SpCu@PSU–PVP-5), M(11)-UV irradiated and M(7) + NaCl 150 mg L^{-1} membranes. Values in brackets show the percentage of metal with respect to the total metal content

It is interesting to note that the rate of release was essentially linear with time, which could be attributed to the difficulty of ions to dissolve and migrate from their nanoparticle support to the bulk. In a previous work, we obtained nanosilver composites with unsupported silver by taking advantage of the reducing effect of PVP. The result was a polymer loaded with silver nanoparticles in the tens of nanometre range. This procedure, however, leads to a rapid leaching of metals during the first hours on stream accompanied by significant nanoparticle detachment [38]. The data presented here show no nanoparticle loss with only a certain preferential release of the more accessible metals on the surface of sepiolite [22].

2.3.4. Antibacterial performance

Fig. 2.10 shows the result of microbial growth tests performed on different membrane specimens. Fig. 2.10 (A) refers to the liquid in contact with membranes after incubation for 20 h at 36 °C while the results for bacteria detached from surface (expressed as CFU per unit membrane surface) are shown in Fig.2. 10 (B). The growth of *E. coli* and *S. aureus* was high for cultures in contact with PSU, not significantly lower than the 1/500 NB control without membrane.

The addition of PVP led to membranes somewhat less prone to microbial adhesion, probably due to their more hydrophilic surface [39, 40]. Other factors, however are involved such as surface charge, which is more negative for membranes with high PVP content, and may explain the higher amount of bacteria attached to M(6) in comparison with M(3) as shown in Fig. 2.10(B).

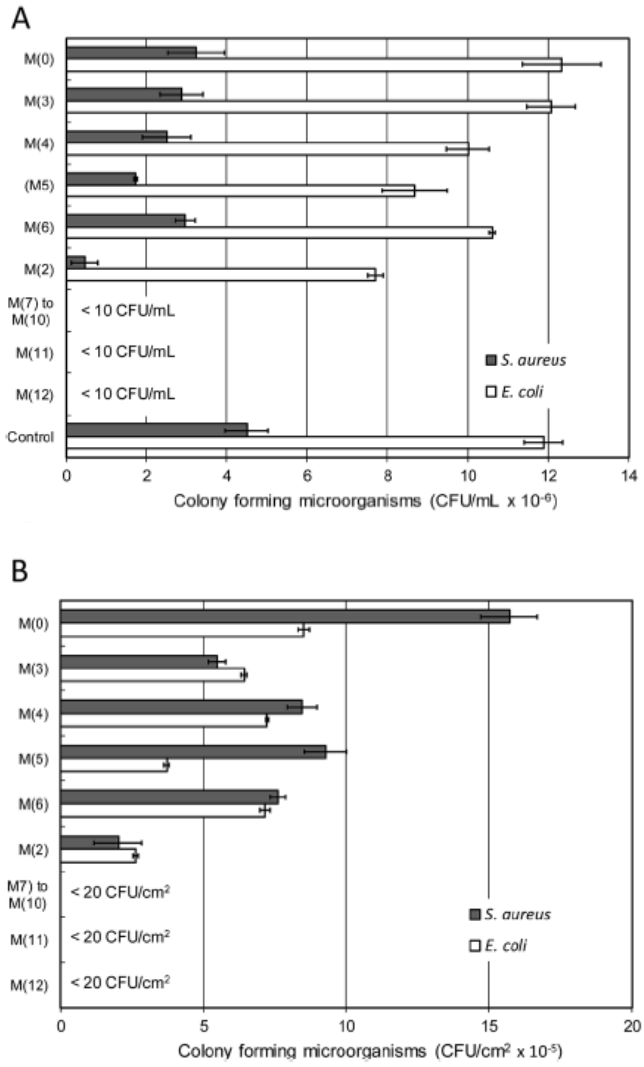

Figure. 2.10. Microbial growth for bacterial cultures exposed to different membranes (A) and culturable bacteria detached from membranes after incubation(B) at 36 °C, 20 h.

Upon contact with metal-loaded membranes the microbial growth was completely inhibited. The effect was considerable for M(2), a membrane prepared without PVP, but was much more marked for composite membranes using PSU-PVP blends, M(7) to M(12). In this case, always for a total content of 5 wt% of metal-loaded sepiolite, microbial growth did not take place at all,

and the combination of PSU-PVP and SpAg, SpAgCu and SpCu led to membranes free of any significant microbial growth after 20 h following inoculation. For the sake of clarity, Fig. 2.10 shows together the results for M(7) to M(10) (SpAg@PSU-PVP-5/10/15/25). All metal loaded membranes were free of bacteria with less than 20 CFU cm^2.

Fig. 2.11 shows SEM micrographs of the surface of membranes put in contact with cultures of *E. coli* and *S. aureus* for 20 h at 36 °C (inoculum 10^6 cells per mL in 1/500 NB, washed, fixed and dried before imaging). The surface of PS-PVP-5 membranes appeared almost entirely colonized with bacteria, while SpAg@PSU-PVP-5 was clean except for a few cells and objects that are probably cell debris.

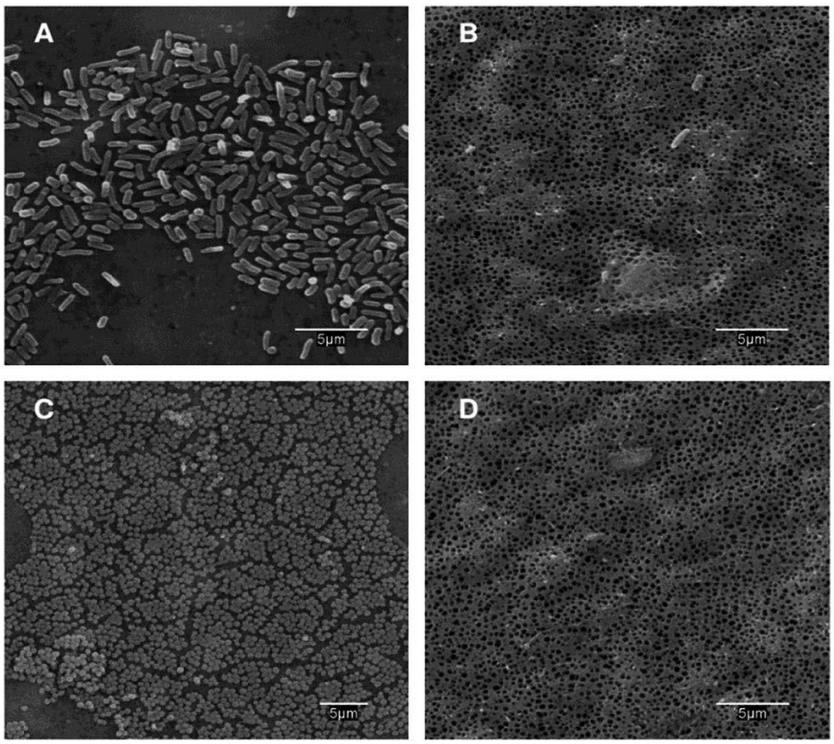

Figure. 2.11. SEM micrographs of PS-PVP-5 (A and C) and SpAg@PSU-PVP-5 (B and D) membranes cultured for 20 h at 36 °C and pH 7.0 with an initial inoculum of 10^6 cells per mL (0.15 mL mg^{-1} membrane) of *E. coli* (A and B) and *S. aureus* (C and D).

The antimicrobial effect of materials containing silver and copper nanoparticles is still controversial, with different pathways suggested for bacterial growth inhibition. In certain cases, nanoparticles can be internalized via phagocytosis and endocytosis, but sepiolite-loaded nanometals were not significantly released during membrane use as shown in Fig. 2.8. The increase in reactive oxygen species because of the interaction with the nanoparticle surface has been suggested to a least partly explain nanotoxicity [41-44]. Other studies suggested that the mechanism of silver nanoparticle toxicity would be essentially explained by the release of silver ions due to the reaction with dissolved oxygen [45]. In our case, membrane surface properties, the good metal dispersion shown by SEM-EDS micrographs and the absence of nanoparticle release from composite membranes suggest that the sepiolite material is well dispersed and entangled into the polymer matrix. Consequently, the amount of nanoparticles in the skin layer that could get in touch with bacterial cells, would be limited if any. Also supporting this claim is that surface charge was similar for all membrane specimens. Consequently, the electrostatic interaction between sepiolite particles and bacterial cells is not playing any significant role in explaining the antimicrobial effect of composite membranes [46]. Our data suggest that the antibacterial action of metal-loaded sepiolite membranes is only due to the release of soluble forms of silver and/or copper. Metals have the potential to bind some proteins but not all biomolecules have a high level of discrimination and many can bind metal ions mimicking the correct cofactor [16]. When the metal homeostasis is affected the overproduction of ROS can induce oxidative stress resulting in cell damage [47]. Metal nanoparticles, attached to sepiolite, would then act as reservoirs for the release of metals that diffuse through the polymer towards the medium surrounding the membranes. Once in contact with living cells, the damage exerted by silver and copper ions proceed via several mechanisms associated or not with the production of reactive oxygen species

(ROS). The following mechanisms have been identified as drivers explaining the antimicrobial activity of metals: (1) increased ROS production due to the in vivo induction of Fenton chemistry, the disruption of cellular donor ligands coordinating iron and thiol mediated reduction of metals; (2) protein dysfunction and loss of enzyme activity as a consequence of metal-catalysed oxidation of proteins in residues adjacent to metal-binding sites; (3) impaired membrane function due to metal binding on electronegative chemical groups; (4) interference with nutrient assimilation and (5) genotoxicity [16, 48-51]. Noteworthy, the release of soluble metal ions from sepiolite fibres has been studied as the antibacterial way of action of natural silicates [52].

The rate at which bacterial inactivation takes place has been studied during the first two hours after contact with membranes. Fig. 2.12 shows the results for membranes M(7), M(11) and M(12) loaded with SpAg, SpAgCu and SpCu respectively.

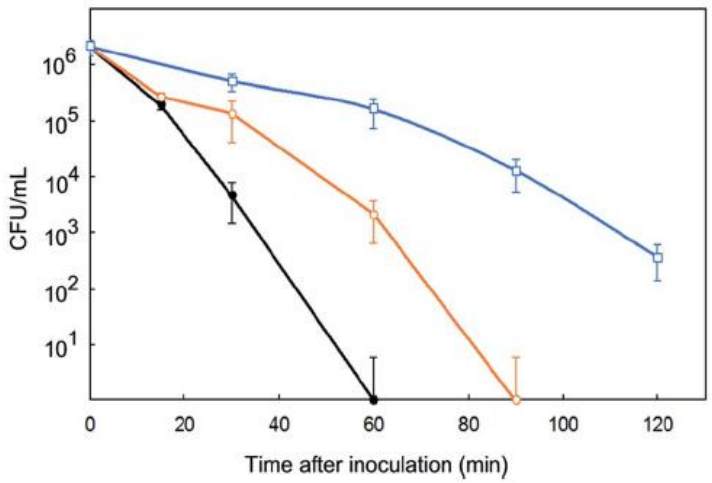

Fig. 2.12. Removal of *E. coli* in contact with M(7) (SpAg ●), M(11) (SpAgCu, ○) and M(12) (SpCu □) membranes during their first use.

In all cases, the membranes were inoculated with 10^6 cell per mL and incubated at 36°C. Samples from the liquid culture in contact with them were taken at prescribed intervals during the first two hours, CFU counted and the results fitted to a first-order decay. The complete set of results for irradiated and non-irradiated membranes is presented in Table 2.2. The antimicrobial effect was clearly faster in the membranes containing more silver, but it was also apparent for copper-loaded specimens. For SpAg@PSU-PVP-5, M(7) in Fig. 2.12, *E. coli* was completely inactivated in 60 min, while for SpCu@PSU-PVP-5, M(11), the decay was about 3 log (99.9%). Comparing successive uses of the same membrane, the rate of decay decreased, most probably due to the loss of the most external metal loading, after which silver, and copper release slowed down.

Table 2.2: Rate constants for CFU decay in cultures in contact with different membranes during first and second use (inoculum: 10^6 cell/mL)

Membrane	**Bacteria**	**Rate constant (h^{-1})**	
		1st use	2nd use
M(7) SpAg@PSU-PVP-5	*E.coli*	5.4 ± 0.6	3.60 ± 0.39
	S.aureus	1.4 ± 0.6	0.36 ± 0.12
M(11) SpAgCu@PSU-PVP-5	*E.coli*	3.5 ± 0.5	2.20 ± 0.10
	S.aureus	0.5 ± 0.2	0.26 ± 0.08
M(12) SpCu@PSU-PVP-5	*E.coli*	2.4 ± 0.5	2.10 ± 0.10
	S.aureus	0.8 ± 0.1	0.42 ± 0.26
M(7)-UV SpAg@PSU-PVP-5	*E.coli*	6.3 ± 0.2	2.40 ± 0.20
	S.aureus	1.0 ± 0.1	0.08 ± 0.02
M(11)-UV SpAgCu@PSU-PVP-5	*E.coli*	6.9 ± 0.2	2.30 ± 0.10
	S.aureus	1.1 ± 0.1	0.11 ± 0.03
M(12)-UV SpCu@PSU-PVP-5	*E.coli*	6.4 ± 0.3	2.50 ± 0.10
	S.aureus	1.3 ± 0.1	0.13 ± 0.08

The repeated reuse of membranes led to the results shown in Fig. 2.13 for M(7), M(11) and M(12) membranes, which were daily inoculated (10^6 cells per mL, 0.15 mL mg $^{-1}$ of membrane), cultured for 24 h at 36 °C in 1/500 NB and, subsequently, washed, dried and reused in the same conditions.

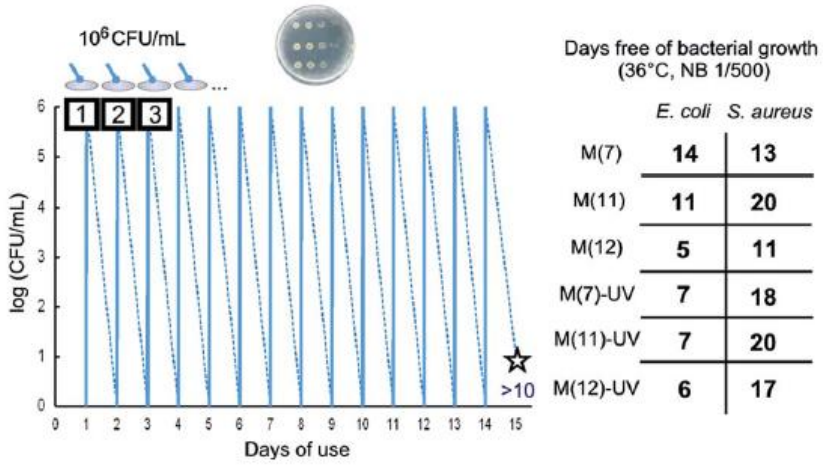

Fig. 2.13. Schematic view of successive daily inoculations until detecting bacterial colonies (the figure corresponds to M(11) incubated with *E.coli)* and days until detecting colonies of *E. coli* and *S. aureus.*

The number of daily reuses without appreciable microbial growth in plate count agar (<10 CFU mL^{-1} or 20 CFU cm^{-2}) was recorded as "days free of bacterial growth" (Fig. 2.13). It has to be taken into account that the number of cycles without significant bacterial count has been recorded under conditions very favourable to bacterial growth at their optimal temperature and without any nutrient restriction. It is interesting to note that SpAg@PSU-PVP-5, M(7), displayed the better results against *E. coli* colonization but SpAgCu@PSU-PVP-5, M(11), which combines silver and copper, performed better against *S. aureus.* These data suggest a synergistic disinfection effect obtained by the combinations of both metals.

The number of cycles free of bacterial growth was generally higher for *S.aureus.* However, the rate of CFU decay for short time contacts (Table 2.2) was lower for *S. aureus*. Gram-negative bacteria exhibit a thin layer of peptidoglycan between the cytoplasmic membrane and the outer cell wall whereas Gram-positive species possess a layer of peptidoglycan many times thicker [53]. This layer is known to help bacteria to overcome physical stresses

and is also believed to reduce the penetration of toxic metal ions. Gram-negative bacteria possess an outer membrane with porins that can act as channels for low molecular weight substances to enter the cell [54]. Therefore, the tolerance to metal ions is generally higher for Gram-positive bacteria in agreement with the kinetic results obtained in this work (Table 2.2). The fact that membranes were more efficient in the long term against *S. aureus* (Fig. 2.13) was not probably related to the vulnerability to silver or copper but to the higher growth rate of *E. coli*, which would overcome an intrinsically higher susceptibility [55, 56].

The data showed that metal release was the factor behind the antimicrobial behaviour of composite membranes. Therefore, the time on service of metal-doped membranes could be estimated from their initial metal content and the rate of metal release. From the data shown in Fig. 2.9, the time on service for metal loaded membranes could be roughly estimated in the order of 100 days (from copper release) or 300 days (calculated from silver release). The rate of metal release can be modulated using the amount of PVP. For example, for M(2), a membranes without PVP, it took 7 days to release >0.5% of the initial silver content (compared to 3 days for 1% in M(7) as shown in Fig.2.9). The antimicrobial efficiency of membranes with lower metal release rate such as M(2) in Fig. 2.10 was considerably lower under the conditions tested in this work (36 °C, 1/500 NB), but under actual service conditions, at lower temperature and without a rich culture media, a material with lower rate of metal release could be competitive.

2.5 Conclusions

PSU-PVP membranes loaded with up to 5 wt% sepiolite containing silver and/or copper were produced. The introduction of PVP and UV-irradiation resulted in permeability increase and higher rate of metal release. Metal-loaded sepiolite became evenly dispersed within the membranes, without evidence of aggregates. Consistent with it, membrane surface charge, measured as ζ-potential, did not change significantly with the introduction of metal-loaded sepiolite. No nanoparticle leaching was detected. The antibacterial performance of sepiolite-loaded membranes was high, with complete removal of bacterial colonies detached from membrane surface (< 20 CFU cm^{-2}) and in the liquid culture in contact with them (<10 CFU mL^{-1}) for 5 wt% silver, copper or silver–copper sepiolite. SEM images showed membranes completely free of bacteria, compared to the high colonisation of PSU-PVP membranes. The antimicrobial action was attributed to the release of metals diffusing from their supports. For membranes loaded with silver or silver-copper, the silver released daily amounted to 0.2-0.4% of the total silver content, which dropped one order of magnitude in the presence of chlorides in the medium. In contact with all metal-loaded composites, *E. coli* was quickly inactivated (<99.999% in 60 min for SpAg@PS-PVP-5). *S. aureus* inactivation was 5-10 times slower, which agrees with its Gram-positive nature. Composite membranes containing silver and/or copper sepiolites could be successfully reused after daily inoculations and subsequent washing up to 20 times with < 99.999% CFU removal. Despite of its initial lower rate of inactivation, the capacity to inactivate *S. aureus* lasted longer (an average of 8 cycles more) that to *E. coli*. Higher rates of metal release limited membrane durability for the removal of *E. coli*, but not for *S. aureus*, indicating that the inactivation of the former requires higher concentrations of metals.

2.6 References:

1. Schewe, J., et al., *Multimodel assessment of water scarcity under climate change.* Proc Natl Acad Sci U S A, 2014. **111**(9): p. 3245-50.
2. Pendergast, M.M. and E.M.V. Hoek, *A review of water treatment membrane nanotechnologies.* Energy & Environmental Science, 2011. **4**(6): p. 1946-1971.
3. Filloux, E., et al., *Ultrafiltration of biologically treated domestic wastewater: How membrane properties influence performance.* Separation and Purification Technology, 2014. **134**: p. 178-186.
4. Fritzmann, C., et al., *State-of-the-art of reverse osmosis desalination.* Desalination, 2007. **216**(1): p. 1-76.
5. Tweddle, T.A., et al., *Polysulfone ultrafiltration membranes.* Industrial & Engineering Chemistry Product Research and Development, 1983. **22**(2): p. 320-326.
6. Nguyen, T., F.A. Roddick, and L. Fan, *Biofouling of water treatment membranes: a review of the underlying causes, monitoring techniques and control measures.* Membranes (Basel), 2012. **2**(4): p. 804-40.
7. Gao, W., et al., *Membrane fouling control in ultrafiltration technology for drinking water production: A review.* Desalination, 2011. **272**(1): p. 1-8.
8. Park, N., et al., *Biofouling potential of various NF membranes with respect to bacteria and their soluble microbial products (SMP): Characterizations, flux decline, and transport parameters*. Vol. 258. 2005. 43-54.
9. Zhao, Y.-F.a.Z., Bao-Ku and Zhu, Li-Ping and Yi, Zhuan and Xu, You-Yi, *Improving the hydrophilicity and fouling-resistance of polysulfone ultrafiltration membranes via surface zwitterionicalization mediated by polysulfone-based triblock copolymer additive.* Journal of Membrane Science, 2013. **440**: p. 40-47.
10. Sun, Q., et al., *Improved antifouling property of zwitterionic ultrafiltration membrane composed of acrylonitrile and sulfobetaine copolymer.* Journal of Membrane Science, 2006. **285**(1): p. 299-305.
11. Ma, Y., et al., *Effect of PEG additive on the morphology and performance of polysulfone ultrafiltration membranes.* Desalination, 2011. **272**(1): p. 51-58.
12. Chakrabarty, B., A.K. Ghoshal, and M.K. Purkait, *Preparation, characterization and performance studies of polysulfone membranes using PVP as an additive.* Journal of Membrane Science, 2008. **315**(1): p. 36-47.
13. Matsuyama, H., et al., *Effect of PVP Additive on Porous Polysulfone Membrane Formation by Immersion Precipitation Method.* Separation Science and Technology, 2003. **38**(14): p. 3449-3458.

14. Han, M.-J. and S.-T. Nam, *Thermodynamic and rheological variation in polysulfone solution by PVP and its effect in the preparation of phase inversion membrane*. Vol. 202. 2002. 55-61.
15. Li, Q., et al., *Antimicrobial nanomaterials for water disinfection and microbial control: potential applications and implications.* Water Res, 2008. **42**(18): p. 4591-602.
16. Lemire, J.A., J.J. Harrison, and R.J. Turner, *Antimicrobial activity of metals: mechanisms, molecular targets and applications.* Nat Rev Microbiol, 2013. **11**(6): p. 371-84.
17. Zodrow, K., et al., *Polysulfone ultrafiltration membranes impregnated with silver nanoparticles show improved biofouling resistance and virus removal.* Water Res, 2009. **43**(3): p. 715-23.
18. Dasari, A., et al., *Antifouling membranes prepared by electrospinning polylactic acid containing biocidal nanoparticles.* Journal of Membrane Science, 2012. **405-406**: p. 134-140.
19. Beer, C., et al., *Toxicity of silver nanoparticles - nanoparticle or silver ion?* Toxicol Lett, 2012. **208**(3): p. 286-92.
20. Xiu, Z.M., et al., *Negligible particle-specific antibacterial activity of silver nanoparticles.* Nano Lett, 2012. **12**(8): p. 4271-5.
21. Grieger, K.D., et al., *Environmental risk analysis for nanomaterials: review and evaluation of frameworks.* Nanotoxicology, 2012. **6**(2): p. 196-212.
22. Quirós, J., et al., *Electrospun cellulose acetate composites containing supported metal nanoparticles for antifungal membranes.* Science of The Total Environment, 2016. **563-564**: p. 912-920.
23. Esteban-Cubillo, A., et al., *The role of magnesium on the stability of crystalline sepiolite structure.* Journal of the European Ceramic Society, 2008. **28**(9): p. 1763-1768.
24. Esteban, A., et al., *Antibacterial Activity of Copper Monodispersed Nanoprticles into sepiolite*. Vol. 41. 2006. 5208-5212.
25. Guo, L.a.S., P, *Ultrafiltration and its Applications to Sampling and Characterisation of Aquatic Colloids*, in *Environmental Colloids and Particles*, H.P.v.L. J. Buffle, K. J. Wilkinson and J. R. Lead, Editor. 2007. p. 159–221.
26. Aerts, P., et al., *Polysulfone–aerosil composite membranes: Part 2. The influence of the addition of aerosil on the skin characteristics and membrane properties.* Journal of Membrane Science, 2000. **178**(1): p. 1-11.
27. Moradihamedani, P. and A.H.B. Abdullah, *Phosphate removal from water by polysulfone ultrafiltration membrane using PVP as a hydrophilic modifier.* Desalination and Water Treatment, 2016. **57**(53): p. 25542-25550.

28. Yeo, H.-T., S.-T. Lee, and M.-J. Han, *Role of a Polymer Additive in Casting Solution in Preparation of Phase Inversion Polysulfone Membranes.* JOURNAL OF CHEMICAL ENGINEERING OF JAPAN, 2000. **33**(1): p. 180-184.
29. Nyström, M. and P. Järvinen, *Modification of polysulfone ultrafiltration membranes with UV irradiation and hydrophilicity increasing agents.* Journal of Membrane Science, 1991. **60**(2): p. 275-296.
30. Kim, K.S., et al., *Surface modification of polysulfone ultrafiltration membrane by oxygen plasma treatment.* Journal of Membrane Science, 2002. **199**(1): p. 135-145.
31. Socrates, G., *Infrared and Raman characteristic group frequencies. Tables and charts. Third Edition.* Journal of Raman Spectroscopy, 2004. **35**(10): p. 905-905.
32. Rivaton, A. and J.L. Gardette, *Photodegradation of polyethersulfone and polysulfone.* Polymer Degradation and Stability, 1999. **66**(3): p. 385-403.
33. Zhu, X., et al., *Studies of UV crosslinked poly(N-vinylpyrrolidone) hydrogels by FTIR, Raman and solid-state NMR spectroscopies*. Vol. 51. 2010. 3054-3063.
34. A. S. Sadjadi, M., et al., *Synthesis and characterization of Ag/PVA nanorods by chemical reduction method*. Vol. 40. 2008. 3183-3186.
35. Lyu, L.-M., W.-C. Wang, and M.H. Huang, *Synthesis of Ag2O Nanocrystals with Systematic Shape Evolution from Cubic to Hexapod Structures and Their Surface Properties.* Chemistry – A European Journal, 2010. **16**(47): p. 14167-14174.
36. Downs, R.T. and M. Hall, *The American Mineralogist Crystal Structure Database*. Vol. 88. 2003. 247-250.
37. Festa, R.A. and D.J. Thiele, *Copper: an essential metal in biology.* Curr Biol, 2011. **21**(21): p. R877-83.
38. Quiros, J., et al., *Antimicrobial electrospun silver-, copper- and zinc-doped polyvinylpyrrolidone nanofibers.* J Hazard Mater, 2015. **299**: p. 298-305.
39. Jucker, C. and M.M. Clark, *Adsorption of aquatic humic substances on hydrophobic ultrafiltration membranes.* Journal of Membrane Science, 1994. **97**: p. 37-52.
40. Habimana, O., A.J.C. Semião, and E. Casey, *The role of cell-surface interactions in bacterial initial adhesion and consequent biofilm formation on nanofiltration/reverse osmosis membranes.* Journal of Membrane Science, 2014. **454**: p. 82-96.
41. Carlson, C., et al., *Unique cellular interaction of silver nanoparticles: size-dependent generation of reactive oxygen species.* J Phys Chem B, 2008. **112**(43): p. 13608-19.

42. Choi, O. and Z. Hu, *Size Dependent and Reactive Oxygen Species Related Nanosilver Toxicity to Nitrifying Bacteria.* Environmental Science & Technology, 2008. **42**(12): p. 4583-4588.
43. Ren, G., et al., *Characterisation of copper oxide nanoparticles for antimicrobial applications.* Int J Antimicrob Agents, 2009. **33**(6): p. 587-90.
44. Ramyadevi, J., et al., *Synthesis and antimicrobial activity of copper nanoparticles.* Materials Letters, 2012. **71**: p. 114-116.
45. Yang, X., et al., *Mechanism of silver nanoparticle toxicity is dependent on dissolved silver and surface coating in Caenorhabditis elegans.* Environ Sci Technol, 2012. **46**(2): p. 1119-27.
46. Kochkodan, V. and N. Hilal, *A comprehensive review on surface modified polymer membranes for biofouling mitigation.* Desalination, 2015. **356**: p. 187-207.
47. Fu, P.P., et al., *Mechanisms of nanotoxicity: generation of reactive oxygen species.* J Food Drug Anal, 2014. **22**(1): p. 64-75.
48. Lin, Y.-s.E., et al., *Inactivation of Mycobacterium avium by copper and silver ions.* Water Research, 1998. **32**(7): p. 1997-2000.
49. Kim, J.H., et al., *Effects of metal ions on the activity of protein tyrosine phosphatase VHR: highly potent and reversible oxidative inactivation by Cu2+ ion.* Arch Biochem Biophys, 2000. **382**(1): p. 72-80.
50. Ruparelia, J.P., et al., *Strain specificity in antimicrobial activity of silver and copper nanoparticles.* Acta Biomater, 2008. **4**(3): p. 707-16.
51. Feng, Q.L., et al., *A mechanistic study of the antibacterial effect of silver ions on Escherichia coli and Staphylococcus aureus.* J Biomed Mater Res, 2000. **52**(4): p. 662-8.
52. Otto, C.C. and S.E. Haydel, *Exchangeable ions are responsible for the in vitro antibacterial properties of natural clay mixtures.* PLoS One, 2013. **8**(5): p. e64068.
53. Silhavy, T.J., D. Kahne, and S. Walker, *The bacterial cell envelope.* Cold Spring Harb Perspect Biol, 2010. **2**(5): p. a000414.
54. Yasuyuki, M., et al., *Antibacterial properties of nine pure metals: a laboratory study using Staphylococcus aureus and Escherichia coli.* Biofouling, 2010. **26**(7): p. 851-8.
55. Yamada, H., et al., *Direct observation and analysis of bacterial growth on an antimicrobial surface.* Applied and environmental microbiology, 2010. **76**(16): p. 5409-5414.
56. Heß, S. and C. Gallert, *Growth Behavior of E. coli, Enterococcus and Staphylococcus Species in the Presence and Absence of Sub-inhibitory Antibiotic Concentrations: Consequences for Interpretation of Culture-Based Data.* Microbial Ecology, 2016. **72**(4): p. 898-908.

CHAPTER 3

Fouling and biofouling resistance of metal-doped mesostructured silica / polyethersulfone ultrafiltration membranes

Chapter 3. FOULING AND BIOFOULING RESISTANCE OF METAL-DOPED MESOSTRUCTURED SILICA/POLYETHERSULFONE ULTRAFILTRATION MEMBRANES

3.1 Abstract

Hybrid polyethersulfone-based ultrafiltration membranes were prepared by incorporating metal (Ag and Cu) and/or amine-functionalized mesostructured SBA-15 silica particles. The doping particles were included into the casting solution to obtain a total solids load of 3.6 wt% in the final membranes. The physicochemical characterization of particles and membranes showed a good dispersion of metals inside the mesoporous structure of silica as well as a reduced skin layer, higher pore interconnectivity, and a larger amount of pores in membranes doped with the hydrophilic fillers. Membrane surface was also slightly less hydrophobic in hybrid membranes. Membrane performance was significantly improved as result of considerable increase of water permeation without affect negatively the membrane selectivity. The organic antifouling properties were enhanced with significant permeability improvement without compromising membrane rejection performance. In addition to it, metal-loaded silica allowed preparing membranes with high antibacterial activity. The removal of colonies of *Escherichia coli* and *Staphylococcus aureus* was complete either on membrane surface or in the liquid in contact with membranes when exposed to a 1/500 nutrient broth medium for 20 h at 36°C. The rate of metal release depended on metal speciation and represented a 0.1-0.6% of the total metal content of membranes.

3.2 Introduction

Ultrafiltration (UF) is a pressure-driven membrane process widely used for the removal of colloidal/particulate matter, pathogenic microorganisms, and oil-

water emulsions [1, 2]. Polyethersulfone (PES) is a thermoplastic polymer extensively used for the fabrication of UF membranes due to its high mechanical strength besides chemical and thermal stabilities [3]. It is well dissolvable in many aprotic polar solvents, as N-methyl-2-pyrrolidone, and can properly be processed into a porous membrane through the non-solvent induced phase method. Despite these advantages, PES material is not enough hydrophilic and water permeability of PES membranes can become insufficient. In addition, the adsorption and deposition of hydrophobic nonpolar solutes on neat PES membranes surface and inside membrane pores leads to serious decrease in permeation flux and the change in separation characteristic during filtration operation that limits the practical application of PES UF membranes [4]. The adsorption of unwanted materials onto membrane surface results in a higher energy demand, shorter membrane lifetime and poorer separation performance [5]. Since membrane fouling is a consequence of the interaction between membrane surfaces and solutes by different mechanisms and hydrophobic interaction is usually accepted as predominant for PES membranes, the dispersion component of surface tension could be a good fouling predictor [6, 7]. Many attempts have been performed to improve the fouling resistance of PES membranes by surface modifications, which include grafting, coating or different surface functionalization treatments with the aim of obtaining enhanced hydrophilicity or biocompatibility [8]. The use of blending additives following surface functionalization has also been successfully explored [9]. Biofouling is another major problem for the application of PES UF membranes. The biofouling is due to cells with altered phenotype that attach and grow on membrane surface forming complex biological communities [10]. Biofilms create their own environment and, once formed, are very difficult to remove often causing permanent permeability loss and irreversible membrane damage [11]. The enhancement of surface hydrophilicity has been extensively

explored for preparing low biofouling PES membranes. Blends with hydrophilic polymers and the inclusion of different nanoparticles have been proposed for biofouling prevention [12, 13]. Also, the use of metal nanoparticles has been frequently reported in view of the toxicity of certain metals against a variety of microorganisms including bacteria and fungi. Metals can cause oxidative stress, either directly of by inactivating the cellular mechanisms normally involved in quenching reactive oxygen species [14]. It has been shown that silver, copper and other metals induce oxidative stress followed by membrane disruption, interference in enzymatic functions, among others [15]. Thanks to it, silver and copper as salts or nanoparticles have been proposed for a number of antimicrobial materials [16, 17].

The incorporation of many diverse types of nanomaterials within the polymer matrix have been proposed for preparing hybrid UF membranes, which include silica, free metals and metal oxides, among others [18, 19]. Particularly, mesoporous silica has been investigated for the preparation of mixed matrix ultrafiltration membranes, which benefit from its hydrophilic and porous nature to improve membrane performance. Mesoporous silica has been shown to enlarge pore size, improve pore interconnectivity and increase hydrophilicity and thermal stability with respect to neat PES, thus providing higher flux and better antifouling performance [20]. Mesoporous silica particles functionalized with amino and carboxylic groups have been studied for enhancing antifouling performance with significant improvements in water permeability, surface porosity, hydrophilicity, and stability [21]. Otherwise, nanometals, particularly silver, have been extensively studied for membrane nanocomposites [22]. Apart from production costs, the incorporation of nanoparticles into polymeric membranes has two important drawbacks. One is the difficulty of getting a good dispersion of nanoparticles within the polymeric matrix. The other is the possibility of releasing engineered nanomaterials into the environment. Nanometals supported on silica particles

or silicates have been proposed to overcome these limitations by preparing stable materials that avoid the dispersion of nanoparticles into the environment [23].

In this work, we prepared new composite polymeric PES ultrafiltration membranes with amino and metal-loaded mesoporous silica as modifying additive incorporated at low weight proportion (less than 4%). The purpose was to obtain UF membranes with mechanical properties similar to those of neat PES, but higher flux, lower organic fouling and an improved resistance to microbial growth. To prove the latter, several bioassays have been performed using the bacteria *Escherichia coli* and *Staphylococcus aureus* as model microorganisms. The inclusion of metals in fillers, rather than their direct dispersion into the polymeric solution or their attachment to membrane was intended to avoid the dispersion of nanoforms into the environment. The purpose was to obtain membranes with higher flux and lower fouling, in which metal-loaded mesoporous silica could act as a vehicle for introducing nanometals without the problems derived from particle aggregation, chemical incompatibility with casting solvents and unintended nanoparticle release. The antimicrobial behaviour was tested using the bacteria *Escherichia coli* and *Staphylococcus aureus* as model microorganisms. To the best of our knowledge, this combination of doping mesoporous silica nanoparticles (amino and metal-loaded) planned to enhance water permeability and mitigate both organic fouling and biofouling of PES membranes has not been previously reported.

3.3 Materials and methods

3.3.1 Materials

Polyethersulfone (PES, 58 kDa) was provided by Solvay Chemicals International (Belgium), and N-Methyl-2-pyrrolidone (NMP) was supplied by

Scharlau (Barcelona, Spain). Pluronic P123 (Sigma Aldrich $EO_{20}PO_{70}EO_{20}$, EO ethylene oxide, PO propylene oxide, MW=5800), tetraethylorthosilicate (TEOS 98% Sigma-Aldrich), N-(3-trimethoxysilylpropyl) diethylenetriamine (97% Sigma-Aldrich), cupric nitrate trihydrate (Fluka) and silver nitrate (Sigma-Aldrich) were used as received. Bovine Serum Albumin (BSA) was purchased from Sigma-Aldrich. The components of culture media were biological grade acquired from Conda-Pronadisa (Spain). Ultrapure water was generated from a Direct-Q™ 5 Ultrapure Water Systems from Millipore (Bedford, MA, USA) with a specific resistance of 18.2 MΩ cm.

Pure SBA-15 sample was synthesized according to a procedure based on triblock copolymer. Pluronic P123 as template and TEOS as a source of silica [24]. During a typical synthesis, 4 g of Pluronic were dissolved in 125 mL aqueous HCl 1.9 M at room temperature. After complete dissolution, TEOS was added and the mixture stirred 20 h at 40 °C. The suspension was then transferred to a tightly closed vessel and kept for 24 h at 110 °C without stirring. The obtained white solid was filtered and washed repeatedly with deionized water. The air-dry white powder was next calcined at 550 °C for 5 h (heating rate 1.8 °C min^{-1}). Amine-functionalized SBA-15 was prepared by co-condensation method using the same procedure except for the addition of 1.8 g of N-(3-trimethoxysilylpropyl) diethylenetriamine 1 h after adding the silica source (TEOS). In this case, the surfactant template was removed by refluxing with ethanol (1 g of sample in 100 mL of ethanol) for 24 h. Amine-functionalized SBA-15 material was referred to as Triamine/SBA-15 in what follows. The metallic impregnation of SBA-15 was carried out by the minimum volume method. Copper or silver nitrate were dissolved in 30 mL of water. The solution was slowly poured over calcined SBA-15 while stirring. The solid was dried at 50 °C overnight and calcined under airflow for 8 h at 500 °C with the same heating ramp of 1 °C min^{-1}. Metal-loaded mesoporous materials, CuO/SBA-15 and Ag/SBA-15, had a content of 8.9 wt% copper (11.2 wt% as

CuO) and 3.5 wt% silver (as Ag). The particle size of SBA-15 and metal-loaded SBA-15 was measured by DLS in polymer solvent medium. The results are shown in Table 3.2. Nitrogen adsorption and desorption isotherms at 77 K were measured using a Micromeritics TRISTAR 3000 system. The data were analysed using the BJH and BET models and the pore total volume (Vt) was assigned at P/P_o=0.975 as single point. X-ray powder diffraction (XRD) patterns were acquired on a PHILIPS X'PERT diffractometer using Cu Kα radiation. The data were recorded from 0.5 to 5° (2θ). Transmission electron microscopy (TEM) microphotographs were carried out on a PHILIPS TECNAI-20 electronic microscope operating at 200 kV.

3.3.2 Membrane preparation and characterization

Membranes were prepared using non-solvent induced phase inversion by means of immersion/precipitation with PES cast from a solution containing 16 wt. % of polymer in NMP. Hybrid membranes were prepared by incorporating SBA-15 (pure, amine-functionalized, or metal-loaded) to NMP with the help of ultrasonic dispersion for 45 min at 40 °C. Subsequently, the polymer was added to the suspension and stirred for at least 24 h at room temperature and allowed aging for at least 24 h. The amount of incorporated particles was that required to obtain 0.6 wt % in the polymer synthesis mixture. After forming a homogenous solution, the films were casted with 200 µm thickness using a filmograph on nonwoven polyester as support layer. The prepared films were immersed in a non-solvent bath (distilled water at 25°C) for precipitation. The membranes were then transferred into another container with fresh ultrapure water and soaked for 24 h before testing. For each polymer solution composition, several identical membrane sheets were made in order to repeatedly test the water flux and solute rejection. Table 3.1 summarizes the composition and particle concentration of casting solutions used in this study

along with the nomenclature proposed to differentiate the tested membranes.

Table 3.1. Membranes prepared in this investigation

Membrane	Filler content (wt%)	Nomenclature
PES	-	PES
PES/SBA-15	SBA-15 (0.6)	SBA@PES
PES/(Triamine/SBA-15)	Triamine/SBA-15 (0.6)	TriSBA@PES
PES/(Ag/SBA-15)	Ag/SBA-15 (0.6)	AgSBA@PES
PES/(Cu/SBA-15)	Cu/SBA-15 (0.6)	CuSBA@PES
PES/(Triamine/SBA-15+Ag/ (SBA-15)	Triamine/SBA-15(0.3) + Ag/SBA-15 (0.3)	AgTriSBA@PES
PES/(Triamine/SBA-15+Cu/ (SBA-15)	Triamine/SBA-15(0.3) + Cu/SBA-15 (0.3)	CuTriSBA@PES

The morphology of membrane cross-section was observed under Scanning Electron Microscopy (SEM, XL-30 Philips). Due to the image magnification required to observe the membrane surface porosity, a Field Emission Gun Scanning Electron Microscope (FEG-SEM, FEI Co.) was used.

Surface ζ-potential was measured by electrophoretic light scattering using the Surface Zeta Potential Cell (ZEN 1020) with a Zeta Sizer (DLS, Malvern Zetasizer Nano ZS). A rectangular section of the membranes was inserted in a dispensable plastic cuvette containing 10 mM KCl aqueous solution with 0.5% (w/w) polyacrilic acid (450 kDa) as negative-tracer, pH was adjusted at 7.0. Measurements were conducted at 25 °C at six different displacements from the sample surface in order to calculate the surface ζ-potential. The experimental data are shown in Table 3.3.

The Surface free energy was determined by measuring contact angles (CA) with water (Milli-Q), glycerol, and diiodomethane using an optical contact angle meter (Krüss DSA25 Drop Shape Analysis System) operating at room temperature. The components of the surface tension were estimated according to the procedure described below.

The Lifshitz-van der Waals (LW), electron donor (−) and electron acceptor (+) components of the surface tension were estimated from CA values for water, glycerol and diiodomethane according to the following expression in which ϑ are the pure liquid contact angles [25].

$$\left(1+\cos\theta\right)\gamma_L = 2\left(\sqrt{\gamma_S^{LW}\gamma_L^{LW}} + \sqrt{\gamma_S^{+}\gamma_L^{-}} + \sqrt{\gamma_S^{-}\gamma_L^{+}}\right) \qquad (1)$$

In this approach, the total surface free energy (γ_S) is the sum of the non-polar London-van der Waals component , γ_S^{LW} , and the acid-base component, γ_S^{AB} , which in turn comprises two non-additive parameters: the electron-acceptor, γ_S^{+} , and the electron-donor, γ_S^{-} , surface tension parameters:

$$\gamma_S = \gamma_S^{LW} + \gamma_S^{AB} = \gamma_S^{LW} + 2\sqrt{\gamma_S^{+}\gamma_S^{-}} \qquad (2)$$

The three components of the solid free surface energy, γ_S^{LW} , γ_S^{+} and γ_S^{-} are unknowns that can be solved by measuring the CA with three liquids taking into account that the components of the liquid free surface energy, γ_L^{LW} , γ_L^{+} and γ_L^{-} for the probe liquids are available in the literature for a number of pure substances [26, 27]. According to Van Oss, the total interfacial tension between the solid film and water, γ_{SL}, can be expressed as follows

$$\gamma_{SL} = \left(\sqrt{\gamma_S^{LW}} - \sqrt{\gamma_L^{LW}}\right)^2 + 2\left(\sqrt{\gamma_S^{+}\gamma_S^{-}} + \sqrt{\gamma_L^{+}\gamma_L^{-}} - \sqrt{\gamma_S^{+}\gamma_L^{-}} - \sqrt{\gamma_L^{+}\gamma_S^{-}}\right) \quad (3)$$

The free energy of interaction between two identical condensed phases immersed gives a direct measure of their hydrophobicity and can be derived from γ_{SL}:

$$\Delta G_{SLS} = -2\gamma_{SL} \qquad (4)$$

The procedure allowed obtaining the free energy of interaction between two identical surfaces immersed in a liquid, ΔG_{SLS}, which gives a measure of the hydrophobicity or hydrophilicity of the surface. If $\Delta G_{SLS} > 0$, the surface is hydrophilic, and if $\Delta G_{SLS} < 0$, it is hydrophobic.

Prior to contact angle measurements, membranes specimens were vacuum-dried at 90 °C for 2 h. In the case of bacterial contact angles, measurements were performed on bacterial lawns deposited on cellulose acetate filters an initial concentration of 10^8 cells/ml. Each measurement was performed in triplicate using the sessile drop technique.

ICP-MS analyses of metal released from membranes were performed on an ICP-MS model X Serie 2 system apparatus from Thermo Scientific. Membranes were submerged in 15 mL of ultrapure water in glass bottles for 24 h in static runs performed at 25 °C. In order to assess the unintended release of nanometals, representative samples of the filtrate recovered after prescribed cumulative times (30, 60, 90 and 120 min) were further ultrafiltrated using Vivaspin 20, 5 kDa, PES centrifuge tubes. The samples were analysed for metals using ICP-MS. In case of nanoparticle release, the amount of metals detected by ICP-MS in the 5 kDa ultrafiltrates would be significantly lower than that of membrane permeate as 5 kDa filters retain particles larger than 2 nm. TMP was set at 2 bar and three replicates of all assays were performed.

3.3.3 Filtration studies

Filtration experiments were carried out by using a crossflow cell module with an effective membrane area of 50 cm^2 connected to a 2 L volume tank. The membrane permeation flux for pure water was determined in a filtration recycle mode at 2 bar, and 0.65 m s^{-1} crossflow velocity. Previously, the linear behavior of water flux against transmembrane pressure (TMP) was confirmed in the 1-4 bar range. Fresh prepared membranes were initially compacted for 2 h at 4 bar and 25 °C.

Membrane fouling was studied by using BSA as organic foulant following the protocol reported elsewhere with BSA solution (1 g L^{-1}, pH 7.2) in 0.1 M phosphate-buffered physiological saline (PBS) [28].

To explore the effect of fouling on the membrane permeation performance, pure water and BSA solution filtration experiments were successively performed at 2 bar TMP and fouling was evaluated through pure water flux ratio as expressed by Eq. (1):

$$\text{Flux ratio } (\%) = \left(\frac{J_w^f}{J_w^i}\right) \times 100 \qquad \text{Eq.1}$$

where pure water flux was measured before filtration of the BSA solution (J_w^i) and after stabilization of the BSA solution flow ($J_w{}^f$), being the membrane repeatedly washed with distilled water preceding the pure water flux measurement.

Solute rejection, R (%), was evaluated from aqueous solutions of BSA (1 g L^{-1}). The permeate (Cp) and feed (Cf) concentrations of BSA were measured by using a Cary 5000 UV-Vis-NIR Spectrophotometer and compared to determine rejection as follows:

$$R(\%) = \left(1 - \frac{C_P}{C_f}\right) \times 100 \qquad \text{Eq.2}$$

For each polymer solution composition, not less than five filtration essays with different membrane samples were made until obtaining reproducible values of flux and solute rejection.

3.3.4 Microbiological assays.

The microorganisms used in these studies were *Escherichia coli* (CETC 516) and *Staphylococcus aureus* (CETC 240). *E.coli* and *S.aureus* are gram-negative and gram-positive strains, respectively, recommended as testing microorganism in the ISO 22196 in order to measure the antibacterial activity on plastic surfaces

[29]. The bacteria were maintained at −80 °C in glycerol (20% v/v) until use. Reactivation was performed using NB nutrient broth culture medium (peptone 10 g L^{-1}, sodium chloride 5 g L^{-1}, meat extract 5 g L^{-1} and, in for solid medium, powder agar 15 g L^{-1}) at 36 °C. The pH was adjusted to 7.0 ± 0.1. The stationary phase was reached and the optimal density optical (OD) were measured at 600 nm.

The antimicrobial behavior of membranes was tested by counting the CFU (Colonies Forming Units) of *E.coli* and *S.aureus* under the standardized conditions of the ISO 22196 test, followed with minor modifications. The initial bacterial concentration was set as 10^6 cells/mL inoculated into sterile 24-well microplates. The volume of inoculum was established at 0.15 mL/mg of membrane. Culture time was 20 h ± 1 h at 36 °C, which was enough to form biofilms on non-modified membranes. The culture conditions ensured that bacteria were cultured in their exponential growth phase without nutrient limitation. After incubation, bacterial suspensions and cells detached from membranes were serially diluted to perform CFU counting. For liquid cultures, 10-fold serial dilutions were performed in PBS following which 10 µL were spot-plated on solid agar. In accordance to the ISO 22196 protocol bacteria were recovered from membrane surface by using 2 mL soybean casein digest lecithin polyoxyethylene sorbitan monooleate (SCDLP broth). Previously membranes were rinsed with PBS for 30 min in an orbital shaker. SCDLP liquid was serially diluted in PBS and spot plated. The counting was performed in triplicate in three independent runs. Routine analyses were performed to ensure all microbial load was recovered from exposed membranes.

SEM and confocal micrographs of membranes colonized by *E.coli* and *S.aureus* were taken after inoculation with 10^6 cells/mL, 0.15 mL/mg membrane, and incubation in NB medium at 36 °C for 20 ± 1 h. For SEM images, membranes were cleaned with distilled water, fixed and dehydrated with ethanol and

acetone. SEM micrographs were obtained in a ZEISS DSM-950 instrument operating at 25 kV.

Live/Dead BacLight Bacterial Viability kit (Molecular Probes, Invitrogen Detection Technologies, Carlsbad, CA, USA) was used to evaluate bacterial viability. This method differentiates viable and no-viability cells using Syto9, a fluorescent nucleic acid stain capable to penetrate cell membrane and bind DNA, and propidium iodide (PI), which is a fluorescent stain marking only membrane-damaged non-viable cells. The excitation/emission maxima were 480/500 nm for Syto9 and 490/635 nm for PI. The micrographs were obtained in a Leica Microsystems Confocal SP5 fluorescence microscope.

3.4 Results and discussion

3.4.1 Particle characterization

Small angle X-ray diffraction patterns of pure, metal-loaded, and amine-functionalized SBA-15 samples are shown in Fig.3.1. All diffractograms evidence the presence of mesophases with hexagonal p6mm symmetry, since the characteristic (1 0 0) diffraction peak is clearly distinguished in all the materials [24]. The diffractograms corresponding to pure SBA-15 and the samples in which the functionality was incorporated by post-synthetic procedure (Ag/SBA-15 and Cu/SBA-15) clearly present two additional peaks of plane families (1 1 0) and (2 0 0). The sample synthesized by co-condensation method, Triamine/SBA-15, also exhibits the same secondary peaks, but very weakly. This fact reflects a reduction of the mesoscopic order due to the structural-distorting phenomena typically observed when the precursors of both mesostructured silica and functionalities are incorporated simultaneously [30].

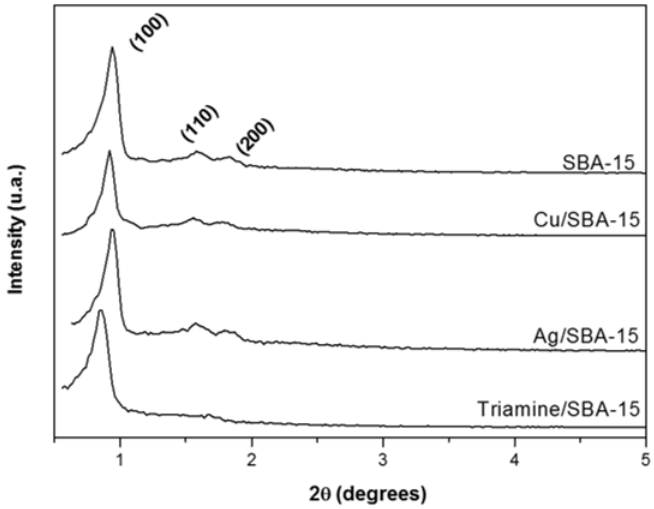

Figure. 3.1. Low angle XRD patterns of pure SBA-15 and functionalized materials.

Nitrogen adsorption-desorption isotherms of the same materials are shown in Fig. 3.2. All the samples displayed type IV isotherms according to the IUPAC classification, with H1 hysteresis loops characteristic of SBA-15-type mesoporous materials [31]. The sharp change in the adsorbed volume around P/P_o=0.6-0.8 in the H1-type hysteresis loop is characteristic of uniform mesopores with open cylindrical geometry [32]. The narrow H1-type hysteresis loop is maintained after the metal incorporation. Consequently, CuO and Ag could penetrate into the porous framework being homogeneously deposited along the cylindrical mesoporous channels. If loaded metal had been placed within the mesoporous structure forming aggregates, it would have provided different wall thicknesses with broader hysteresis loop in the N_2 isotherm [33]. In the case of Triamine/SBA-15 sample, a significant deformation of the hysteresis loop can be appreciated, which could be attributed to the perturbation promoted by amine-organosilane molecules during the silicate condensation process [30].

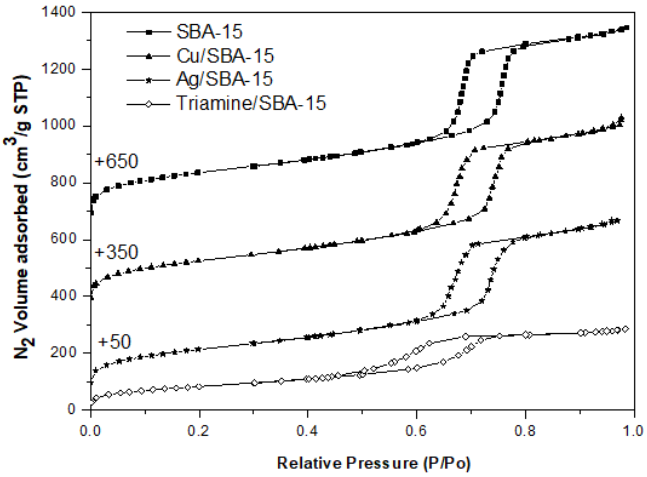

Figure. 3.2. Nitrogen adsorption-desorption isotherms of SBA-15 and functionalized materials.

Table 3.2 summarizes the textural properties of the synthesized materials. A decrease in BET surface area, S_{BET}, and total pore volume, $V_{t,}$ is observed for the functionalized samples in comparison with pure SBA-15. The highest reduction was observed for Triamine/SBA-15 where the total pore volume decreases around 35%. This is a common fact when large functionality amount is incorporated by co-condensation route [34]. It should be noted that Cu/SBA-15 and Ag/SBA-15 exhibit pore size values similar to pure SBA-15 corroborating homogeneous metal deposition into the Mesoporous SBA-15 channels.

Table 3.2. Textural properties of particles.

Sample	S_{BET} (m^2/g)	V_t[a] (cm^3/g)	D_p[a] (nm)	*Particle size*[b] *(μm)*
SBA-15	675	1.06	8.0	1.4 ± 0.2
Cu/SBA-15	589	1.00	8.0	1.5 ± 0.4
Ag/SBA-15	549	0.95	7.9	1.5 ± 0.2
Triamine/SBA-15	481	0.68	7.0	2.2 ± 1.0

[a] Total pore volume and pore size calculated by BJH method from the adsorption branch of the N_2 isotherm. [b] Measured in NMP (polymer solvent).

Fig. 3.3 shows TEM images of synthesized samples. SBA-15 internal structure was not modified by the incorporation of functionalities and all the synthesized materials exhibited similar mesoporous ordered patterns in accordance with the XRD results (Fig.3.1). The pore diameter was graphically estimated around 8 nm for SBA-15, Cu/SBA-15, and Ag/SBA-15 and around 7 nm for Triamine/SBA-15 in fair agreement with values calculated from nitrogen isotherms (Fig. 3.2). Since silver density is much higher than that of SiO_2, Ag was visible in TEM micrographs as black dots embedded inside the mesoporous channels (Fig. 3.3-C).

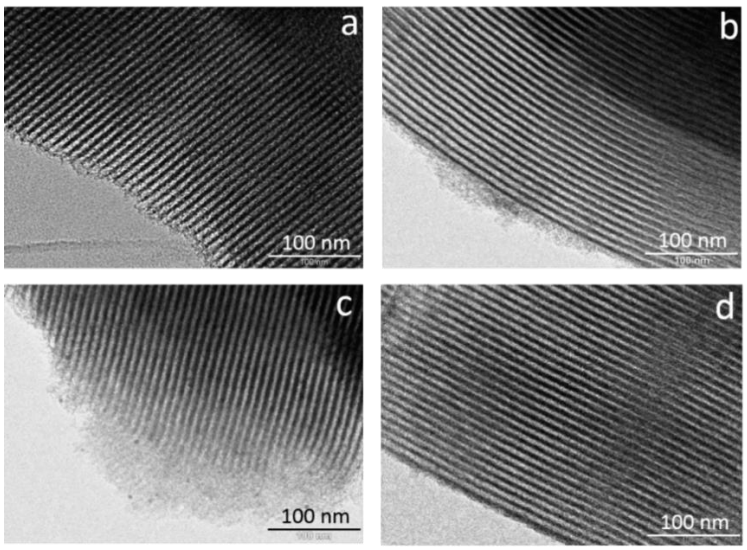

Figure. 3.3. TEM micrographs of (a) SBA-15, (b) Cu/SBA-15, (c) Ag/SBA-15 and (d) Triamine/SBA-15.

3.4.2 Membrane characterization

Cross-sectional images of membranes structure are shown in Fig. 3.4. PES and modified membranes displayed asymmetric structure with relatively dense skin layer below which finger-like sublayer and porous substrate were fully developed. However, SBA-15 loaded specimens exhibited morphological changes in both skin layer and finger-like structure sublayer.

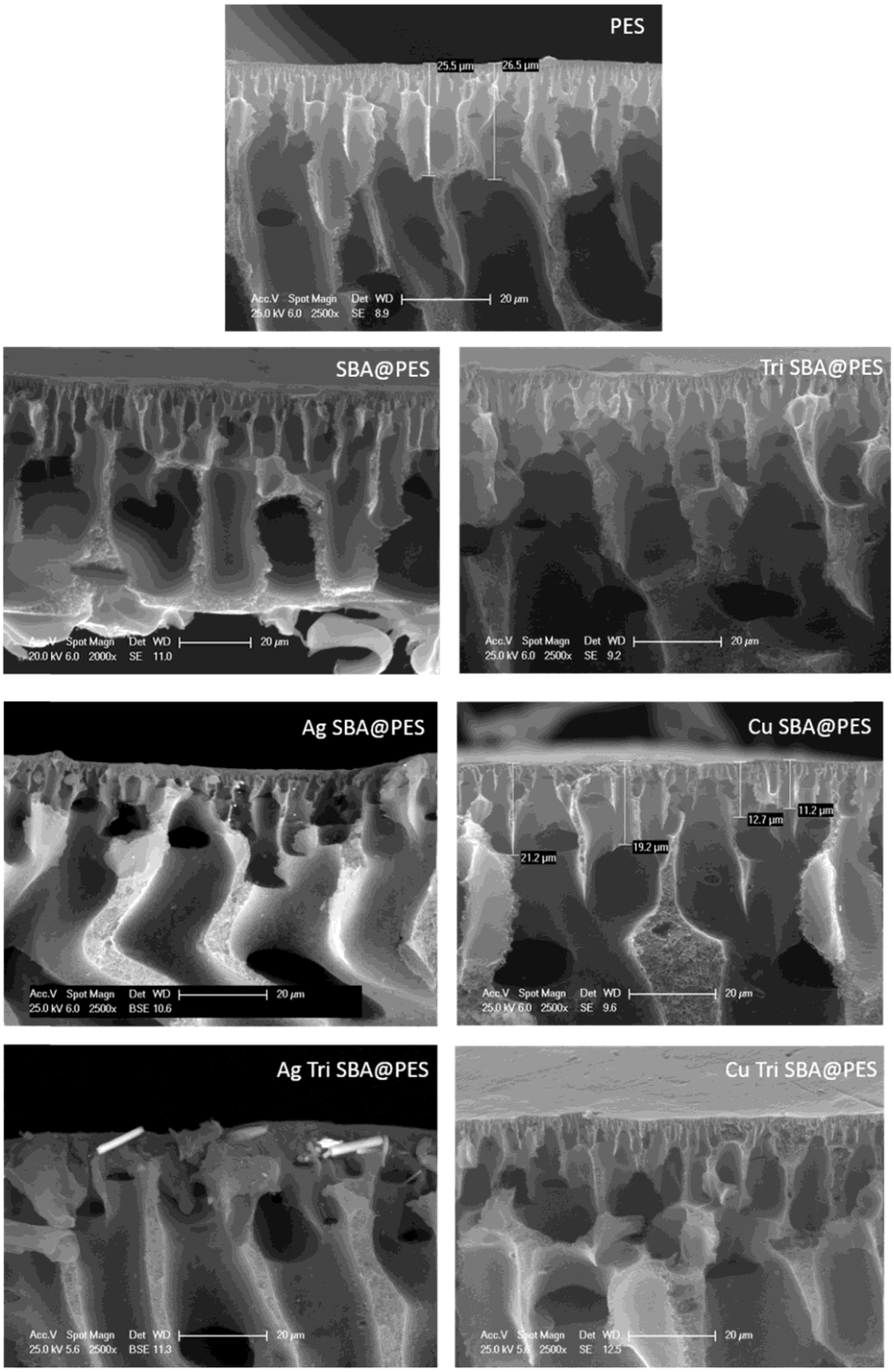

Figure.3.4. Cross-sectional SEM micrographs of membranes manufactured in this investigation

Comparing images of neat PES with modified membranes, the presence of enlarged macrovoids is apparent in hybrid membranes. In addition, the skin layer thickness decreased with the presence of particles. Both effects could be explained in terms of faster interdiffusion process (exchange between solvent and non-solvent) during membrane formation as a result of the addition of hydrophilic particles to the ternary thermodynamic system [35]. These morphological changes promote a better pore connectivity throughout the membrane cross-section, which is crucial to the membrane permeation performance. In addition, metal-loaded particles were visible on membrane surface, as shown in AgTriSBA@PES membrane image, which could be act as biofouling inhibitors. The effect of fillers addition on the membrane morphology was also investigated in terms of surface porosity (Fig. 3.5). The number of pores formed and their spatial distribution onto membrane surface significantly changed as a result of membrane doping. First, it is apparent that the presence of proposed fillers into the polymeric solution promoted an abrupt formation of new pores: it has been stated that hydrophilic fillers can act as pore formation agents during the inversion-precipitation process [18]. Second, the pore spatial distribution for neat PES membrane appeared more uniform than that of the doped membrane. Before membrane formation, the dispersion power of solvent determined the spatial configuration of polymer chains inside the polymeric solution. Filler addition reduced the number of polymer chain configurations, promoting the formation of more polymer-lean zones that resulted in nucleation points for pore formation. Besides, the distribution of polymer chains was also affected by the hindrance effect of particles leading to a non-uniform distribution of new pores, because polymer chains can become disrupted in different ways depending on the physicochemical properties of polymer-particle interface [36]. In order to visualize the enhanced pore formation for modified membranes in comparison with neat PES specimen, yellow circles have been drawn around

pores in Fig. 3.5 for PES and TriSBA@PES samples so remarking the number of formed pores and its spreading on the membrane surface.

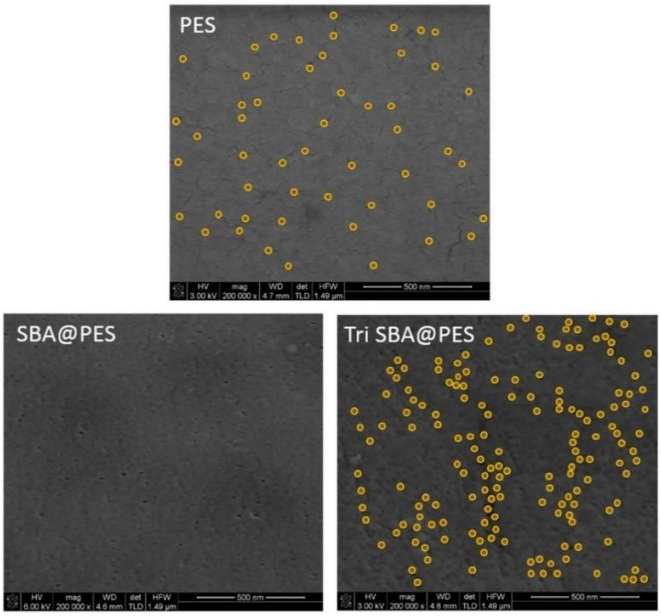

Figure.3.5. FE-SEM images of manufactured membranes surfaces. Yellow circles have drawn around pores to facilitate visual interpretation.

The values of the CA for water, glycerol and diiodomethane are shown in Table 3.3 together with the surface free energy components and the values of ΔG_{SLS}. Neat PES membrane was hydrophobic with ΔG_{SLS} ~ -40 mJ/m^2, which slightly decreased with the introduction of metal-loaded SBA-15 and, to a higher extent, with amine-functionalized SBA-15. For lawns of *E. coli* and *S. aureus* cells, the surface appeared clearly hydrophilic. Surface charge measured as surface zeta potential is also shown in Table 3.3. All membrane surfaces were negatively charged with a zeta potential near -40 mV, except for specimens containing triamine moieties, for which the charge was less negative as a consequence of the positive charge imparted by amine moieties at pH 7. The surface ζ-potential of prepared membranes was in the -28.3 to -47.6 mV range (in water at pH 7.0), the lowest values corresponding to triamine functionalized membranes.

Table 3.3. Membrane surface ζ -potential, contact angle measurements and surface free energy components.

Material	ζ -potential (mV)	Contact angle (°)			Surface free energy components (mJ/m²)					
		Water	Glycerol	Diiodo-methane	γ_S^{LW}	γ_S^+	γ_S^-	γ_S^{AB}	γ_S	ΔG_{SLS}
PES	-42.6 ± 4.0	65.2 ± 0.4	58.5 ± 2.2	20.8 ± 0.5	47.5	0.04	12.3	1.5	49.0	-39.8
SBA@PES	-36.6 ± 6.1	64.8 ± 0.6	61.8 ± 3.2	36.4 ± 2.8	41.4	0.06	15.6	1.9	43.2	-27.3
TriSBA@PES	-31.9 ± 1.2	64.1 ± 1.8	62.7 ± 1.5	42.8 ± 0.4	38.2	0.10	17.6	2.6	40.8	-20.8
AgSBA@PES	-47.6 ± 5.7	64.2 ± 0.7	61.9 ± 1.2	31.0 ± 0.8	43.8	0.05	16.1	0.6	44.3	-28.2
CuSBA@PES	-43.7 ± 0.1	65.1 ± 1.7	62.2 ± 0.3	38.6 ± 2.7	40.3	0.07	15.7	2.1	42.5	-26.5
AgTriSBA@PES	-32.5 ± 4.8	64.3 ± 1.0	62.3 ± 0.7	36.2 ± 2.3	41.5	0.03	16.6	1.4	42.8	-25.4
CuTriSBA@PES	-28.3 ± 2.7	66.3 ± 1.6	62.5 ± 1.8	33.7 ± 0.3	42.6	0.03	14.2	1.2	43.9	-32.0
E.coli	-	16.7 ± 1.3	44.0 ± 3.5	58.7 ± 0.5	29.3	1.1	62.0	16.3	45.6	+44.2
S.aureus	-	25.8 ± 3.1	38.3 ± 2.8	56.7 ± 2.6	40.4	0.8	45.6	11.9	52.3	+22.6

3.4.3 Filtration performance

The water permeability of neat and modified PES membranes was determined within 1-4 bar TMP range, where flux and pressure displayed a linear relationship demonstrated by exploring the pure water flux over the mentioned range. Permeability was calculated from the slope of the linear correlation between pure water flow and TMP.

The results are shown in Fig. 3.6 from which the enhancement of water permeability against neat PES membrane is apparent for all hybrid membranes.

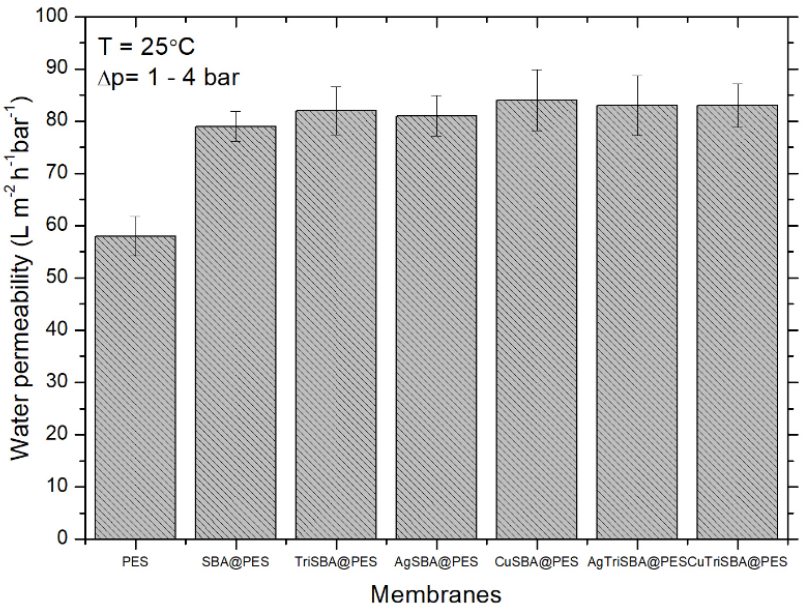

Figure.3.6. Pure water permeability for neat PES and hybrid membranes.

The addition of 0.6 wt% doping particles resulted in over 30% permeability increase in all cases, which should be explained by the three morphological changes observed in membrane structure as a consequence of particle incorporation: enhanced porosity, thinner skin layer, and better pore interconnectivity (Fig.3.4). No significant differences between the diverse hybrid membranes were found, although permeability of SBA@PES sample

was systematically lower than membranes containing functionalized SBA-15 nanoparticles. In comparison with previously reported hybrid PES membranes exclusively prepared with amine-functionalized SBA-15 nanoparticles, these new membranes also containing metal-doped mesoporous silica exhibited rather similar permeability values that largely improved the corresponding to neat PES sample. Thus, the expected antimicrobial ability due to silver and copper content was not threatened by water permeability reduction [21].

Since fouling properties of UF membranes were studied by filtering 1 g L^{-1} BSA aqueous solutions, rejection experiments were also conducted at 2 bar TMP. Fig. 3.7 shows the rejection performance found for all the PES prepared membranes, neat and hybrid, calculated from Eq. (2). As observed, the rejection was thoroughly high, above 94%. The incorporation of SBA-15 based materials to polymer matrix barely affected protein retention that even slightly improved for four of the new hybrid membranes.

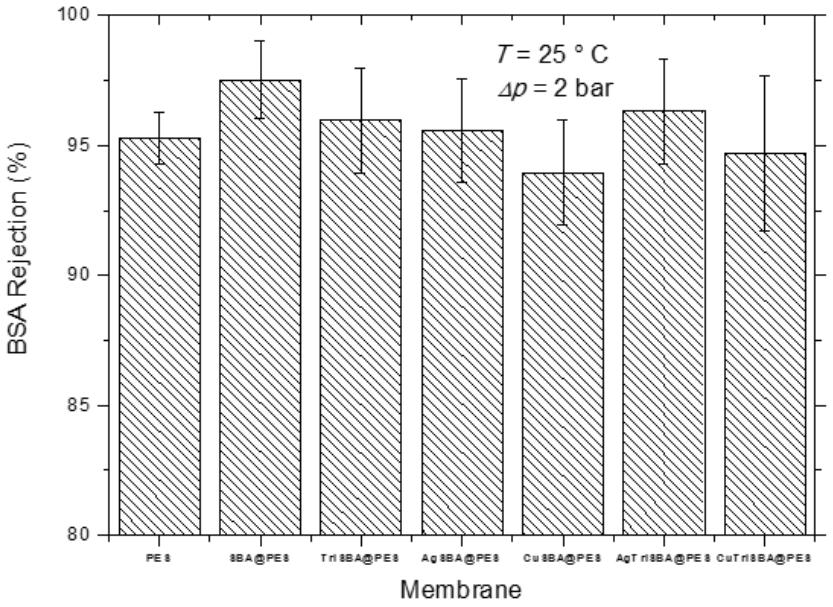

Figure.3.7. BSA rejection of manufactured membranes for 1 g/L BSA aqueous solutions at 2 bar TMP.

3.4.4 Organic antifouling

The antifouling capacity of membranes was evaluated through pure water flux decline determined before and after filtration of BSA solution. Experiments were initially carried out with perfectly clean specimens; then, the permeate flux of 1 g L^{-1} BSA solution at 2 bars was monitored until stabilization; after washing, pure water flux was subsequently obtained. Flux ratios calculated with Eq. (1) are displayed in Fig. 3.8 that shows how the addition of a small amount (0.6 wt%) of SBA-15 particles to PES membrane reduced fouling between 14% and 29%. Taking into account that the polymer type and concentration were the same for all membranes, the flux ratio improvement observed for all doped membranes should be exclusively associated to the incorporation of fillers.

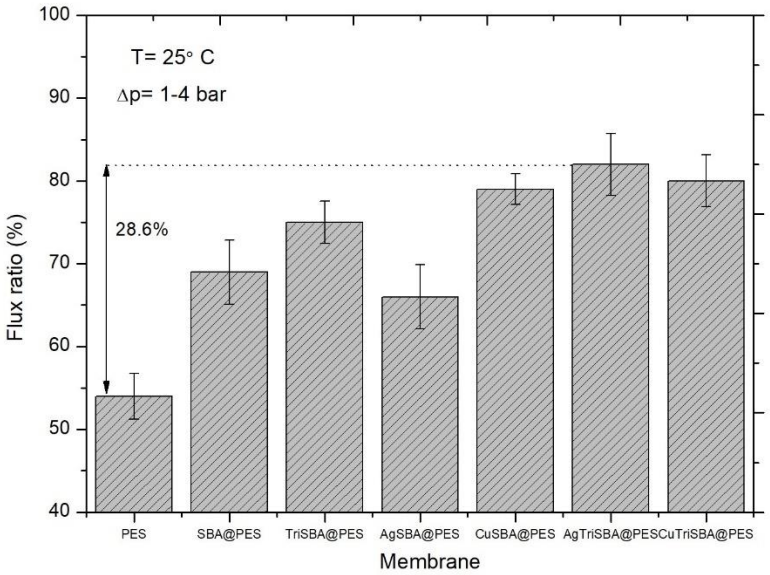

Figure.3.8. Evaluation of irreversible fouling of membranes in terms of pure water flux decline after filtration of 1 g L^{-1} BSA solution.

It is expected that protein adsorption on the skin membrane layer and pore plugging could be prevent by increasing surface hydrophilicity due to a high affinity for water as compared to BSA [37]. The addition of hydrophilic fillers

should fulfil this goal besides the above mentioned enhancing of macrovoids and pore interconnectivity, which would result in a superior permeability for similar retention properties [22, 38]. Nevertheless, no strict correlation was found between flux ratio decline and the hydrophilicity evidences summarized in Table 3.3. Water contact angles exhibited no significant differences between the prepared membranes, as expected due to the low nanoparticles content; however, the hydrophilicity estimation from surface free energy (less negative value of ΔG_{SLS} refers to more hydrophilic character) revealed an acceptable correspondence to specimens displaying higher flux ratio (e.g.,TriSBA@PES and AgTriSBA@PES in Fig. 3.8).

In order to quantitatively describe the fouling resistance for neat and hybrid membranes, the intrinsic, reversible, and irreversible resistances were considered [28]. As observed in Fig. 3.9, all the calculated resistances for doped membranes were lower than the value corresponding to the neat PES sample. The intrinsic membrane resistance exhibited the dominant contribution to the total membrane resistance in all of tested specimens, suggesting that the membrane permeation is mainly limited by the inherent morphological characteristics of membranes and less influenced by fouling-induced flux restrictions. Reversible resistances were low in all cases and no important difference between neat PES and doped membranes was found. Conversely, the contribution of irreversible fouling of PES membrane was significantly higher than for hybrid ones. The irreversible adhesion of foulants on membrane surface is recognized as the cause for permanent permeation loss due to the forming of patches around the pores that eventually expand to form a continuous gel layer [39, 40].

The modification of membranes by embedding metal-doped SBA-15 nanoparticles mitigated the severity of organic fouling over 60% in all tested specimens, as previously found for PES UF hybrid membranes exclusively charged with amine-functionalized mesoporous silica [21]

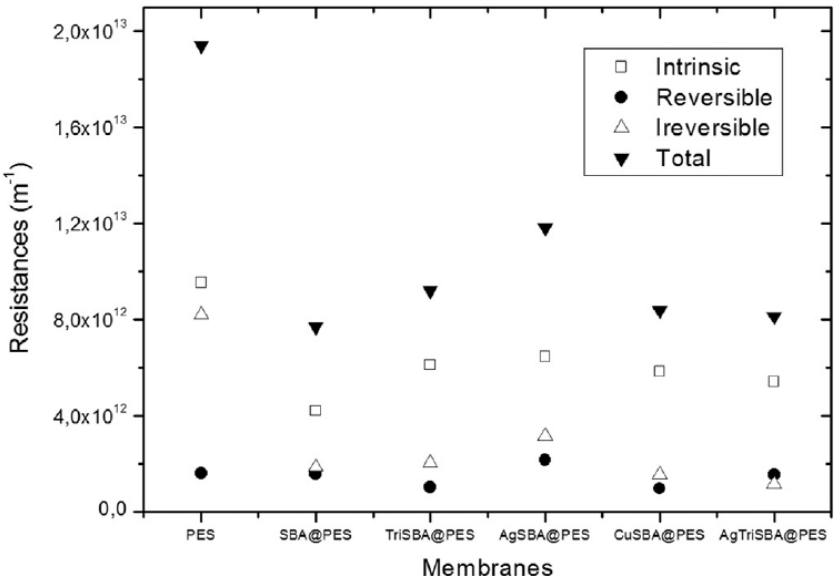

Figure.3.9. Membrane fouling resistances determined from filtration experiments.

3.4.5 Antimicrobial behavior

Fig. 3.10 shows the results of microbial growth tests performed on different membrane specimens exposed to *E. coli* or *S. aureus*. Fig. 3.10-A refers to colony counting of microorganisms in the 1/500 NB liquid culture in contact with membranes after 20 h of incubation at 36 °C. The growth of *E. coli* and *S.aureus* was not significantly different on SBA@PES, TriSBA@PES and the copper-containing materials CuSBA@PES and CuTriSBA@PES from the control PES membranes. The introduction of silver, either in AgSBA@PES (0.3 wt% Ag/SBA-15) or in AgTriSBA@PES (0.6 wt% Ag/SBA-15) resulted in a decrease in the number of viable colonies below the quantification limit of 10 CFU/mL.

The results for microorganisms detached from membrane surface using PBS-SCDLP after removing the culture liquid in contact with them are shown in Fig. 3.10-B expressed as CFU/cm^2. There is a higher tendency of *E. coli* to colonize PES membranes with respect to *S.aureus*. *E. coli* and *S. aureus*, being gram-negative and gram-positive bacteria respectively, have quite different bacterial envelopes. Gram negative bacteria possess an outer membrane and a thin layer of peptidoglycan between this and the cytoplasmic membrane, whereas gram-positive species have a much thicker layer of peptidoglycan [41]. The thick peptidoglycan layer protects bacteria against external stresses including the exposure to toxic metal ions while the outer membrane of gram-negative bacteria possesses porins, which allow the internalization of ions and low molecular weight substances [42]. The data obtained in this work can be rationalized taking into account the higher growth rate of *E. coli* respect to *S.aureus* [43]. The number of viable cells recovered from surface decreased for SBA@PES and for TriSBA. In close contact with surface, the copper loaded membranes, CuSBA@PES and CuTriSBA@PES displayed a statistically significant antibacterial action for both bacterial strains with > 50% reduction for TriSBA@PES materials and over 1-log reduction for CuSBA@PES (with double amount of copper). AgSBA@PES and AgTriSBA@PES membrane surfaces were essentially free of bacteria capable of forming new colonies microorganisms, with colony counting below the quantification limit of 1 CFU/cm^2.

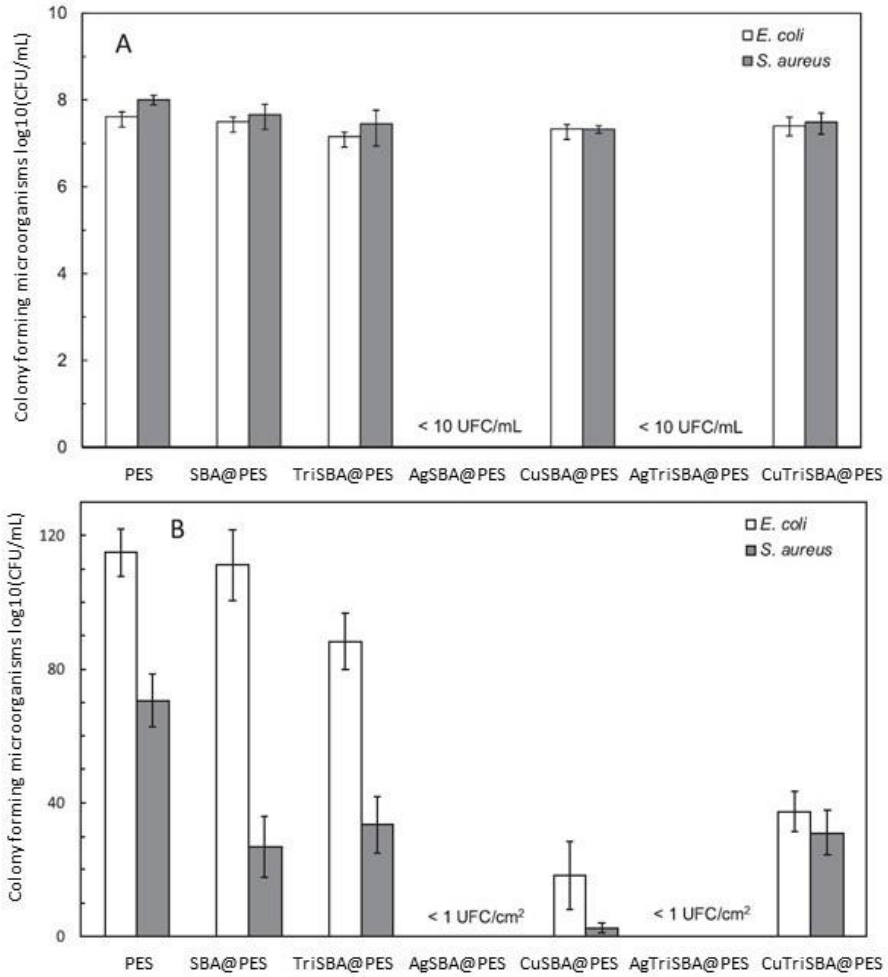

Figure.3.10. Microbial growth for bacterial cultures exposed to membranes (A) and culturable bacteria detached from membranes after incubation (B) at 36ºC, 20 h.

Fig. 3.11 - 3.12 and 3.13 show SEM micrographs of the surface of membranes kept in contact with *E. coli* (Fig. 3.11) or *S. aureus* (Fig. 3.12) for 20 h at 36 °C following an inoculation of 10^6 cells/mL in NB and the corresponding washing, fixing and drying procedures before imaging. The surface of AgSBA@PES and AgTriSBA@PES membranes appeared almost free of bacteria, only displaying a few cells and scattered objects, probably cell debris.

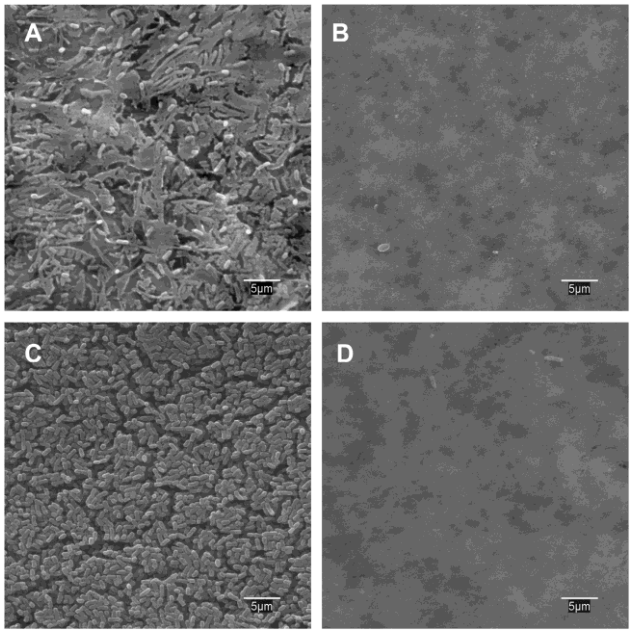

Figure. 3.11. Microbial colonization of membranes exposed to *E.coli* cultures (20h, 36ºC). PES(A), AgSBA@PES (B), TriSBA@PES (C) and AgTriSBA@PES (D)

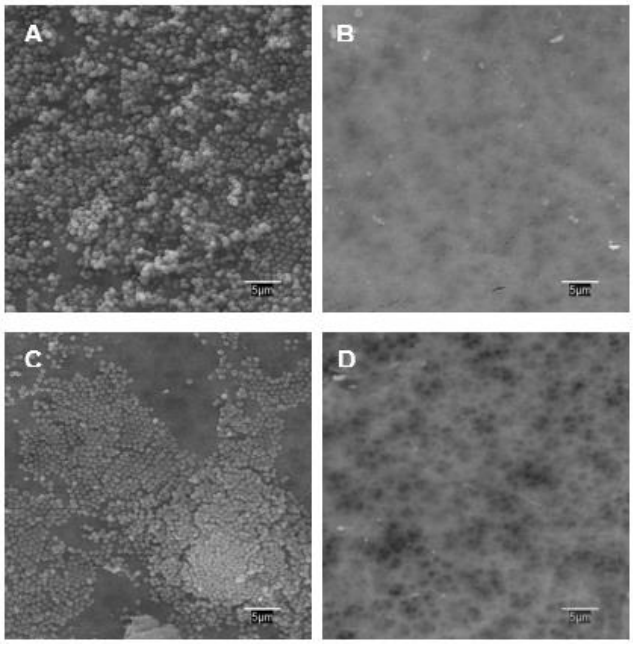

Figure. 3.12. Microbial colonization of membranes exposed to *S. aureus* cultures (20h, 36 °C). PES (A), AgSBA@PES (B), TriSBA@PES (C) and AgTriSBA@PES (D).

However, PES membranes (Fig. 3.11 and 3.12) appeared almost entirely covered by bacteria with already formed biofilm matrix clearly observed. The other non-silver loaded membranes (from which TriSBA@PES is shown in Fig. 3.11 and 3.12-3.13) displayed certain parts of their surface relatively clean, while others exhibit a bacterial lawns and evidences of biofilm formation. It has to be pointed out that the cultures for Fig. 3.11 and 3.12-3.13 were obtained after incubation in full NB medium, which is much more favorable for bacterial attachment and colonization than the ISO 22196 1/500 NB used in colony counting experiments.

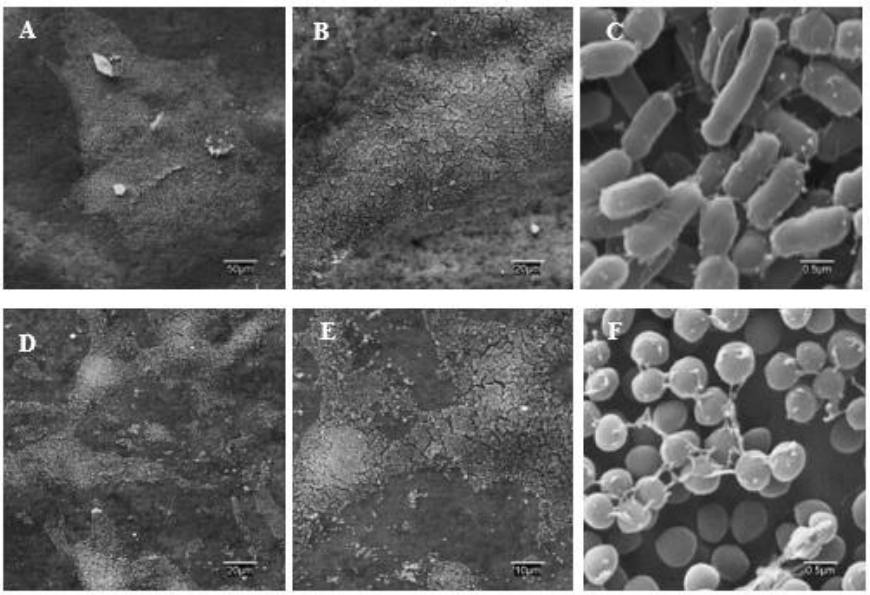

Figure. 3.13. Microbial colonization of TriSBA@PES membranes exposed to *E. coli* (A-B-C) and *S. aureus* (D-E-F) for 20 h at 36 °C. The different magnifications show irregular colonization patterns and biofilm formation.

Figs. 3.14 and 3.15 show the results of live/dead bacterial viability staining. The images correspond to representative confocal micrographs of membrane surfaces exposed to *E. coli* (Fig. 3.14) or *S. aureus* (Fig. 3.15) cultures for 20 h at 36 °C in contact with complete NB medium for all membranes but

SBA@PES, excluded for simplicity because the micrographs were not significantly different from those of TriSBA@PES.

The presence of membrane-damaged bacteria is apparent in all metal loaded specimens (Figs. 3.14 B-C-E-F for *E. coli* and the corresponding images in Fig. 3.15 for *S. aureus*), but also in TriSBA@PES (Figs. 3.14/3.15-D) in a slightly higher proportion with respect to control. Figs. 3.14 and 3.15 show silver-loaded membranes essentially free of viable bacteria, a result in agreement with colony counted performed for membranes in contact with 1/500 NB medium. The presence of red marked damaged cells was also apparent for CuSBA@PES and CuTriSBA@PES specimens in agreement with the SEM results shown before. Hydrophilic bacteria tend to adhere on hydrophilic surfaces, but this simple thermodynamic approach assumes direct contact between bacteria and surface and ignores the presence of cell appendages, such as pili and flagella, which makes direct contact a quite unrealistic scenario [44].

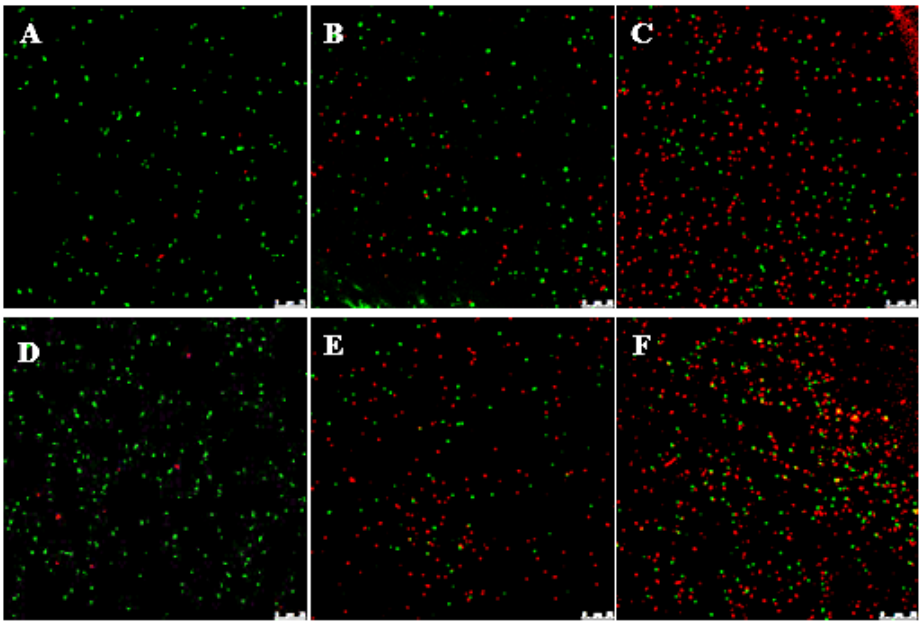

Figure. 3.14. Live/dead confocal micrographs of *E. coli* cultured on (A) PES, (B) CuSBA@PES, (C) AgSBA@PES, (D) TriSBA@PES, (E) CuTriSBA@PES and (F) AgTriSBA@PES.

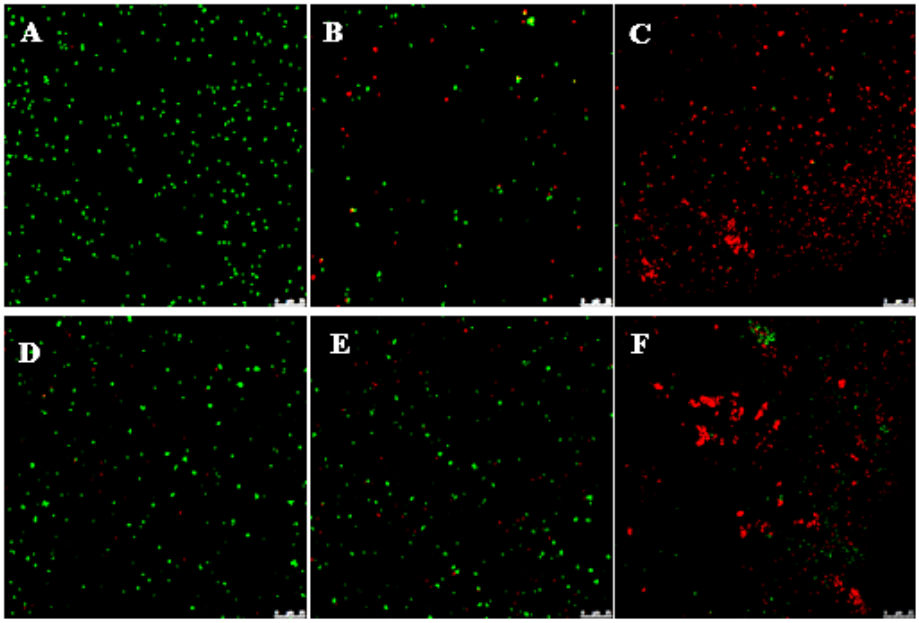

Figure. 3.15. Live/dead confocal micrographs of *S. aureus* cultured on (A) PES, (B) CuSBA@PES, (C) AgSBA@PES, (D) TriSBA@PES, (E) CuTriSBA@PES and (F) AgTriSBA@PES.

The other physicochemical factor affecting bacterial adhesion is surface charge, which we measured as surface zeta potential (Table 3.3). All the surfaces of tested membranes were negatively charged and, therefore, electrostatic repulsion is expected to limit bacterial adhesion as a consequence of the negative surface charge of bacterial outer membranes. The ζ-potential of *E. coli* and *S. aureus* is approximately −40 mV at pH 7 [45]. All the membranes tested in this work displayed similar surface charge, with ζ-potential mostly in the −30 to −40 mV range. Consequently, surface charge is not expected to play any significant role in explaining the differential effect observed in this work with the possible exception of membranes containing triamine-functionalized SBA-15. The data showed a slightly lower tendency to favor the microbial attachment of *E. coli* on membranes containing triamine/SBA-15 in comparison with other metal-free specimens even

considering they are more hydrophilic than PES of SBA@PES materials. The reason could be the presence of positively charged domains associated to protonated amines, but the effect is weak. It has been shown that hydrophobicity and charge, while theoretically related to the attachment of different strains, are not good biofouling predictors for most practical situations [46].

Moreover, the surfaces exposed to microbial culture media exhibit complex interfaces with organic and inorganic compounds adsorbed, which modify the way in which microorganisms adhere. More specifically, the free energy of adhesion calculated from surface energy components is strongly affected by the growth medium used for culturing microorganisms, which has a significant impact on bacterial adhesion [47].

3.4.6 Metal realized analyses

Fig.3.16 shows the amount of copper and silver released by metal containing membranes (Cu/AgSBA@PES and Cu/AgTriSBA@PES) after 24 h in water at pH.7 and 20 °C and in 1/500 NB medium. The total amount of silver was 1.26 mg/g of AgSBA@PES membranes (0.63 for AgTriSBA@PES) and that of copper 3.2 mg/g of CuSBA@PES membranes (1.6 for CuTriSBA@PES). This represented 0.1% in water and 0.2% in 1/500 NB medium of the total amount of silver loaded in AgSBA@PES membranes. For copper materials the figures were 0.6% and 0.3% respectively. The amount of silver released was substantially lower in 1/500 NB medium with respect to pure water, with the opposite behavior found for copper materials.

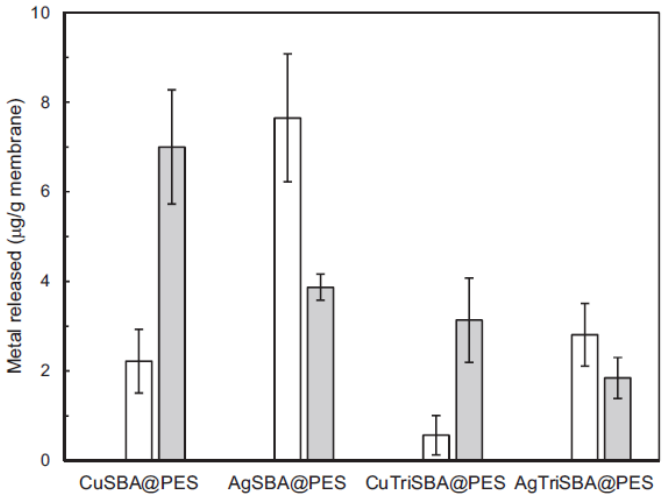

Figure. 3.16. Metal released per unit mass of membrane after 20 h in contact with water (empty bar) or NB 1/500 culture medium (grey bar)

The reason for the difference was, most probably, the different speciation of metals, which migrate to the bulk in the form of solvated cations (Ag^{+}, Cu^{2+}) or as hydroxylated species. Visual MINTEQ (version 3.1, KTH, Stockholm, Sweden) allowed determining that the dominating speciation of copper were $CuOH^{+}$, $Cu_2(OH)_2^{2+}$ and $Cu_3(OH)_4^{2+}$. In the presence of chloride, the amount of silver released was considerably lower due to the formation of insoluble AgCl. The higher amount of copper detected in solution could be attributed to the interaction with the organic constituents of the culture medium.

The absence of nanoparticle release with membrane filtrate is shown in the results represented in Fig. 3.17. The amount of metals in membrane filtrate and 5 kDa subsequent ultrafiltrate were quantified using the same membranes by ICP-MS. The samples correspond to filtrates recovered during four periods of 30 min following each other. The results show no significant differences between silver and copper concentration before and after 5 kDa filtration, meaning that no nanoparticles higher than 5 kDa membrane pore size (about 2 nm) were present in the filtrate of AgSBA@PES and CuSBA@PES membranes.

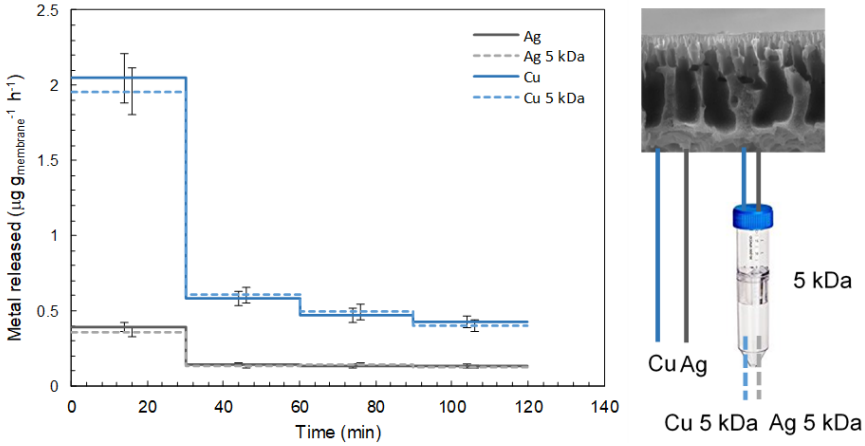

Figure 3.17. ICP-MS analyses of permeate from AgSBA@PES and CuSBA@PES before (solid lines) and after (dashed lines) 5 kDa ultrafiltration of membrane permeate. Error bars show no significant differences for silver (in grey) and copper (in blue).

The antibacterial effect of silver materials in cases in which silver nanoparticles are not released to the medium in contact with microorganisms is the release of silver ions [48, 49]. Moreover, it has been proposed that silver release due to the reaction with dissolved oxygen is the only mechanism explaining the antimicrobial activity of silver materials, either or not in nanoforms [50]. Copper and copper oxide materials also display considerable antimicrobial activity [51]. In the metal-containing particles used in this work, silver (Ag°) and copper (CuO) were essentially included inside the mesoporous structure of SBA-15, which is in turn embedded in the polymer structure of the hybrid membranes. Therefore, the possibility of particle detaching and migration to the membrane surface was not realistic. Moreover, no silicon was found in ICP analyses of water and culture medium in contact with membranes. The damage produced by silver and copper ions to living cells has been shown to be primarily due oxidative stress followed by several associated impairments such as membrane damage or enzymatic dysfunction [15].

Many membrane modifications pursuing antibiofouling behavior have been proposed up to date. Most deal with surface modification with antimicrobials, mostly silver compounds or nanoparticles [52]. Park et al. covalently immobilized silver nanoparticles after surface functionalization and found reduced irreversible biofouling and significant inhibition of bacterial growth [53]. However, and even if nanoparticles were not released from membrane surface due to their covalent attachment the loss of active metal was intense and almost 50% was loss during the initial filtration stages. Kim et al. attached silver containing macromolecules and showed that silver concentrations at membrane surface resulted in 85% reduction of the specific growth rate of *E. coli* [54]. Also, in this case a considerable amount of silver detached from membrane surface. In general, the issue of silver leaching during membrane fabrication and application has been recognized as critical. Moreover, in case of using metal salts, the leaching is highly dependent on the ion exchange with dissolved salts [55]. In contrast with surface-functionalization approaches, we used metal loaded particles with the active substances in reduced form as a way of reducing the rate of metal passing to the solution. We demonstrated that no nanoparticle leaching occurred and that a sustained release of metal ions is possible from their reduced forms, which can be easily dispersed in casting solutions without using complex functionalization procedures

3.5 Conclusion

Hybrid PES ultrafiltration membranes were prepared by incorporating mesostructured silica particles functionalized with silver, copper, and amine moieties. Composite membranes displayed asymmetric structure with relatively dense skin layer and a porous finger-like sublayer. The amount of surface pores significantly increased in doped membranes. All membranes were negatively charged and slightly hydrophobic with free energy of interaction slightly decreasing with the introduction of fillers.

The addition of particles increased permeability > 30% in all cases, without reduction of membrane performance expressed as BSA rejection. The addition of mesoporous silica particles, functionalized or not, allowed fouling reduction up to 29% during protein filtration. All flow resistances were lower for composite membranes with respect to neat PES. The intrinsic membrane resistance was dominant suggesting that membrane permeation was limited by the inherent morphological characteristics of membranes.

Silver-loaded composites exhibited high antimicrobial activity, with complete removal of bacterial colonies either on membrane surface (< 1 CFU/cm^2) and in the liquid culture in contact with them (< 10 CFU/mL). The effect was lower, but also significant for copper-loaded materials. The antimicrobial action could be attributed to the release of metals, which diffused from loaded mesoporous silica and PES matrix to the bulk. The release of dissolved metals represented a 0.1-0.6% of the total content of metal of the tested membranes.

3.6 References

1. Chakrabarty, B., A.K. Ghoshal, and M.K. Purkait, *Ultrafiltration of stable oil-in-water emulsion by polysulfone membrane.* Journal of Membrane Science, 2008. **325**(1): p. 427-437.
2. Liu, P., et al., *Hollow-fiber ultrafiltration for simultaneous recovery of viruses, bacteria and parasites from reclaimed water.* J Microbiol Methods, 2012. **88**(1): p. 155-61.
3. Boussu, K., et al., *Characterization of commercial nanofiltration membranes and comparison with self-made polyethersulfone membranes.* Desalination, 2006. **191**(1): p. 245-253.
4. Prince, J.A., *Synthesis and characterization of PEG-Ag immobilized PES hollow fiber ultrafiltration membranes with long lasting antifouling properties.* Journal of Membrane Science, 2014. **v. 454**: p. pp. 538-548-2014 v.454.
5. Van der Bruggen, B., *Chemical modification of polyethersulfone nanofiltration membranes: A review.* Journal of Applied Polymer Science, 2009. **114**(1): p. 630-642.
6. Maximous, N., G. Nakhla, and W. Wan, *Comparative assessment of hydrophobic and hydrophilic membrane fouling in wastewater applications.* Journal of Membrane Science, 2009. **339**(1): p. 93-99.
7. Choo, K.H. and C.H. Lee, *Understanding Membrane Fouling in Terms of Surface Free Energy Changes.* Journal of Colloid and Interface Science, 2000. **226**(2): p. 367-370.
8. Zhu, L.J., et al., *Hydrophilic and anti-fouling polyethersulfone ultrafiltration membranes with poly(2-hydroxyethyl methacrylate) grafted silica nanoparticles as additive.* Journal of Membrane Science, 2014. **451**: p. 157-168.
9. Zhao, Y.F., et al., *Improving the hydrophilicity and fouling-resistance of polysulfone ultrafiltration membranes via surface zwitterionicalization mediated by polysulfone-based triblock copolymer additive.* Journal of Membrane Science, 2013. **440**: p. 40-47.
10. Shirtliff, M.E., J.T. Mader, and A.K. Camper, *Molecular Interactions in Biofilms.* Chemistry & Biology, 2002. **9**(8): p. 859-871.
11. Liu, C.X., et al., *Modification of membrane surface for anti-biofouling performance: Effect of anti-adhesion and anti-bacteria approaches.* Journal of Membrane Science, 2010. **346**(1): p. 121-130.
12. Rahimpour, A. and S.S. Madaeni, *Polyethersulfone (PES)/cellulose acetate phthalate (CAP) blend ultrafiltration membranes: Preparation, morphology, performance and antifouling properties.* Journal of Membrane Science, 2007. **305**(1): p. 299-312.

13. Akar, N., et al., *Investigation of characterization and biofouling properties of PES membrane containing selenium and copper nanoparticles.* Journal of Membrane Science, 2013. **437**: p. 216-226.
14. Hobman, J.L. and L.C. Crossman, *Bacterial antimicrobial metal ion resistance.* J Med Microbiol, 2015. **64**(Pt 5): p. 471-97.
15. Lemire, J.A., J.J. Harrison, and R.J. Turner, *Antimicrobial activity of metals: mechanisms, molecular targets and applications.* Nat Rev Microbiol, 2013. **11**(6): p. 371-84.
16. Ruparelia, J.P., et al., *Strain specificity in antimicrobial activity of silver and copper nanoparticles.* Acta Biomater, 2008. **4**(3): p. 707-16.
17. Raffi, M., et al., *Investigations into the antibacterial behavior of copper nanoparticles against Escherichia coli*. Vol. 60. 2010. 75-80.
18. Kim, J. and B. Van der Bruggen, *The use of nanoparticles in polymeric and ceramic membrane structures: Review of manufacturing procedures and performance improvement for water treatment.* Environmental Pollution, 2010. **158**(7): p. 2335-2349.
19. Teli, S.B., et al., *Fouling Resistant Polysulfone–PANI/TiO_2 Ultrafiltration Nanocomposite Membranes.* Industrial & Engineering Chemistry Research, 2013. **52**(27): p. 9470-9479.
20. Huang, J., et al., *Fabrication of polyethersulfone-mesoporous silica nanocomposite ultrafiltration membranes with antifouling properties.* Journal of Membrane Science, 2012. **423-424**: p. 362-370.
21. Martín, A., et al., *Enhanced ultrafiltration PES membranes doped with mesostructured functionalized silica particles.* Desalination, 2015. **357**: p. 16-25.
22. Ng, L.Y., et al., *Polymeric membranes incorporated with metal/metal oxide nanoparticles: A comprehensive review.* Desalination, 2013. **308**: p. 15-33.
23. Quirós, J., et al., *Electrospun cellulose acetate composites containing supported metal nanoparticles for antifungal membranes.* Science of The Total Environment, 2016. **563-564**: p. 912-920.
24. Zhao, D., et al., *Triblock Copolymer Syntheses of Mesoporous Silica with Periodic 50 to 300 Angstrom Pores.* Science, 1998. **279**(5350): p. 548.
25. Van Oss, C.J., M.K. Chaudhury, and R.J. Good, *Interfacial Lifshitz-van der Waals and polar interactions in macroscopic systems.* Chemical Reviews, 1988. **88**(6): p. 927-941.
26. Holländer, A., *On the Selection of Test Liquids for the Evaluation of Acid-Base Properties of Solid Surfaces by Contact Angle Goniometry.* Journal of Colloid and Interface Science, 1995. **169**(2): p. 493-496.
27. Van Oss, C.J., *Development and applications of the interfacial tension between water and organic or biological surfaces.* Colloids Surf B Biointerfaces, 2007. **54**(1): p. 2-9.

28. Lin, J., et al., *Nano-WS2 embedded PES membrane with improved fouling and permselectivity.* J Colloid Interface Sci, 2013. **396**: p. 120-8.
29. 22196, ISO, *Measurement of Antibacterial Activity on Plastics and Other Nonporous Surfaces, International Organization for Standardization, Geneva, Switzerland* 2011.
30. Wang, X., et al., *Direct Synthesis and Catalytic Applications of Ordered Large Pore Aminopropyl-Functionalized SBA-15 Mesoporous Materials.* The Journal of Physical Chemistry B, 2005. **109**(5): p. 1763-1769.
31. Rouquerol, F., J. Rouquerol, and K. Sing, *CHAPTER 3 - Methodology of Adsorption at the Gas–Solid Interface*, in *Adsorption by Powders and Porous Solids*, F. Rouquerol, J. Rouquerol, and K. Sing, Editors. 1999, Academic Press: London. p. 51-92.
32. Kruk, M., et al., *Characterization of Regular and Plugged SBA-15 Silicas by Using Adsorption and Inverse Carbon Replication and Explanation of the Plug Formation Mechanism.* The Journal of Physical Chemistry B, 2003. **107**(10): p. 2205-2213.
33. Choi, M., et al., *Controlled Polymerization in Mesoporous Silica toward the Design of Organic–Inorganic Composite Nanoporous Materials.* Journal of the American Chemical Society, 2005. **127**(6): p. 1924-1932.
34. Morales, G., et al., *Sulfonated polystyrene-modified mesoporous organosilicas for acid-catalyzed processes.* Chemical Engineering Journal, 2010. **161**(3): p. 388-396.
35. Aerts, P., et al., *Polysulfone–aerosil composite membranes: Part 2. The influence of the addition of aerosil on the skin characteristics and membrane properties*. Vol. 178. 2000. 1-11.
36. Sotto, A., et al., *Effect of nanoparticle aggregation at low concentrations of TiO_2 on the hydrophilicity, morphology, and fouling resistance of PES–TiO_2 membranes.* Journal of Colloid and Interface Science, 2011. **363**(2): p. 540-550.
37. Wavhal, D.S. and E.R. Fisher, *Membrane Surface Modification by Plasma-Induced Polymerization of Acrylamide for Improved Surface Properties and Reduced Protein Fouling.* Langmuir, 2003. **19**(1): p. 79-85.
38. Jadav, G.L. and P.S. Singh, *Synthesis of novel silica-polyamide nanocomposite membrane with enhanced properties.* Journal of Membrane Science, 2009. **328**(1): p. 257-267.
39. Peng, W., I.C. Escobar, and D.B. White, *Effects of water chemistries and properties of membrane on the performance and fouling—a model development study.* Journal of Membrane Science, 2004. **238**(1): p. 33-46.

40. Chang, Y. J. and M.M. Benjamin, *Modeling Formation of Natural Organic Matter Fouling Layers on Ultrafiltration Membranes.* Journal of Environmental Engineering, 2003. **129**(1): p. 25-32.
41. Thomas J. Silhavy, D.K., and Suzanne Walker, *The Bacterial Cell Envelope.* Cold Spring Harb Perspect Biol, 2010. **2:14**.
42. Miyano, Y., et al., *Antibacterial properties of nine pure metals: A laboratory study using Staphylococcus aureus and Escherichia coli*. Vol. 26. 2010. 851-8.
43. Hess, S. and C. Gallert, *Growth Behavior of E. coli, Enterococcus and Staphylococcus Species in the Presence and Absence of Sub-inhibitory Antibiotic Concentrations: Consequences for Interpretation of Culture-Based Data.* Microb Ecol, 2016. **72**(4): p. 898-908.
44. Hori, K. and S. Matsumoto, *Bacterial adhesion: From mechanism to control.* Biochemical Engineering Journal, 2010. **48**(3): p. 424-434.
45. Kłodzińska, E., et al., *Effect of zeta potential value on bacterial behavior during electrophoretic separation.* ELECTROPHORESIS, 2010. **31**(9): p. 1590-1596.
46. Tang, X., et al., *Factors affecting the attachment of micro-organisms isolated from ultrafiltration and reverse osmosis membranes in dairy processing plants.* J Appl Microbiol, 2009. **107**(2): p. 443-51.
47. Zhao, Q., et al., *Evaluation of bacterial adhesion on Si-doped diamond-like carbon films*. Vol. 253. 2007. 7254-7259.
48. Sharma, V.K., et al., *Organic-coated silver nanoparticles in biological and environmental conditions: Fate, stability and toxicity.* Advances in Colloid and Interface Science, 2014. **204**: p. 15-34.
49. Yang, X., et al., *Mechanism of silver nanoparticle toxicity is dependent on dissolved silver and surface coating in Caenorhabditis elegans.* Environ Sci Technol, 2012. **46**(2): p. 1119-27.
50. Xiu, Z.M., et al., *Negligible Particle-Specific Antibacterial Activity of Silver Nanoparticles.* Nano Letters, 2012. **12**(8): p. 4271-4275.
51. Ramyadevi, J., et al., *Synthesis and antimicrobial activity of copper nanoparticles.* Materials Letters, 2012. **71**: p. 114-116.
52. Sawada, I., et al., *Development of a hydrophilic polymer membrane containing silver nanoparticles with both organic antifouling and antibacterial properties.* Journal of Membrane Science, 2012. **387-388**: p. 1-6.
53. Park, S.Y., et al., *Amphiphilic thiol functional linker mediated sustainable anti-biofouling ultrafiltration nanocomposite comprising a silver nanoparticles and poly(vinylidene fluoride) membrane.* ACS Appl Mater Interfaces, 2013. **5**(21): p. 10705-14.
54. Kim, Y., et al., *Towards antibiofouling ultrafiltration membranes by blending silver containing surface modifying macromolecules.* Chemical Communications, 2012. **48**(5): p. 693-695.

55. Mansouri, J., et al., *Biofouling performance of silver-based PES ultrafiltration membranes.* Desalination and Water Treatment, 2016. **57**(58): p. 28100-28114.

CHAPTER 4

Surface functionalization of Poly (vinyl chloride) ultrafiltration membranes using a hyperbranched polyamidoamine for antifouling and antibiofouling properties

Chapter 4. SURFACE FUNCTIONALIZATION OF POLY (VINYL CHLORIDE) ULTRAFILTRATION MEMBRANES USING A HYPERBRANCHED POLYAMIDOAMINE FOR ANTIFOULING AND ANTIBIOFOULING PROPERTIES

4.1 Abstract

Poly(vinyl chloride) (PVC) ultrafiltration membranes with improved antifouling and antibiofouling properties were prepared by non-solvent induced phase inversion using a hyperbranched polyamidoamine as additive. PVC directly reacted into the casting solution with the commercial polyamidoamine nanomaterial Helux-3316 by means of a nucleophilic substitution reaction. The composition of neat and functionalized membranes was studied by ATR-FTIR analysis and elemental composition. Amino groups were tracked using the fluorescent dye fluorescamine. Surface ζ potential and water contact angles were used to measure surface charge and hydrophilicity of tested membranes. The incorporation of amino groups increased the membrane hydrophilicity, which resulted in enhanced water permeability. Functionalized membranes displayed antifouling behaviour revealed upon filtering BSA solutions and displayed lower irreversible fouling than PVC membranes. The attachment of Helux moieties to PVC resulted in membranes with antibiofouling functionality explained by the interaction of positively charged Helux moieties with the negatively charged cell envelopes. Growth reduction for cells attached to the membrane surface during filtration reached up to 1-log for the Gram-positive bacterium *S. aureus*. This investigation revealed that the incorporation of the hyperbranched nanomaterial in concentrations in the order of 1 wt% in the casting solution provides significant benefits to the membrane performance, in terms of permeability and antifouling potential.

4.2 Introduction

Membrane processes are key technologies for sustainable industrial development. They are able provide efficient separations with the potential to replace other conventional and energy-intensive techniques. Membrane efficiency is based on the absence of phase changes as well as on the possibility they offer to reduce energy consumption by recycling product and waste streams [1]. Ultrafiltration is a pressure-driven separation widely used for the separation of particulate matter and macromolecules from soluble compounds and for the treatment of stable oil-in-water emulsions. Ultrafiltration is widely used as desalination pre-treatment, and for wastewater reclamation, either from domestic or industrial effluents [2]. Increased regulatory pressure is increases the use of water filtration operations, and, therefore, the demand for membranes is steadily increasing even despite certain recent slowdown due to the lower world economic growth. Technological advancements in membrane technologies are expected to lead to cost reductions and additional market growths. One of the main drawbacks of membranes in water treatment operations is their tendency to flux decline due to the interaction with organic or inorganic substances or with growing microbial cells. Inorganic fouling is due to the accumulation of particles on membrane surface and inside the pores, eventually creating a cake layer. Organic fouling is the consequence of the adsorption of natural organic matter on external and internal membrane surfaces, thus blocking or constricting pores. Natural organic matter, particularly extracellular polymeric substances and soluble macromolecules have been reported as the main organic foulants [3]. Biofouling refers to the growth of microbial cells on membrane surface where they adhere and form biofilms. The interaction between membranes and bacteria starts by non-specific adsorption followed by adherence mediated by the exopolysaccharides (EPS) segregated by bacterial cells during biofilm forming process [4]. Biofilms are complex biological communities that

evolved to protect bacteria. One formed, biofilms modify their microenvironment and are very difficult to remove, therefore leading to permanent flux declines [5]. The usual strategy to control fouling and biofouling in ultrafiltration processes is back-washing with cleaning agents or disinfectants. Chlorinated water is the usual way used to inactivate microorganisms on the surface of chlorine-resistant membranes [6]. Backwashing is needed to remove EPS binding microorganisms [7]. Many authors reported new types of antifouling or antibacterial membranes based on several principles. The use of metal nanoparticles has been frequently proposed due to the toxic effect of many metals to bacterial cells. Copper, silver and other metals, either by direct contact or mediated by the release of different ions have been showed to induce oxidative stress, membrane disruption, and interference with core enzymatic activities [8]. Accordingly, metal nanomaterials have been incorporated to the polymeric matrix to prepare hybrid antifouling ultrafiltration membranes [9, 10]. Apart from metal-based nanomaterials non-metal releasing nanoparticles proved antifouling capacity due to enhanced membrane hydrophilicity [11]. The incorporation of hydrophilic nanofillers in the polymer casting solution was shown to increase permeate flux in mixed matrix ultrafiltration membranes [12]. Zeolites, mesoporous silica and related materials have been investigated in view of their capacity to modify pore size and interconnectivity as well as surface hydrophilicity with the purpose of increasing membrane permeability and durability. Enhanced antifouling activity has been reported in silica particles upon functionalization with positively and negatively charged amino and carboxylic moieties together with improvements in hydrophilicity, permeability, and pore structure [13]. The incorporation of nanoparticles into polymeric membranes has some disadvantages. One technical, namely the difficulty of creating homogeneous membranes with good particle dispersion due to the tendency of nanoparticles to aggregate in organic solvents. Besides,

the possible release of nanomaterials into the environment poses additional concerns. Helux-3316 is a hyperbranched polymeric nanomaterial that consists of a polyamide backbone with terminal primary amine end-groups together with a lower amount of carboxylic acids. Hyperbranched polymers are a class of dendritic materials, also comprising dendrimers, created from a central core upon random branching. Unlike dendrimers, hyperbranched polymers are irregularly shaped and their relatively facile, one-step synthesis make them readily available [14]. Due to their relatively low cost, hyperbranched polymers have large-volume applications. Lupasol® is a hyperbranched poly(ethyleneimine) used as crosslinker of epoxy resins [15]. Boltorn® hyperbranched materials are in use as ink component [16]. Chemically, hyperbranched polymers are characterized by having a large number of reactive groups, higher solubility than similar molecules of comparable weight and low viscosity, which grant a variety of uses diverse fields [17]. In this work, we used the hyperbranched polyamidoamine Helux-3316 manufactured by Polymer Factory (Sweden) to functionalize poly(vinyl chloride) ultrafiltration membranes. The approach followed was to chemically bind the polyamidoamine nanomaterial to poly(vinyl chloride) backbone by means of a nucleophilic substitution reaction of chlorine atoms. The concentration of the hyperbranched nanomaterial was in the order of 1 wt% in the casting solution. Here, a new type of modified ultrafiltration membranes has been studied in terms of permeability, organic fouling and antibiofouling/antimicrobial functionality of the resulting membranes.

4.3 Materials and methods

4.3.1 Materials

Hyperbranched polyamidoamine (Helux-3316) was supplied from Polymer Factory (Stockholm, Sweden). Helux-3316 contains primary amines end-groups with a theoretical molecular weight of 5108 g/mol. The chemical

structure of Helux-3316 is shown in Fig. 4.1. Poly (vinyl chloride) (PVC, average molecular weight 43 kDa) and polyvinylpyrrolidone (PVP, average molecular weight 40 kDa) were acquired from Sigma-Aldrich. N, N-dimethylacetamide (DMAc, 99,9%), dimethyl sulfoxide (DMSO, 99,9%), glutaraldehyde solution (25% in H_2O), sodium cacodylate, bovine serum albumin (BSA) and fluorescamine were obtained from Sigma-Aldrich. Ultrapure water with a specific resistance of 18.2 MΩ cm $^{-1}$ was produced by a Direct-Q 5 Ultrapure Water Systems (Millipore, USA). Live/Dead BacLight kits were acquired from Invitrogen (Thermo-Fisher, Waltham, MA). The components of culture media were purchased from Laboratorios Conda (Spain).

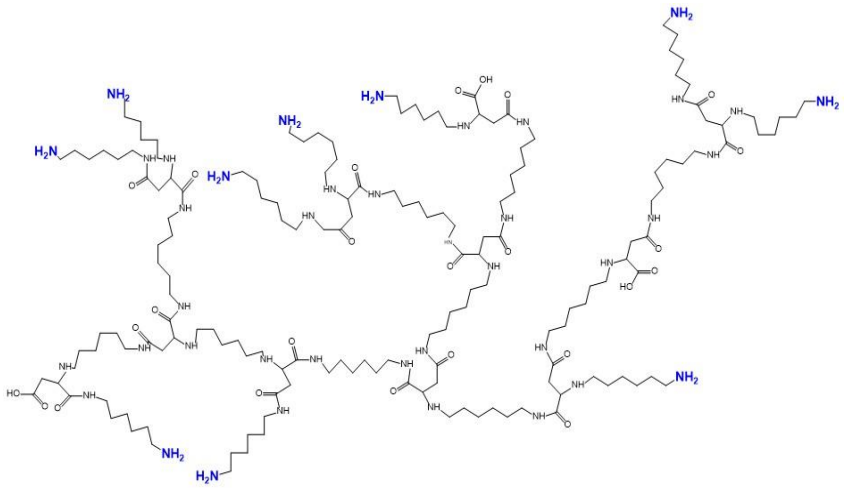

Figure 4.1. Chemical structure of Helux-3316. Primary amine end-groups (-NH_2) are shown in blue. Adapted from reference [27].

4.3.2 Membrane preparation

Membranes were prepared via non-solvent induced phase inversion method from a casting solution containing 15 wt% of PVC polymer as base material, 5 wt% of PVP in DMAc. PVP was used as pore forming additive due to its role of polymer surfactant during gelation process, which is known to result in higher porosity and permeation fluxes [18]. For Helux-PVC membranes, Helux-3316 was added into the casting solution, and heated at 60 ºC for 10 h under stirring. After complete dissolution, or after heating in the case of Helux-PVC

membranes, the solution was kept stagnant for at least 12 h at room temperature in order to remove any air bubbles present. Afterwards, the solution was cast to 200 µm thickness films onto a glass plate using an automatic film applicator AB3120 (TQC, The Netherlands) and immediately immersed into a water coagulation bath where the solvent (DMAc) and the non-solvent (water) exchanged. Finally, membranes were washed and stored in a new container containing fresh distilled water.

Some specimens were prepared without PVP for comparison purposes and for allowing the assessment of Helux-PVC coupling by tracking their nitrogen content without the interference of nitrogen from PVP. Table 4.1 summarizes the concentrations used and the nomenclature used in what follows.

Table 4.1. Composition of casting solutions.

Membrane	PVC (% w/w)	PVP (% w/w)	Helux (% w/w)
PVC	15	-	-
PVC-PVP	15	5	-
PVC-PVP-H [0.8]	15	5	0.8
PVC-PVP-H [1.6]	15	5	1.6
PVC-H [0.8]	15	-	0.8
PVC-H [1.6]	15	-	1.6

4.3.3 Membrane characterization

The morphology of membranes was studied by observing their cross-section under scanning electron microscopy (SEM, Zeiss DSM-950 apparatus operating at 25 kV). Prior to observation, the membranes were frozen in liquid nitrogen and covered with gold. The composition of PVC and Helux-PVC membranes was analysed by Attenuated total reflectance Fourier transform infrared (ATR-FTIR) spectra using a Thermo-Scientific Nicolet iS10 apparatus with a Smart iTR-Diamond ATR module. Elemental composition analyses were performed using a LECO CHNS-932 Analyzer.

Surface ζ-potential was determined by electrophoretic light scattering using a Zetasizer Nano apparatus (ZEN1020) from Malvern (Malvern Instruments, UK). Surface zeta potential measurement consisted of holding a rectangular section of each membrane between two electrodes using araldite adhesive. The sample is then immersed into an appropriate aqueous solution containing 10 mM KCl (pH 7.0) and 0.5 % (w/w) of polyacrylic acid (450 kDa) acting as a tracer. The electrophoresis mobility of the tracer was measured at six different distances from the sample surface. Measurements were conducted at room temperature (25 ºC). Static water contact angles (WCA) were studied by the sessile drop technique using a Krüss DSA25 equipment. Surface ζ-potential and WCA were calculated using at least four replicates with different specimens. All measurements were performed at room temperature.

In order to assess the grafting of amino groups from Helux to PVC in Helux-PVC membranes, we used fluorescamine as probe for confocal microscopy imaging. Fluorescamine is a non-fluorescent compound that reacts with primary amines forming a stable and highly fluorescent product. A fresh stock solution of fluorescamine (3 mg/mL in acetone) was prepared, extended onto membrane surface, and incubated for 15 min at room temperature. Immediately after, the membranes were washed and visualized using a confocal microscope with fluorescence module (TCS-SP5 Leica Microsystems) at excitation/emission wavelengths of 365 nm/470 nm respectively. PVC membranes without any source of nitrogen in their structure were also treated with fluorescamine as a negative control. The stability of Hellux-3316 as a source of nitrogen in the aminated membranes was tracked, after 48 h of water filtration at 2 bars transmembrane pressure (TMP).

4.3.4 Filtration and fouling assays

Filtration assays were conducted using a crossflow stainless-steel module connected to a 2 L volume tank kept at 25 ºC. The effective area of the membrane samples was 20 cm^2 (40 mm x 50 mm). Pure water flux (J_w) was measured at different transmembrane pressures (TMP) in the 1 to 4 bar range. Prior to permeability tests, membranes were compacted for about 2 hours at 4 bars with deionized water in order to obtain reproducible and representative flux measurements. Four specimens of each membrane were tested.

Pure water flux (J_w^i) was calculated using following equation:

$$J_w^i = \frac{V}{A \cdot \Delta t} \qquad (1)$$

Where V (L) is the volume of permeate collected, A (m^2) is the membrane effective area and Δt (h) is the operation time.

Membrane fouling was studied using BSA as model of organic foulant. For it, BSA was dissolved in 0.1 M phosphate-buffered physiological saline (PBS) at a concentration of 1.0 g/L, pH 7.2. Once pure water flux was measured in permeation tests, water was replaced by the BSA solution and flux allowed to stabilize. Then, BSA solution was kept flowing for 3 h, after which the flux of fouled membranes was recorded (J_p, before cleaning specimens). Then, membranes were rinsed with distilled water and pure water flux of cleaned specimens (J_w^f) was recorded again. At least five filtration experiments were carried out for each polymer composition until reproducible values were obtained. All values were recorded at 2 bat TMP.

Flux recovery ratio was calculated as follows:

$$\text{Flux recovery ratio (\%)} = \left(\frac{J_w^f}{J_w^i}\right) \times 100 \qquad (2)$$

Flux loss was analysed in terms of total, reversible and irreversible fouling ratio as indicated in the following equations:

$$\text{Total Fouling Ratio (\%)} = \left(1 - \frac{Jp}{J_w^i}\right) \times 100 \quad (3)$$

$$\text{Reversible Fouling Ratio (\%)} = \left(\frac{J_w^f - J_P}{J_w^i}\right) \times 100 \quad (4)$$

$$\text{Irreversible Fouling Ratio (\%)} = \left(\frac{J_w^i - J_w^f}{J_w^i}\right) \times 100 \quad (5)$$

Rejection efficiency (R) was calculated according to the following equation:

$$\text{R (\%)} = \left(1 - \frac{C_P}{C_f}\right) \times 100 \quad (6)$$

Where C_p and C_f represent the concentration of BSA in permeate and feed solutions, respectively. The concentration of foulant was recorded by UV spectrophotometry using at wavelength of 280 nm.

4.3.5 Antibiofouling assays

The antimicrobial activity of the prepared membranes was tested using two different bacterial strains, *S. aureus* (CECT 240, strain designation ATCC 6538P) and *E. coli* (CECT 516, strain designation ATCC 8739), Gram-positive and Gram-negative respectively. The microorganisms were maintained in glycerol at -80 ºC until use. Nutrient broth culture medium (NB) was used to reactivate bacterial growth using a pH 6.8-7.0, after which bacterial cultures were kept at 36 ºC under constant stirring (250 rpm). Bacterial growth for initial cultures was monitored by tracking optical density (OD) at 600 nm.

The antibiofouling behaviour of membranes was estimated by counting the CFU (colonies Forming Units) according to the standard procedure described in the ISO 22196, with minor modifications. For it, cultures with an initial bacterial concentration of 10^6 cells/mL were prepared and inoculated in sterile 24-wells microplates, using a NB medium diluted 500-fold. Membranes were sterilized and then soaked in bacterial cultures, maintaining them for 20h at

36 ºC. The amount of inoculum used was 0.3 mL/mg of membrane. After incubation, bacterial cells present in the culture medium and cells detached from membranes were quantified by counting colony-forming units (CFU). For that, 10-fold serial dilution were performed in PBS, then 10 µL of each dilution was spot-plated on solid agar and incubated at 36 ºC for 24 h before counting colonies. Adhered cells were obtained using soybean casein digest broth with lecithin and polyoxyethylene sorbitan monooleate, following the guideline described in ISO 22196. Prior to it, membranes were washed with PBS for 30 min in an orbital shaker in order to remove the non-adhered cells. Each sample was measured in triplicate in three independent runs. Colonized membranes were visualized using SEM images. Membranes were incubated for 20 h with bacterial cultures of initially 10^6 cells/mL of *E. coli* or *S. aureus*. Afterwards, membranes were cleaned with distilled water, fixed using glutaraldehyde (5% v/v) in sodium cacodylate (0.2 M) and dehydrated using different concentrations of ethanol (25%-50%-70-90-100 % v/v) and acetone (100 % v/v). SEM micrographs were obtained in a ZEISS DSM-950 instrument operating at 25 kV. Bacterial viability was examined by means of the Live/Dead BacLight Bacterial Viability kit. This method uses two different fluorescent nucleic acid stains, SYTO 9 and propidium iodide (PI) which differentiate viable and non-viable cells, respectively. It is based in their ability to penetrate healthy bacterial cells. SYTO 9 can penetrate intact and damaged membranes, marking cells in green. In contrast, propidium iodide is only internalized by membrane-damaged cells, marking cells in red. The images were obtained by the confocal laser microscopy (LEICA TCS-SP5) using an excitation/emission wavelength of 472 nm/ 580 nm respectively.

4.4 Results and discussion

The reactivity of chloride atoms in the poly(vinyl)chloride main chains allows chemical modification without affecting the polymer backbone by means of nucleophilic substitution reactions [19, 20]. In this study, the hyperbranched polyamidoamine Helux-3316 was used as a nucleophile for the amination reaction of PVC chains by means of the SN_2 reaction. Helux substituted chlorine atoms from PVC chains giving rise to aminated-PVC chains in DMAc solution. Fig. 4.2. shows a schematic representation of the production process of Helux-PVC ultrafiltration membranes.

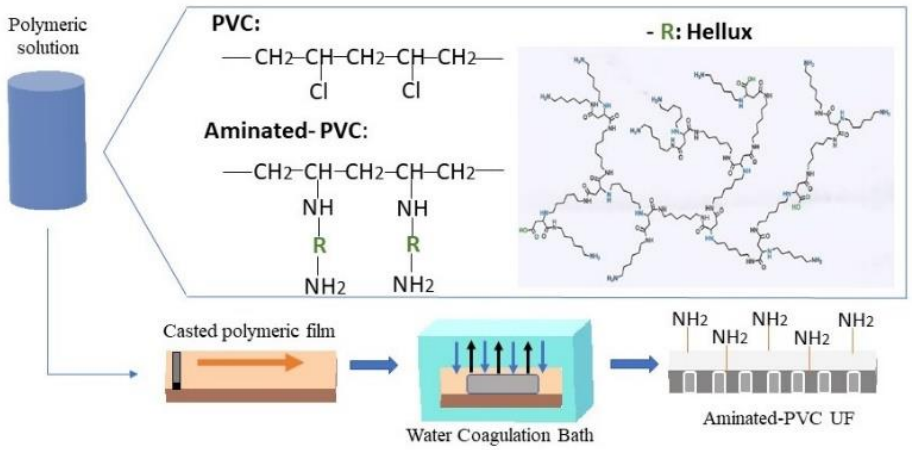

Figure 4.2. Schematic representation of the preparation of Helux-PVC ultrafiltration membranes.

Fig. 4.3 shows cross-sectional SEM images of PVC and Helux-PVC membranes displaying asymmetric structure with dense skin layer on top of a finger-like porous sublayer. The formation of larger finger-like pores structures is clear in modified PVC membranes. It could be explained by the faster diffusion exchange between solvent and non-solvent during the phase inversion process due to the action of hydrophilic components into the polymer solution. Morphological changes include improved pore interconnectivity, which enhances water permeation [10].

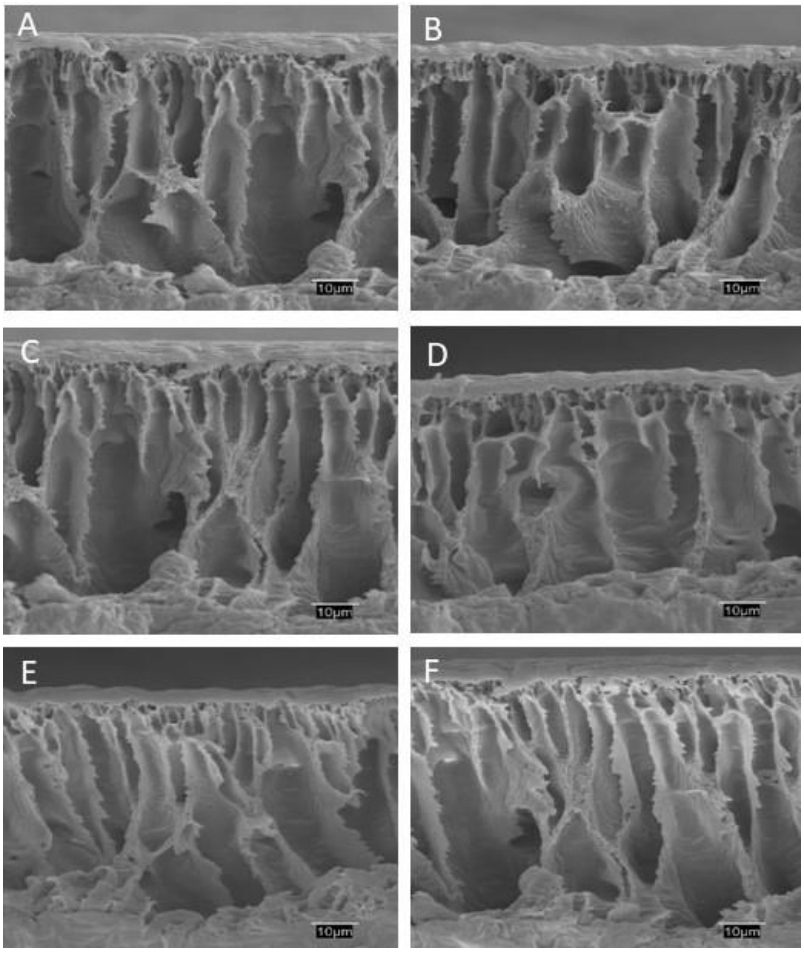

Figure 4.3. SEM cross-sectional images of neat PVC (A), PVC-PVP (B), PVC-PVP-H [0.8] (C) and PVC-PVP-H [1.6] (D) PVC-H [0.8] (E) and PVC-H [1.6] (F) membranes.

FTIR spectra confirmed the presence of the main functional groups of polymers on membranes (Figure 4.4). Fig. 4.4A displays the FTIR spectra of neat PVC, PVP-PVC and Helux-PVC membranes showing the characteristic peaks of the polymers. The band at 2890–2958 cm^{-1} corresponded to C-H stretching mode. CH_2 deformation appeared at 1320 cm^{-1}, out of plane angular deformation of CH at 1230 cm^{-1}, trans CH wagging at 960 cm^{-1}, C-Cl stretching at 845 cm^{-1}, and cis CH wagging at 650 cm^{-1} [21]. The spectra of PVP-doped membranes also revealed the characteristic bands of PVP. Besides the

absorptions corresponding to hydrocarbon backbone, the peak at 1660 cm^{-1} was attributed to the stretching vibration of the carbonyl groups, C=O, from the pyrrolidone ring [22, 23].

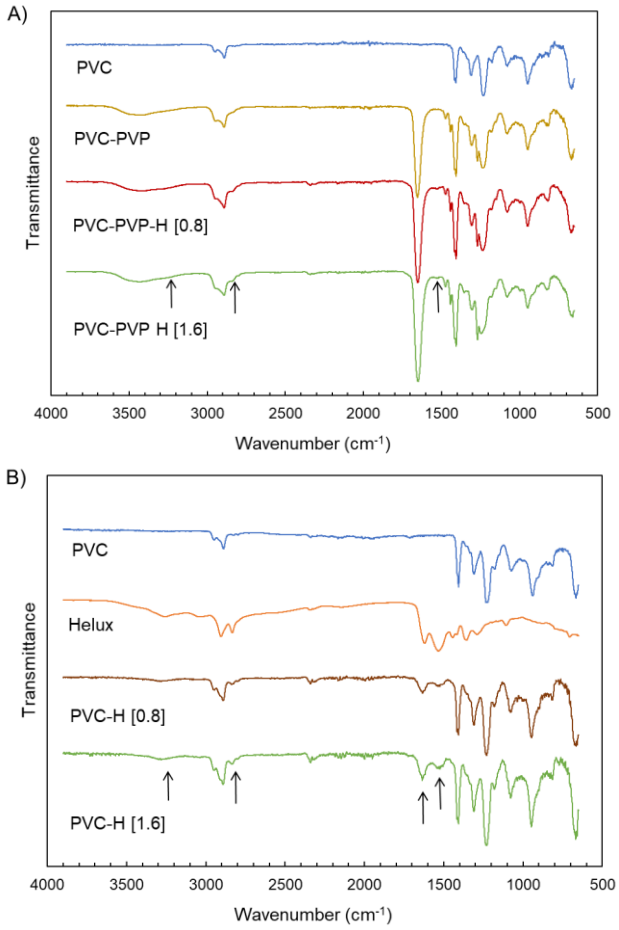

Figure 4.4. A) ATR-FTIR spectra of PVC, PVC-PVP, and Helux-PVC membranes PVC-PVP-H [0.8] and PVC-PVP-H [1.6]. B) FTIR spectra of pure PVC and Helux, and Helux-PVC membranes prepared without PVP: PVC-H [0.8] and PVC-H [1.6].

The presence of Helux in Helux-PVC membranes can be confirmed by the FTIR spectra of these membranes from the shoulder at 3240 cm^{-1} corresponding to N-H stretching of amides, the C-H stretching signal in the 2800-2900 cm^{-1}, and the peak at 1528 cm^{-1}, which corresponded to the N-H bend in amides and

amines. In order to clarify the presence of aminated groups, some additional specimens were prepared without PVP, namely PVC-H [0.8 and 1.6]. In this case, membranes showed a new peak at 1648 cm^{-1} corresponding to the amide C=O stretch, which confirmed the incorporation of Helux functional groups into the structure of PVC membranes. Their spectra together with that of pure Helux are shown in Fig. 4.4B. Coincidences with Helux peaks in FTIR spectra are indicated with arrows.

Surface ζ-potential was used to characterize membrane surface charge [24]. The surface ζ-potential at pH.7.0 of representative specimens are shown in Table 4.2.

Table 4.2. Membranes properties

Membranes	Surface ζ-potential (mV) [a]	WCA (º)	Permeability (LMH)[b]	Rejection (%)[b]
PVC-C	-34.1 ± 1.3	78.4 ± 2.7	89.5 ± 2.7	89.2 ± 0.8
PVC-PVP	-31.7 ± 1.3	73.4 ± 1.7	114.4 ± 1.3	88.1 ± 1.1
PVC-PVP-H[0.8]	-24.0 ± 2.6	69.9 ± 1.6	131.2 ± 2.0	89.6 ± 1.6
PVC-PVP-H[1.6]	-14.0 ± 2.5	65.9 ± 2.1	149.4 ± 0.6	87.6 ± 1.7
PVC.H [0.8]	-26.4 ± 1.3	72.3 ± 2.6	128.2 ± 1.0	88.9 ± 0.6
PVC.H [1.6]	-18.3 ± 1.1	69.3 ± 1.9	137.6 ± 1.3	87.9 ± 1.4
Helux-3316 pure	+8.9 ± 2.1[c]	-	-	-

[a] Surface zeta potential was measured at pH.7.0
[b] Operation at 2 bar TMP
[c] ζ-potential in aqueous dispersion (Mili-Q ultrapure water)

Neat PVC membranes displayed a zeta potential value of -34.1 ± 1.3 mV. Negative surface charge in polymeric membranes is a usual finding, attributed to the preferential adsorption of negative ions [25]. As result of Helux addition (a compound bearing 10 primary amino groups), the ζ-potential values of Helux-PVC membranes increased to -24.0 ± 2.6 mV and -14.0 ± 2.5 mV for Helux concentration in the casting solution of 0.8 % and 1.6 %, respectively. The pK_a values of aliphatic primary and secondary amines is ~10 and,

therefore, they are positively charged at neutral pH [26]. The reduction of the negative charge of PVC upon amination indicated that the introduction of positively charged $-NH_3^+$ or $-NH_2^+$- groups partly compensated PVC negative charge, leading to less negative ζ-potential values [23].

The hydrophilicity of PVC and Helux-PVC membranes was studied by measuring the water contact angles (WCA) created between water drop and membrane surface. The results obtained are also represented in Table 4.2. The incorporation of Helux resulted in slightly decreased water contact angles values, compared to neat PVC membranes. The effect is most probably due to the presence of charged amines that stabilise intermolecular hydrogen bonds with water molecules, leading to higher hydrophilicity for Helux-PVC membranes.

The incorporation of amino groups into PVC membranes was visually assessed using the fluorescent dye fluorescamine, which is a molecule that interacts with primary amines, forming stable Helux-fluorescamine conjugates [27]. Fig. 4.5 shows confocal images of neat PVC and Helux-PVC membranes after exposure to fluorescamine dye. Helux-PVC membranes revealed a blue fluorescent colour distributed across their surface, indicating the presence of aminated groups. The intensity of Helux-fluorescamine conjugate increased with increasing concentration of Helux in the casting solution. PVC membranes used as a negative control were treated with the same concentration of fluorescamine and showed absence of any blue fluorescence.

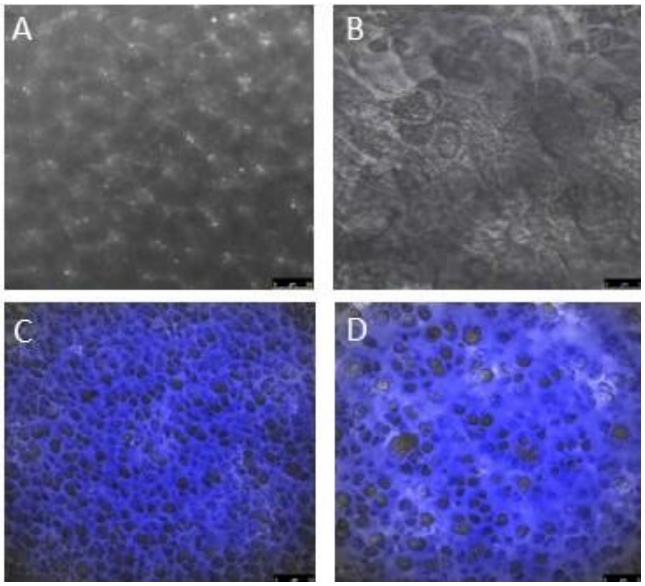

Figure 4.5. Confocal images of PVC (A), PVC-PVP (B), PVC-PVP-H [0.8] (C) and PVC-PVP-H [1.6] (D) membranes exposed to fluorescamine dye.

Elemental analysis was used to quantify the amount of Helux-3316 grafted into PVC membranes. The percentage of nitrogen was measured in PVC-H [0.8] and PVC-H [1.6] membranes, which contain Helux as the only source of nitrogen. Membrane specimens containing PVP were not analysed due to the interference of nitrogen from PVP. Fig 4.6 shows that as the concentration of Helux increased from 0.8 % to 1.6 % in the casting solution, the percentage of nitrogen included in membranes increased from 1.1 ± 0.3 % to 2.2 % ± 0.7, respectively. These figures support the assumption that the Helux used in casting solutions became effectively incorporated into the final membranes.

In order to assess the stability of Helux included in membranes, a series of filtration assays were performed at 2 bar TMP for 48 h. The results of nitrogen measurements showed that Helux did not significantly release from membranes during operation, indicating stable functionalization.

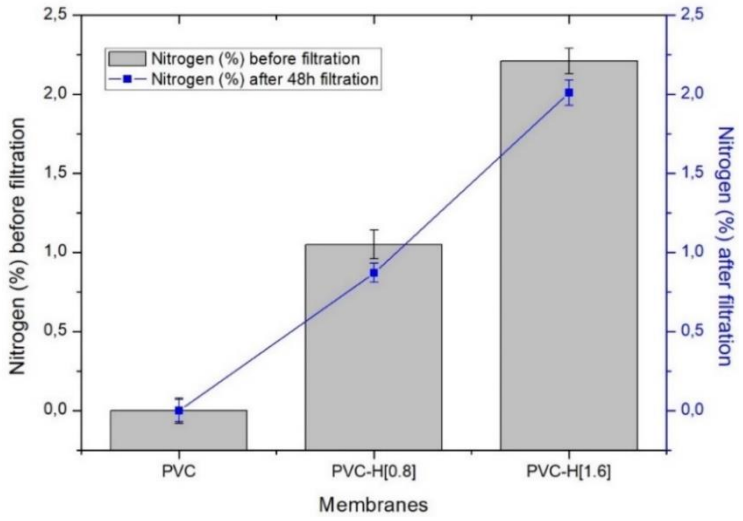

Figure 4.6. Percentage of nitrogen in PVC and Helux-PVC membranes before and after 48h of water filtration at 2 bar TMP. Error bars represent standard deviation.

Pure water permeability of neat PVC, PVC-PVP and Helux-PVC membranes is indicated in Table 4.2. The results showed that the permeability increased from 89.4 ± 2.7 LMH obtained for neat PVC membranes up to 114.4 ± 1.3 and 149.4 ± 0.6 LMH for PVC-PVP membranes and Helux-functionalized PVC membranes, respectively. It is a known fact that hydrophilic additives such as PVP or polyethylene glycol are excellent pore-forming agents [28]. Such additives enhance phase-separation during membrane fabrication and contribute to the increase the number of membrane pores, which results in higher membrane permeability [13]. The higher hydrophilicity of Helux-PVC membranes is also expected to increase water permeability and to mitigate membrane surface fouling.

Table 4.3: Fouling parameters of PVC and Helux-functionalized membranes

Membrane	TFR (%)	RFR (%)	IFR (%)	FRR (%)
PVC	37.8 ± 1.0	17.9 ± 1.3	19.9 ± 0.3	77.7 ± 3.6
PVC-PVP	33.3 ± 2.1	17.1 ± 0.7	16.2 ± 1.3	83.0 ± 0.5
PVP-PVP-H [0.8]	28.6 ± 1.2	16.7 ± 2.4	11.9 ± 1.1	88.1 ± 1.1
PVP-PVP-H [1.6]	32.5 ± 2.0	18.5 ± 3.5	14.8 ± 2.4	84.6 ± 3.2

The antifouling behaviour of PVC and Helux-PVC membranes was studied using BSA as a protein model for organic fouling. The decrease in permeability due to the adsorption and deposition of organic fouling was measured by recording water flux before and after BSA filtration. BSA solution (1g/L) was kept flowing for 3 h at 2 bar TMP after stabilization, and pure water flux was recorded as indicated before. Fouling parameters Total Fouling Ratio (TFR), Reversible Fouling Ratio (RFT), Irreversible Fouling Ratio (IFR) and Flux Recovery Ratio (FFR) were calculated as shown in equations 2-5. The results are summarized in Table 4.3. The effect on the antifouling character of prepared membranes is clearly positive taking into account the obtained results as consequence of modification proposed in all of cases .TFR decreased from 38 % for neat PVC membranes up to 29-33 % for PVC-PVP and Helux-PVC membranes, without differences that could be attributed to the introduction of the hyperbranched polyamidoamine additive. The results can be attributed to their higher membrane hydrophilicity due to the presence of PVP or Helux, indicating better antifouling properties. Total flux loss can be produced by reversible or irreversible fouling. Irreversible fouling was higher in neat PVC membranes (19.9 %). Hydrophobic membranes are prone to suffer the adsorption of proteins due to hydrophobic interactions, blocking membrane pores and inducing the formation of a surface cake layer [29]. Irreversible fouling is only partially removed by chemical cleaning, which is known to damage membrane surface, thereby reducing membrane life [30]. Both TFR and IFR decreased in Helux-functionalized membranes, a fact that can be attributed to their higher hydrophilicity. A possible reason for not observing significantly lower RFR might be the electrostatic interaction between the positively charged amino groups of Helux-PVC membranes and negative charged BSA [23]. BSA rejection tests carried out by measuring the protein concentration in permeates allowed calculating rejection efficiency, which is shown for all tested specimens in Table 4.2.

Similar retention properties were obtained for PVC and Helux-functionalized membranes, with only a slight non-significant reduction in membranes containing PVP, which could eventually be related to pore size increase during membrane preparation.

The microorganisms tested in this work as biofoulants were the Gram-negative *E. coli* and the Gram-positive *S. aureus*, strains commonly used as representative for both types of microorganisms in antimicrobial activity tests. Figure 4.7 shows the number of viable bacteria, express as a CFU (colony forming units) present in the liquid medium (NB 1/500) kept in contact for 20 h at 36 ºC with different membranes specimens. The results showed that the growth of *E. coli* and *S. aureus* decreased for Helux-functionalized specimens, most probably due to the presence of positively charged amines on their surface. Anti-biofouling behaviour was measured by counting cells adhered to the membrane surface after detaching them using the procedure given in the ISO 22196 and outlined before.

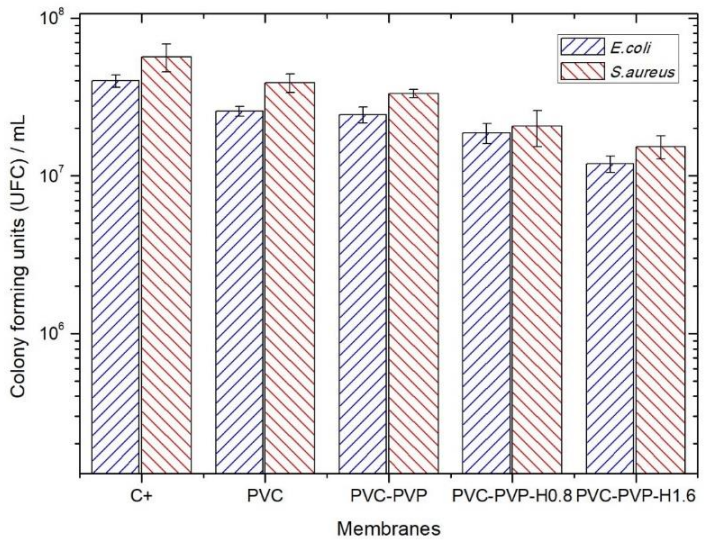

Figure 4.7. Microbial growth of *E.coli* (▨) and *S.aureus* (▨) cultures kept in contact with different membrane specimens at 36 ºC for 20 h.

Figure. 4.8 showed that after 20 h in contact with the membranes at 36 ºC, the bacterial cells responsible for biofilm formation, were considerably reduced in Helux-PVC membranes. About 1-log reduction was observed for *S. aureus* growth, with a somewhat lower effect for *E. coli*. The differences between both strains are due to evolutionary reasons that provided Gram-negative bacteria additional protection. A higher resistance of Gram-negative bacteria to antimicrobials is a usual finding, usually attributed to their different structure as explained below.

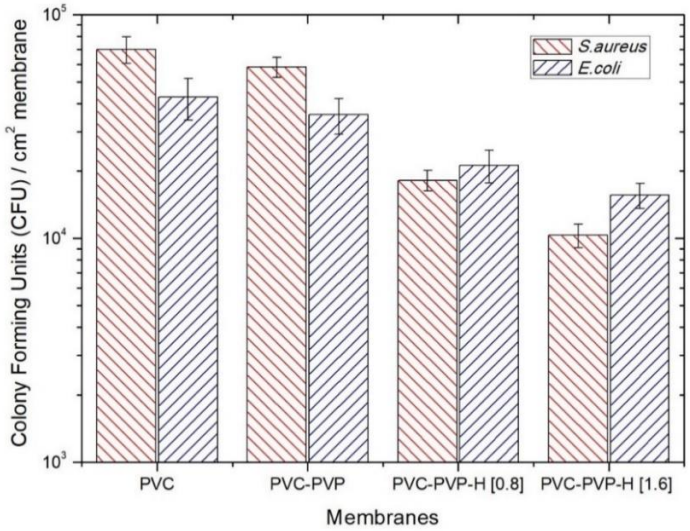

Figure 4.8. Viable microorganism detached from membranes specimens exposed to *S. aureus* (▨) and *E. coli* (▨) cultures after 20 h at 36 ºC. Errors bars indicate standard deviation.

The antimicrobial behaviour of Helux-PVC membranes can be attributed to the presence of primary or secondary amines in functionalized membranes. Helux molecules displays polycationic character at physiological pH, due to its protonated amine groups as revealed by its ζ-potential of +8.9 ± 2.1 mV. Table 4.2 showed that surface zeta potential became less negative upon Helux functionalization of PVC membranes that partially neutralize the negative charge of PVC. Overall, membrane surface should contain positively charged domains associated to Helux moieties, which are susceptible to interact with

the negatively charged bacterial wall, therefore, contributing to the disruption of membrane structures. The external difference between cell wall structures of Gram-positive and Gram-negative could explain this behaviour. Gram-negative bacteria contain a thin cell wall surrounded by two plasma membrane layers, the outer membrane (OM) contains polyanionic lipopolysaccharides (LPS) neutralized by divalent cations, as a Ca^{2+} and Mg^{2+} [31, 32]. Gram-positive bacteria contain a thick cell wall composed by different layers of peptidoglycan and lipoteichoic acids that also requires cationic counterions to stabilize the assembly [33]. Cation-binding sites are essential for maintaining the cell wall structure. However, amino charged groups could interact with divalent cations competing for the electronegative sites on cell membranes [34]. These electrostatic interactions may disrupt cell wall structure leading to increased membrane permeability [35-37]. Although the exact mechanism of action varies between polycations, membrane damage leads to osmotic imbalances and, finally, cell lysis [38, 39].

The disruption of the cell wall membrane was confirmed by confocal images using Live/Dead assay. This method distinguishes viable and non-viable cells according to cell membrane integrity using two fluorescent stains: propidium iodide and Syto9. Propidium iodide is a nucleophilic dye that only penetrates through the damaged membrane, marking the cells in red. Syto9 marks viable cells in green, indicating non-damaged bacterial cells. Figure. 4.9 shows PVC and PVC-PVP membranes covered only by green-labelled viable cells. However, Helux-PVC membranes revealed a considerable number of red-marked cells indicating cells with damaged membrane integrity and only a few scattered green-marked viable cells.

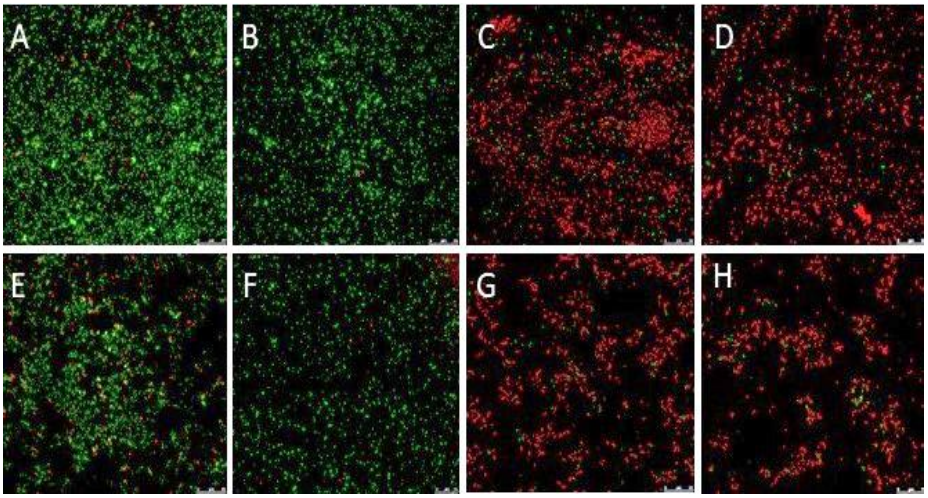

Figure 4.9. Confocal images of PVC (A, E) PVC-PVP (B, F) PVC-PVP-H [0.8] (C, G) and PVC-PVP-H [1.6] (D, H) membranes after exposure to *S. aureus* (A-D) and *E. coli* (E-H) cultures for 20 h at 36 ºC. Viable bacteria are green marked by viability stain, whereas red dots indicate membrane-damaged cells.

The anti-biofouling behaviour of Helux-PVC membranes was studied using SEM micrographs. Fig. 4.10 (B-D) shows that and PVC-PVP-H [1.6] membranes considerably reduce biofilm formation. Although certain colonization was observed, the comparison with PVC membranes (A-C) indicated significantly reduced bacterial growth and biofilm formation. The microbial colonization of PVC-PVP and PVC-PVP-H [0.8] membranes are shown in Fig. 4.10 (E-H) Combining physicochemical and biological data, we showed that the introduction of the hyperbranched polymeric nanomaterial Helux reduced biofouling by affecting the integrity of microbial cell membranes. Besides, the higher hydrophilicity of Helux-functionalized membranes resulted in higher permeability and decreased irreversible organic fouling. Overall, better hydrodynamic performance and fouling and biofouling resistance would benefit membranes with lower energy consumption, reduced use of chemicals for cleaning procedures and increased membrane life.

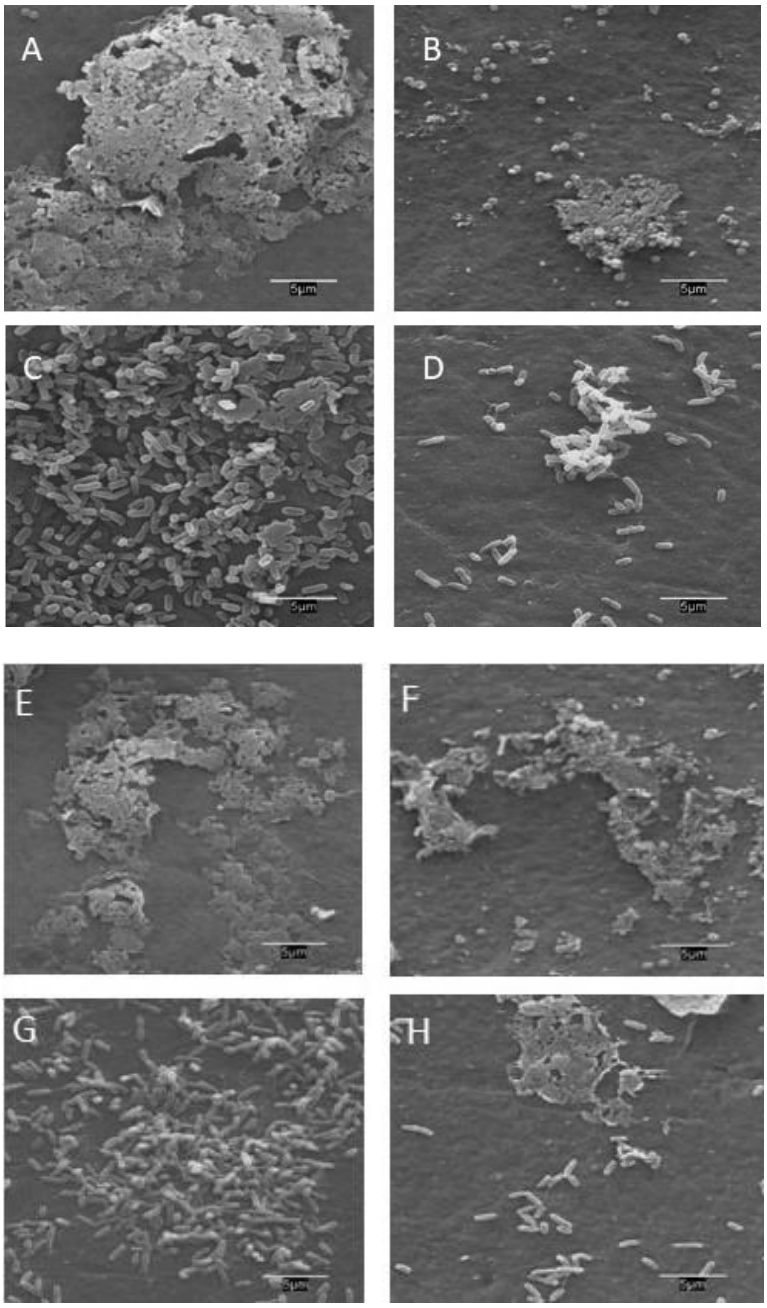

Figure 4.10. Microbial colonization of *S. aureus* (A-B-E-F) and *E. coli* (C-D-G-F) after exposure of PVC (A-C), PVC-PVP-H [1.6] (B-D), PVC-PVP (E-G) and PVC-PVP-H [0.8] (F-H) membranes to bacterial cultures for 20 h at 36 ºC.

4.5 Conclusions

In this study, new PVC ultrafiltration membranes functionalized with the hyperbranched polymeric nanomaterial Helux-3316 were prepared. The incorporated amine groups were evenly distributed within functionalized membranes and became firmly attached to the polymeric material by covalent bonds. No loss of nitrogen was observed during operation.

The surface ζ potential of Helux-PVC membranes increased from -34.1 ± 1.3 mV in PVC membranes to -14.0 ± 2.5 mV for Helux-loaded specimens, because of positively charged amines at neutral pH.

Helux-PVC membranes displayed higher water permeability due to their increased of hydrophilicity compared to PVC membranes and displayed significant resistance against irreversible organic fouling as observed from BSA filtration experiments.

The modified Helux-PVC membranes exhibited clear anti-biofouling character, with up to 1.0-log reduction of bacterial growth on membranes surface. The antimicrobial activity was attributed to the presence of positively charged groups in functionalized membranes, which induced damage of bacterial cell envelopes, eventually rendering cells non-viable.

4.6 References:

1. Buonomenna, M.G., *Membrane processes for a sustainable industrial growth.* RSC Advances, 2013. **3**(17): p. 5694-5740.
2. Koyuncu, I., et al., *Advances in water treatment by microfiltration, ultrafiltration, and nanofiltration* in *Advances in Membrane Technologies for Water Treatment: Materials, Processes and Applications*, A. Basile, A. Cassano, and N.K. Rastogi, Editors. 2015, Woodhead Publishing, Elsevier. p. 83-128.
3. Subhi, N., et al., *Organic fouling of ultrafiltration membrane: Detailed characterization by liquid chromatography with organic carbon detector (LC-OCD).* Separation Science and Technology, 2012. **48**(2): p. 199-207.
4. Shao, S., et al., *Biofouling in ultrafiltration process for drinking water treatment and its control by chlorinated-water and pure water backwashing.* Science of The Total Environment, 2018. **644**: p. 306-314.
5. Liu, C.X., et al., *Modification of membrane surface for anti-biofouling performance: Effect of anti-adhesion and anti-bacteria approaches.* Journal of Membrane Science, 2010. **346**(1): p. 121-130.
6. Yu, W., et al., *Pre-treatment for ultrafiltration: effect of pre-chlorination on membrane fouling.* Scientific Reports, 2014. **4**(1): p. 6513.
7. Nguyen, T., F.A. Roddick, and L. Fan, *Biofouling of water treatment membranes: A review of the underlying causes, monitoring techniques and control measures.* Membranes, 2012. **2**(4): p. 804-840.
8. Lemire, J.A., J.J. Harrison, and R.J. Turner, *Antimicrobial activity of metals: mechanisms, molecular targets and applications.* Nature Reviews Microbiology, 2013. **11**(6): p. 371-384.
9. Xu, Z., et al., *Antimicrobial polysulfone blended ultrafiltration membranes prepared with Ag/Cu_2O hybrid nanowires.* Journal of Membrane Science, 2016. **509**: p. 83-93.
10. Díez, B., et al., *Fouling and biofouling resistance of metal-doped mesostructured silica/polyethersulfone ultrafiltration membranes.* Journal of Membrane Science, 2017. **526**: p. 252-263.
11. Dong, L.X., et al., *Fabrication and anti-biofouling properties of alumina and zeolite nanoparticle embedded ultrafiltration membranes.* Desalination, 2015. **365**: p. 70-78.
12. Luque-Alled, J.M., et al., *Polyethersulfone membranes: From ultrafiltration to nanofiltration via the incorporation of APTS functionalized-graphene oxide.* Separation and Purification Technology, 2020. **230**: p. 115836.

13. Martín, A., et al., *Enhanced ultrafiltration PES membranes doped with mesostructured functionalized silica particles.* Desalination, 2015. **357**: p. 16-25.
14. Zheng, Y., et al., *Hyperbranched polymers: advances from synthesis to applications.* Chemical Society Reviews, 2015. **44**(12): p. 4091-4130.
15. Román, F., et al., *Study of hyperbranched poly(ethyleneimine) polymers of different molecular weight and their interaction with epoxy resin.* Materials, 2018. **11**(3): p. 410.
16. Żołek-Tryznowska, Z. and J. Izdebska, *Flexographic printing ink modified with hyperbranched polymers: Boltorn™ P500 and Boltorn™ P1000.* Dyes and Pigments, 2013. **96**(2): p. 602-608.
17. Gao, C., D. Yan, and H. Frey, *Promising dendritic materials: An introduction to hyperbranched polymers*, in *Hyperbranched Polymers: Synthesis, Properties, and Applications*, D. Yan, C. Gao, and H. Frey, Editors. 2011, Wiley. p. 1-26.
18. Xu, J. and Z.L. Xu, *Poly(vinyl chloride) (PVC) hollow fiber ultrafiltration membranes prepared from PVC/additives/solvent.* Journal of Membrane Science, 2002. **208**(1): p. 203-212.
19. Kameda, T., et al., *Chemical modification of poly(vinyl chloride) by nucleophilic substitution.* Polymer Degradation and Stability, 2009. **94**(1): p. 107-112.
20. Shaglaeva, N., et al., *Nucleophilic substitution of chlorine atoms in polyvinyl chloride.* Russian Journal of Applied Chemistry, 2008. **81**: p. 131-134.
21. Ramesh, S., et al., *FTIR studies of PVC/PMMA blend based polymer electrolytes.* Spectrochimica acta. Part A, Molecular and Biomolecular Spectroscopy, 2007. **66**(4-5): p. 1237-1242.
22. Kamaruddin, et al., *Synthesis of polyvinylpyrrolidone (PVP)-green tea extract composite nanostructures using electrohydrodynamic spraying technique.* IOP Conference Series: Materials Science and Engineering, 2017. **202**: p. 012043.
23. Zhu, J., et al., *Improved antifouling properties of poly(vinyl chloride) ultrafiltration membranes via surface zwitterionicalization.* Industrial & Engineering Chemistry Research, 2014. **53**(36): p. 14046-14055.
24. Qi, Y., et al., *Polythyleneimine-modified original positive charged nanofiltration membrane: Removal of heavy metal ions and dyes.* Separation and Purification Technology, 2019. **222**: p. 117-124.
25. Burns, D.B. and A.L. Zydney, *Buffer effects on the zeta potential of ultrafiltration membranes.* Journal of Membrane Science, 2000. **172**(1): p. 39-48.
26. Bryantsev, V.S., M.S. Diallo, and W.A. Goddard, *pKa calculations of aliphatic amines, diamines, and aminoamides via density functional*

theory with a Poisson−Boltzmann continuum solvent model. The Journal of Physical Chemistry A, 2007. **111**(20): p. 4422-4430.
27. Martín, I., et al., *Hyperbranched polymeric nanomaterials impair the freshwater crustacean Daphnia magna.* Environmental Pollution, 2019. **249**: p. 581-588.
28. Aryanti, P.T.P., et al., *Performance and characterization of PEG400 modified PVC ultrafiltration membrane.* Membrane and Water Treatment, 2015. **6**(5): p. 379-392.
29. Singh, R., *Introduction to Membrane Technology*, in *Membrane Technology and Engineering for Water Purification*, R. Singh, Editor. 2015, Butterworth-Heinemann. p. 1-80.
30. Kimura, K., et al., *Irreversible membrane fouling during ultrafiltration of surface water.* Water Research, 2004. **38**(14): p. 3431-3441.
31. Exley, S.E., et al., *Antimicrobial peptide mimicking primary amine and guanidine containing methacrylamide copolymers prepared by raft polymerization.* Biomacromolecules, 2015. **16**(12): p. 3845-3852.
32. Martins, A.F., et al., *Antimicrobial activity of chitosan derivatives containing N-quaternized moieties in its backbone: a review.* International Journal of Molecular Sciences, 2014. **15**(11): p. 20800-20832.
33. Malanovic, N. and K. Lohner, *Antimicrobial peptides targeting gram-positive bacteria.* Pharmaceuticals, 2016. **9**(3): p. 59.
34. Yang, Y.F., et al., *Membrane surface with antibacterial property by grafting polycation.* Journal of Membrane Science, 2011. **376**(1): p. 132-141.
35. Timofeeva, L. and N. Kleshcheva, *Antimicrobial polymers: Mechanism of action, factors of activity, and applications.* Applied Microbiology and Biotechnology, 2010. **89**: p. 475-92.
36. Giano, M.C., et al., *Injectable bioadhesive hydrogels with innate antibacterial properties.* Nature Communications, 2014. **5**(1): p. 4095.
37. Goetz, L., et al., *Superhydrophilic anti-fouling electrospun cellulose acetate membranes coated with chitin nanocrystals for water filtration.* Journal of Membrane Science, 2016. **510**: p. 238-248.
38. Azevedo, M.M., et al., *Polyethyleneimine and polyethyleneimine-based nanoparticles: novel bacterial and yeast biofilm inhibitors.* Journal of Medical Microbiology, 2014. **63**(9): p. 1167-1173.
39. Phillips, D.J., et al., *Evaluation of the antimicrobial zctivity of cationic polymers against Mycobacteria: Toward antitubercular macromolecules.* Biomacromolecules, 2017. **18**(5): p. 1592-1599.

CHAPTER 5

Electrospun composite membranes for fouling and biofouling control

Chapter 5. ELECTROSPUN COMPOSITE MEMBRANES FOR FOULING AND BIOFOULING CONTROL

5.1 Abstract

Composite ultrafiltration membranes were prepared by directly electrospinning a top layer of poly(acrylic acid) (PAA) and poly(vinyl alcohol) (PVA) onto polysulfone (PSU). The electrospun layer was cross-linked by heat curing and the previous irradiation of the PSU support allowed creating stable composites that did not detach under crossflow operation. The physicochemical properties of the composites were measured using FTIR spectroscopy, water contact angle, surface ζ-potential and permeation measurements. PAA-PVA electrospun layers increased membrane hydrophilicity and reduced organic fouling without affecting permeability and protein rejection performance. The antibacterial performance of the top-layer composites was investigated using *Escherichia coli* and *Staphylococcus aureus* strains and tracked counting colony forming units, SEM images of colonized specimens, and cell viability using confocal microscopy. The results showed that PAA-PVA coating resulted in clear antimicrobial performance, particularly for the bacterium *S. aureus,* which was attributed to the chelating of the cations stabilizing cell envelopes. Composite membranes were compared with neat PSU membranes in 48 h crossflow experiments. The composites showed good mechanical integrity and antimicrobial behaviour under flow conditions with average reduction of 1-log for electrospun composites exposed to *S.aureus* over PSU. This work demonstrates that top-layer nanofiber composites can lead to ultrafiltration membranes with enhanced functionalities.

5.2 Introduction

Membrane technology plays a leading role in providing a sustainable use of water and energy resources because of its better efficiency compared to other approaches [1, 2]. Ultrafiltration (UF) is membrane process suitable for large volume operations such as feed pre-treatment of reverse osmosis desalination units or the removal of colloids and microorganisms from reclaimed wastewater [3, 4]. Polysulfone (PSU), poly(ether sulfone) (PES), and poly(vinylidene difluoride) are widely used for producing UF membranes due to their high mechanical and chemical resistance [5]. However, the membranes prepared from these materials are prone to suffer the deposition of nonpolar solutes due to hydrophobic interactions [6]. As a consequence, permeate flux, separation efficiency and membrane lifetime decline during operation [7, 8]. The approaches proposed to limit the adsorption of organic solutes on ultrafiltration membranes include surface functionalization treatments and the use of blending additives to improve surface hydrophilicity or pore architecture [9-12]. Biofouling is the biotic form of organic fouling that describes the accumulation of microorganisms on membrane surface [13]. Biofouling decreases membrane permeability, reduces membrane performance, and supposes a risk of pathogen dissemination [14]. Once attached to a surface, microorganisms tend to originate biofilms in which cell communities grow protected by an extracellular polymeric matrix acting as defence against adverse conditions that makes their eradication a very difficult task [15, 16]. The strategies followed to prevent or limit membrane biofouling include the use of disinfecting agents and the design of low-biofouling surfaces [17, 18]. The use of antimicrobial nanoparticles to decorate the active layer of membranes or incorporated into the casting solution has also been explored [19-21].

Electrospinning is a electrohydrodynamic technique suitable for the production of submicron polymeric fibres in which a jet of fluid is charged by a high-voltage power source and flows of a capillary tube when the electrostatic force overcomes fluid surface tension [22]. During the path to a grounded electrode, the solvent evaporates, and the solid fibre is collected as nonwoven mat or as an ordered array of fibres depending on the collector geometry [23]. The fabrication of electrospun submicrometric fibres have received increased attention in recent years due to the many potential uses of nanofibers in diverse fields [24]. Their main advantages are a high surface to-volume ratio, the versatility to produce different materials via chemical modification, and the creation of coaxial structures [25, 26]. The incorporation of high-porosity nanofiber layers onto conventional ultrafiltration membranes has been explored to improve fouling resistance, which was tentatively attributed to the decreased contact time between protein and filtrating layer [27]. A similar approach consisting of placing electrospun nonwovens onto commercial scaffolds was able to create ultrafiltration composites from microfiltration fabrics [28]. Nanofibrous composites have also been prepared from electrospun poly(ethylene terephthalate) and polyacrylonitrile nanofibers acting as support layer of thin active coatings with the purpose of increasing membrane resistance or water permeability [29, 30]. The replacement of UF layer in conventional thin-film membranes by electrospun nanofibrous membranes has also been explored to provide improved flux [31]. Additionally, electrospun polymeric substrates have been proposed as low tortuosity porous layer in thin film composite nanofiltration membranes with improved permeability [32].

The purpose of this work was to create composite ultrafiltration membranes by directly electrospinning a top layer onto the surface of PSU ultrafiltration membranes, which were previously irradiated to create anchoring points. The polymers chosen were poly(acrylic acid) (PAA) and poly(vinylalcohol) (PVA).

Both are water-soluble polymers that can be easily cross-linked to produce insoluble materials [33]. Besides, it has been shown that PAA-containing nanofibers fibres exhibit important antibacterial activity attributed to the quelation of the divalent cations stabilizing bacterial envelopes [34, 35]. The composites were characterized using SEM spectroscopy, FTIR, water contact angle (WCA), surface ζ-potential, and permeation measurements. The antibacterial and antibiofilm behaviour was studied using the bacteria *Escherichia coli* and *Staphylococcus aureus.*

5.3 Materials and methods

5.3.1 Chemicals.

Polysulfone (PSU, molecular weight 60 kDa) and 1-methyl-2-pyrrolidone (NMP) were obtained from Across Organics. Poly(vinylpyrrolidone) (PVP, molecular weight 40 kDa), poly(vinyl alcohol) (PVA, molecular weight 89−98 kDa, and poly(acrylic acid) (PAA, molecular weight 450 kDa) were acquired from Sigma-Aldrich. Dimethyl sulfoxide (DMSO, 99.9%) and bovine serum albumin (BSA) were obtained purchased from Sigma-Aldrich. Live/Dead BacLight kit and FilmTracer FM 1-43 Green Biofilm Stain were purchased from Invitrogen (Thermo-Fisher, Waltham, MA). Ultrapure water with a resistivity of 18.2 MΩ cm^{-1} was produced by a Direct-Q 5 Ultrapure Water Systems (Millipore, USA) The components of culture media were purchased from Laboratorios Conda (Spain).

5.3.2 Preparation of Electrospun Composite Membranes.

The composite membranes were created by electrospinning a layer of PAA−PVA nanofibers on the top surface of PSU ultrafiltration membranes and are named in what follows as PAA-PVA [number]@PSU, where “number” refers to the weight density of electrospun layer as indicated in Table 5.1 and PAA−PVA@PSU refers to any of the composites.

Table 5.1. Properties of the Synthesized Composites.

Membrane	UV	Weight density of fibers (mg/cm^2)	Surface ζ-potential (mV) at pH.7	Water contact angle (WCA º)	-COOH (mmol/g)
PSU	-	-	-30.1±1.8	65.3±3.1	0.0±0.5
PSU[0]	+	-	-29.3±0.4	60.1±0.8	0.0±0.6
PAA-PVA[1]@PSU	-	0.03±0.01	-31.9±0.6	65.5±0.9	0.9±0.1
PAA-PVA[2]@PSU	-	0.04±0.02	-31.6±0.9	62.6±1.3	2.9±1.4
PAA-PVA[3]@PSU	-	0.05±0.01	-31.1±2.8	58.8±1.4	4.1±0.1
PAA-PVA[4]@PSU	-	0.12±0.03	-33.5±2.8	55.6±1.1	4.2±0.1
PAA-PVA[5]@PSU	+	0.46±0.07	-35.2±3.8	52.1±4.2	5.8±0.1
PAA-PVA[6]@PSU	+	0.83±0.19	-37.1±1.9	48.2±3.3	8.5±0.2
PAA-PVA[7]@PSU	+	1.18±0.28	-38.1±1.4	43.8±0.9	8.9±0.3
PAA-PVA[8]@PSU	+	1.85±0.32	-41.2±0.1	39.0±1.7	11.6±0.2

The support membranes were ultrafiltration membranes prepared using phase inversion from a casting solution containing 5 wt % PVP and 15 wt % PSU with NMP as solvent. The casting solution was stirred until total dissolution and kept at least 24 h at room temperature. Once the homogeneous solution was prepared, the films were cast to 200 µm thickness using an automatic film applicator AB3120 (TQC, The Netherlands). The prepared films were immediately immersed in a coagulation bath of distilled water for phase separation. The membranes were rinsed in distilled water for at least 24 h before drying. For a set of membranes, and prior to the electrospinning process, the surface of PSU membranes was functionalized with UV light using a cross-linker equipped with 254 nm lamps. The irradiation time was set at 5 min, which was enough to obtain a clear FTIR carbonyl band at 1710 cm^{-1} (Figure 5.3) without compromising the integrity of the skin layer. The latter was assessed by the absence of significant permeability changes and BSA rejection over PSU non-treated membranes. The purpose was to provide anchoring points for the reaction with carboxyl or hydroxyl groups of the electrospun fibres to ensure enough mechanical resistance for the electrospun composite [36].

The coating step with PAA-PVA nanofibers was performed by electrospinning on the top of the skin layer of PSU membranes held on the grounded collector. The electrospinning solution consisted of PAA (100 mL, 8 wt %) and PVA (11 mL, 15 wt %) in ultrapure water. The solution containing PAA and PVA was stirred (2h) and degassed before being electrospun. Details on the electrospinning process and parameters can be found elsewhere [35].

The electrospinning time was set to less than 90 min, which corresponded to < 2 mg/cm^2 for the membranes with higher PAA-PVA loadings as indicated in Table 5.1. This was consistent with the purpose of creating a layer functionalizing the outer surface of the ultrafiltration membrane that did not introduce additional hydraulic resistance or microfiltration functionality. The electrospinning apparatus consisted of a Glassman dc power connected to the needle tip and the grounded collector. The collector was a flat piece of steel covered with aluminium foil in which specimens of the PSU membranes prepared as described previously were carefully placed with the skin layer outward. The electrospun membranes were dried (50 °C, 24 h), after which they were cross-linked at 140 °C (30 min), washed with ultrapure water, and vacuum-dried (50 °C, 24 h). The whole preparation process is synthesized in the scheme shown in Figure 5.1.

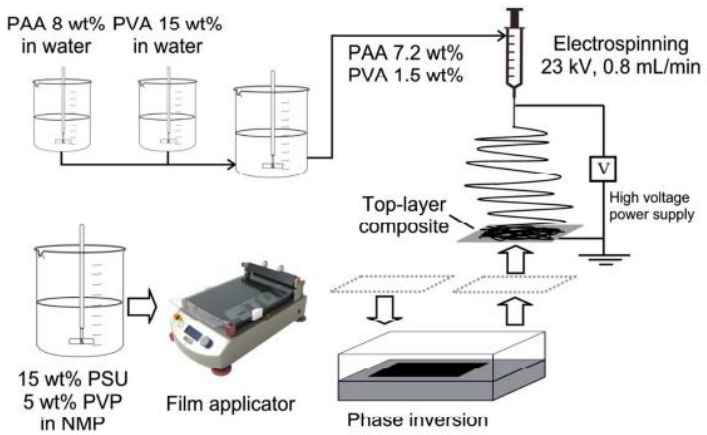

Figure 5.1. Scheme showing the preparation of composite membranes.

5.3.3 Membrane Characterization.

Attenuated total reflectance Fourier transform infrared (ATR-FTIR) spectra were recorded using a Thermo-Scientific Nicolet iS10 equipment.

The surface morphology of membranes was studied by scanning electron microscopy (SEM) in a Zeiss DSM-950 apparatus operating at 25 kV on gold-coated samples.

The surface charge of membranes was determined by electrophoretic light scattering in a Zetasizer NanoZS apparatus equipped with a ZEN 1020 Cell (Malvern Instruments, U.K.). The measurements consisted of determining the electrophoretic mobility of a tracer (0.5 wt % PAA, 450 kDa) as a function of the distance to the surface of specimens glued to the sample holder. Further details are given elsewhere [37].

Water contact angle (WCA) was used to determine surface membrane hydrophilicity. Measurements were performed using the sessile drop technique in a Krüss DSA25 equipment at room temperature. At least four drops in different positions were taken for each measurement.

The content of carboxyl groups in composite membranes was measured by titrating deprotonated samples with hydrochloric acid under inert atmosphere.

5.3.4 Membrane Filtration Performance.

Pure water flux, protein rejection, and water flux recovery ratio were measured under continuous flow conditions by means of a crossflow cell module with 20 cm^2 (40 mm × 50 mm) membranes of connected to a 2 L vessel. Membrane permeation flux was determined for transmembrane pressure (TMP) in the 1-4 bar range. Four specimens of each membrane were tested, and all of them were maintained in distilled water during 24 h and

compacted for at least 30 min at 4 bar at room temperature before measurements.

Fouling measurements were performed using BSA as a model for protein rejection. BSA solution 1 g L^{-1} prepared in phosphate-buffered saline (PBS, 0.1 M, pH 7.2) was used for fouling assays, which were performed at 2 bar TMP and 0.80 m s^{-1} linear velocity. Pure water filtration and BSA filtration experiments were performed to evaluate water fluxes, J^{i}_{w}, before and after BSA filtration followed by membrane cleaning for at least 30 min, J^{f}_{w}. The experiments with BSA were conducted at the time required to filter 0.5 g/cm^2 BSA.

Flux recovery ratio (FRR) was calculated according to the following expression:

$$\text{FRR (\%)} = \left(\frac{J_w^f}{J_w^i}\right) \times 100 \qquad \text{Eq.1}$$

FRR represents the irreversible fouling and the part of the reversible fouling due to the formation of a cake layer (excluding concentration polarization).

$$\text{R (\%)} = \left(1 - \frac{c_p}{c_f}\right) \times 100 \qquad \text{Eq.2}$$

Solute rejection, R, was determined from BSA concentration in permeate and feed, C_f and C_p, respectively, measured from UV absorbance at 261 nm in a Shimadzu SPD-6AV spectrophotometer.

5.3.5 Antimicrobial Effect and Antibiofouling Behaviour.

Neat PSU and PAA-PVA@PSU composites were tested for their antibacterial activity against two different microbial strains, the Gram-positive bacterium *S. aureus* (CECT 240, strain designation ATCC 6538P) and the Gram-negative bacterium *E.coli* (CECT 516, strain designation ATCC 8739). The microorganisms were reactivated using nutrient broth (NB) at pH 7.0 ± 0.1 and 36 °C under agitation (250 rpm) and followed by optical density (OD) at 600

nm. For the antimicrobial runs, NB was diluted 500-fold. The antimicrobial effect of composite membranes was evaluated by determining colony-forming units (CFU) under static and crossflow conditions as prescribed in ISO 22196 with minor modifications.

For the static test, dried membranes in accurately weighed pieces were placed into sterile 24-well plates with neat PSU membranes as negative controls. A bacterial suspension was prepared by diluting 0.4 mL of a 10^6 cell/mL cultures in 2.0 mL NB 1/500, which was added into the each well and incubated for 20 h at 36 °C. After exposure, the membranes were washed with PBS and shaken 10 min at 5 °C to remove non-adhered cells. Adhered cells were recovered using SCDLP (soybean casein digest broth with lecithin and poly(oxyethylene) sorbitan monooleate) following ISO 22196. The supernatant liquid after 20 h exposure and the suspension resulting from cell detachment were serially diluted in PBS, and colony counting was performed after inoculation of Petri dishes containing NB and incubation at 36 °C for 16 h. At least three replicates of at least two serial dilutions were used for each sample, and all experiments were replicated until obtaining sufficient accuracy.

In the crossflow device, the antimicrobial effect of composite membranes was tested by checking specimens with the maximum amount of PAA-PVA against the growth of *S. aureus*. For it, neat PSU and PAA-PVA@PSU composites were located in the crossflow module and connected to the feed flask that contained an initial bacterial concentration of 10^6 cells/mL in diluted nutrient broth medium (NB 1/500) at 25 °C. Before every experiment the cross-flow unit was carefully cleaned and disinfected using a method adapted from Jeong et al. [38]. Briefly, 0.5% sodium hypochlorite was circulated for 2 h followed by twice water rinsing for 10 min. Afterward, trace organic matter was removed by circulating 5 mM EDTA, pH 11, for 30 min, followed by water rinsing and 2 mM sodium dodecyl sulfate, pH 11, for 30 min, followed by new

water rinsing. Sterilization was performed by autoclaving the entire unit at 121 °C for 2 h. The connecting tubes were also sterilized as described previously [39]. After 48 h samples from the retentate were collected and CFU counted according to the procedure describe before. Forty-eight hours was set as a practical limit because the device could not be stopped or left unattended. The membranes were then removed, carefully washed in PBS, and incubated in SCDLP medium to detach the bacterial and determinate the number of viable cells attached to the membrane surface.

Bacterial viability was assessed by means of Live/Dead BacLight Bacterial Viability kit (Molecular Probes). The method is based on two fluorescent nucleic acid probes, one of which, SYTO9, penetrates intact cell membranes marking viable cells in green, while the other, propidium iodide (PI), is only internalized by membrane-damaged cells that become red-stained. Confocal micrographs were taken in a fluorescent microscope Leica Microsystems SP5. Cell bodies on membrane surface were visualized by means of FilmTracer FM 1-43. Green Biofilm Cell Stain used as indicated by the manufacturer. Stained cells were visualized by confocal laser microscopy (LEICA TCS-SP5) using an excitation/emission maxima wavelength of 472/580 nm. The nonfluorescent water-soluble dye inserts into the surface of bacterial membranes where they become intensely fluorescent. The formation of biofilms onto membrane surface was also assessed by SEM using membrane specimens previously cleaned, fixed, and dehydrated.

5.4 Results and discussion

5.4.1 Membrane Characterization.

The properties of base and irradiated PSU membranes and the electrospun PAA-PVA@PSU composites are shown in Table 5.1. Specimens PAA-PVA[1] @PSU to PAA–PVA[4]@PSU were prepared onto non-irradiated PSU membranes, while membranes designated as PAA-PVA[5]@PSU to

PAA−PVA[8]@PSU corresponded to the higher coating coverage of the electrospun top layer. Irradiated PSU membranes, marked as "+" in Table 5.1, were UV treated for 5 min. The reason for this procedure was that PAA-PVA loadings above 0.1 mg cm^{-2} tended to detach from non-irradiated PSU base membranes when running 24 h experiments in cross-filtration regime (2 bar TMP, linear velocity 0.80 m s^{-1}) as shown by visual inspection of micrographs. However, preirradiated membranes kept fibres attached to the PSU membrane for all tested loadings (up to 1.85 mg cm^{-2}). Cross-linking treatment (30 min, 140 °C) was used to stabilize the electrospun layer rendering water insoluble composites. The electrospun PAA-PVA layers deposited and cross-linked onto irradiated supports preserved their fibrous structure after 48 h in all cases, the stability being attributed to the interaction between PAA-PVA moieties and oxygenated groups from the surface of irradiated PSU [40].

Accordingly, WCA decreased for irradiated PSU membranes as shown in Table 5.1. Membrane surface charge measured using surface ζ-potential at pH 7.0 is also shown in Table 5.1. Surface charge was negative in all cases with more negative values for PAA-PVA composite membranes, and even more negative for increasing amounts of the electrospun layer up to a value as low as -41.2 ± 0.13 mV. Uncoated PSU displayed negative charge, with ζ-potential -30.1 ± 1.8 mV. The negative charge of PSU membranes, which does not contain charged groups, is usually explained by the adsorption of hydroxide ions on membrane surface [41]. The reason for the more negative charge of PAA-PVA loaded composites was the presence of carboxylate moieties in the PAA backbone [35].

Membrane surface hydrophilicity was studied by measuring the WCA between the membrane surface and the air-water interface. The values obtained are also presented in Table 5.1. WCA decreased for increasing amounts of the electrospun layer, which can be explained by two factors: first, because of the

presence of hydrophilic groups in PAA-PVA polymeric fibre, and second, because surface roughness decreases the measured contact angles in hydrophilic surfaces (and increases in hydrophobic surfaces) from the values measured in the chemically identical flat surfaces.

Figure 5.2 shows the ATR-FTIR spectra of the outer layer of uncoated PSU and PAA-PVA@PSU composites. For the PSU membrane, the bands at 1585, 1504, 1489, and 1100 cm^{-1} are due to the vibrations of PSU aromatic ring (C=C stretching). The peak at 1244 cm^{-1} corresponds to the PSU aromatic ether bond (−C−O−C−), while the weak stretching vibrations of the C−H bonds of PSU were observed in the 2860−2900 cm^{-1} region [42].

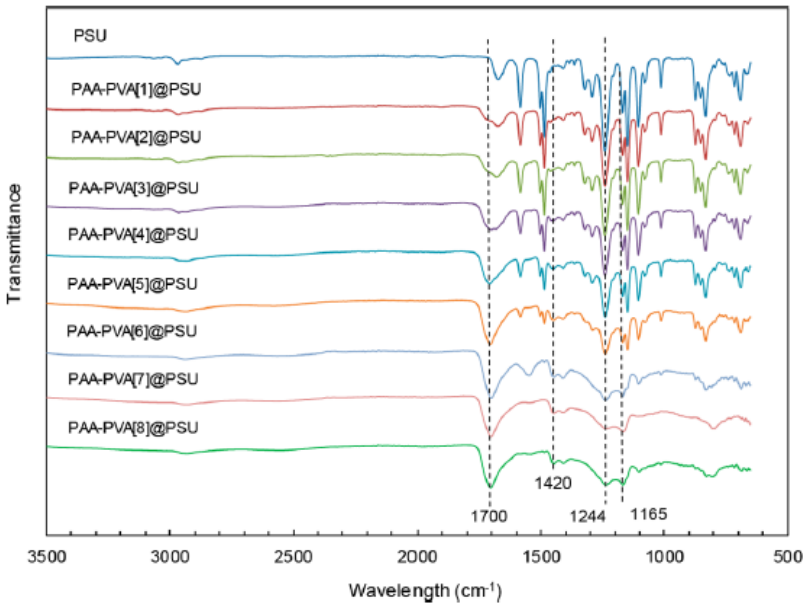

Figure 5.2. ATR-FTIR spectra of PAA−PVA@PSU composite membranes

Most new peaks appearing in the composite membrane are characteristic of the PAA-PVA coating such as the C-H alkyl stretching vibration (2850-3000 cm^{-1}). The characteristic carboxyl stretching band of PAA appears at 1700 cm^{-1}. The symmetric and antisymmetric stretching of carboxylate ion (COO-) appeared at 1420 cm^{-1} [43]. The formation of anhydride and ester moieties

during heat curing of PAA−PVA blends was assessed elsewhere by tracking the decrease of the C=O stretching vibration and the growth of the C−O−C stretching bands, observed here at 1165 cm^{-1} [35, 44]. The IR spectrum of the composite samples with lower amount of polymeric coating was dominated by the bands attributed to PSU, which decreased for higher PAA-PVA loadings as the surface of the composite material became covered by the polymeric electrospun layer.

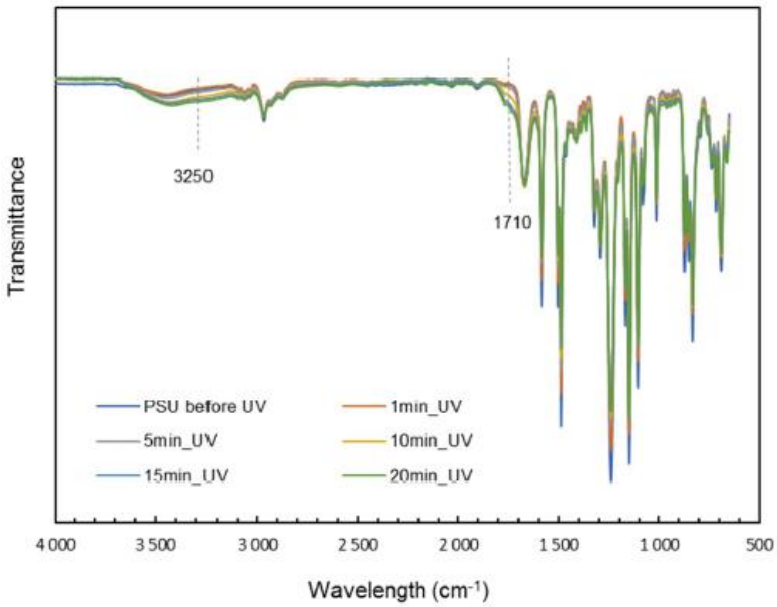

Figure 5.3. ATR-FTIR spectra of PSU base membranes before and after UV irradiation

ATR-FTIR spectra irradiated and non-irradiated PSU membranes are shown in Figure 5.3. PSU irradiated membranes showed a clear OH stretching band at 3400 cm^{-1} and a broad band at 1725 cm^{-1} due to the C=O stretching of carboxyl groups. The changes can be explained by the oxidative photolysis of aromatic moieties [45]. The broad band at 1500-1900 cm^{-1} corresponded to carbonyl (C=O) groups, the band in the 2500-3700 cm^{-1} region was due to the presence of hydroxyl groups, and the band at 1100-1350 cm^{-1} region was due to C−O single bonds [46]. The decrease observed in the band at ~1325 cm^{-1}, due to

bond scissions of C−O and C−S (Figure 5.3), agreed with the formation of common photoproducts of the diphenylethersulfone units [47].

The morphology of composite membranes is shown in Figure 5.4 as a series of surface SEM images of representative specimens. Figures 5.4 a-c correspond to the upper view of membranes prepared with different PAA-PVA loadings after heat curing. The images indicated that PAA-PVA electrospun material formed a continuous layer on top of the PSU support consisting of well-formed fibres without beading or other flaws that kept their fibrous structure after heat curing. Figures 5.4 d-f show cross-sectional SEM images of PSU and composite membranes. Figure 4d corresponds to neat PSU and displayed the usual asymmetric structure with a top skin layer over a porous substrate. Composite specimens (Figures 4e and 4f) exhibited similar morphological structure with a well-developed layer of electrospun fibres with a thickness in the few microns range.

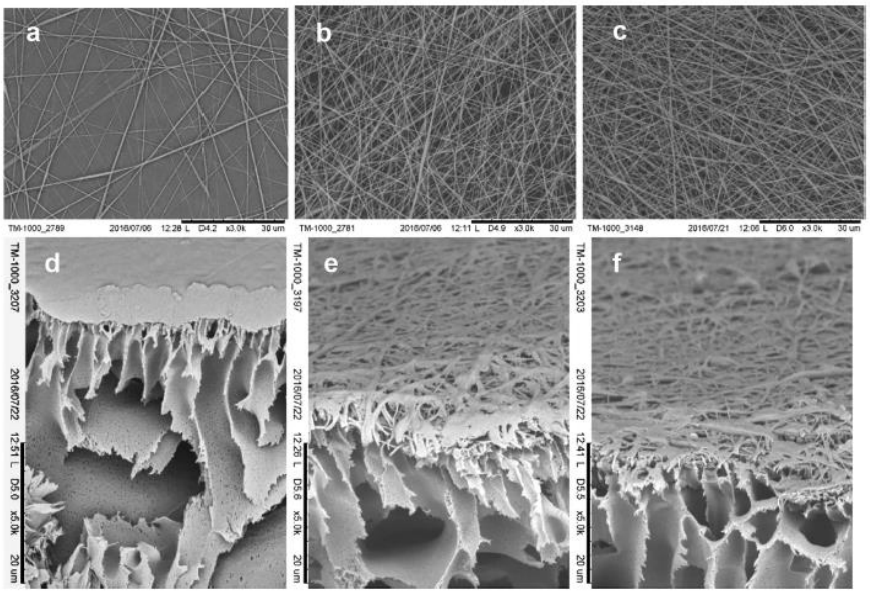

Figure 5.4. (Upper row) SEM images of composite membranes in upper view: (a) PAA−PVA[1]@PSU, (b) PAA−PVA[5]@PS U, and (c) PAA−PVA[8]@PSU. (Lower row) Cross-sectional SEM images of (d) neat PSU, (e) PAA−PVA[5]@PS, and (f) PAA−PVA[8]@PSU.

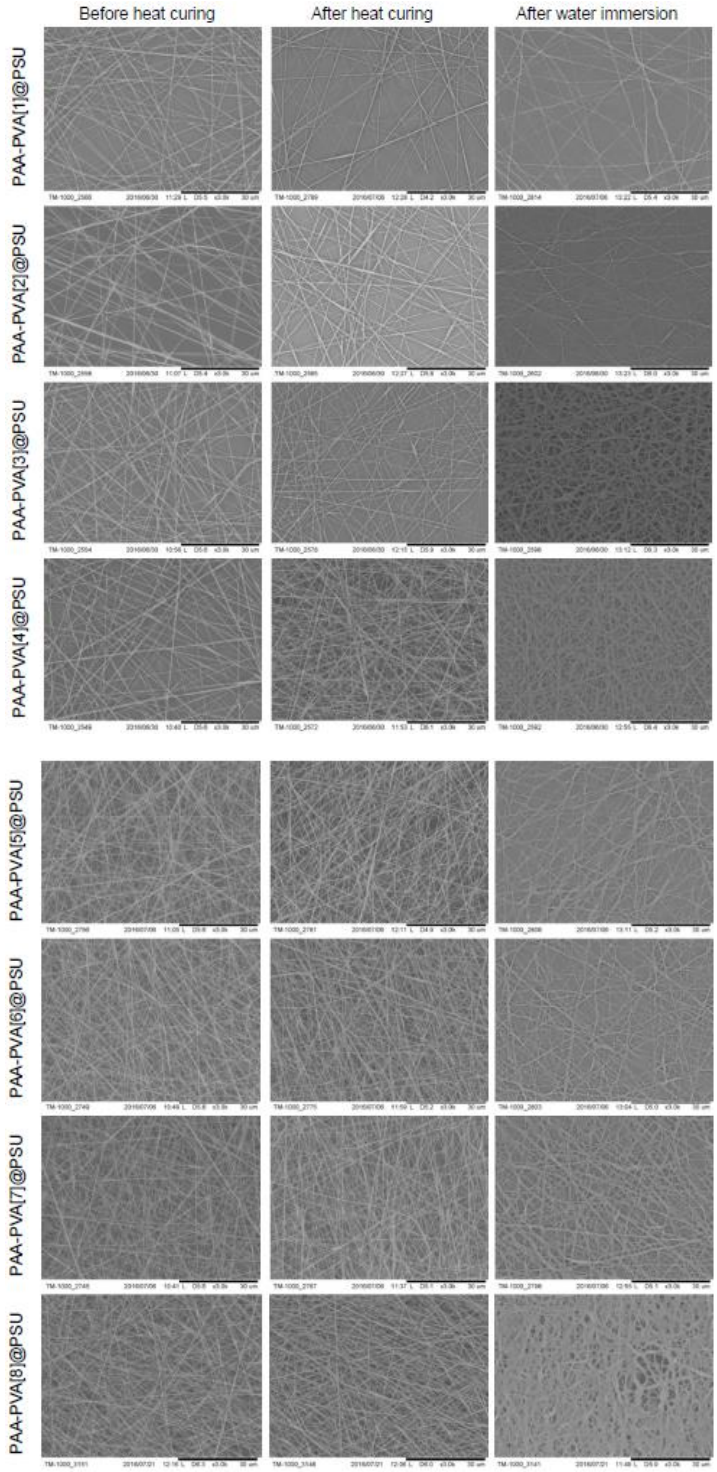

Figure 5.5. SEM micrographs of PAA.PVA electrospun layer (upper view) before and after heat curing and after water conditioning.

Figure 5.5 shows a complete set of upper view SEM micrographs before and after heat curing and after water conditioning. The electrospun layer preserved its fibrous structure after 24 h water immersion and did not detach from the support. The average diameter of fibres in the electrospun layer was 220 ± 50 nm that increased after water immersion to 440 ± 80 nm due to the swelling behaviour of the polymeric material [48].

5.4.2 Filtration Performance.

The results of water permeability for composite PSU membranes are shown in Figure 5.6 that shows a slight increase in water permeability as the weight load of PAA-PVA increased. Irradiation treatment resulted in a slight increase of water permeability compatible with the higher surface polarity. The permeability of composite specimens also increased slightly with the incorporation of the electrospun layer.

The results showed that the incorporation of the electrospun layer did not add an important additional hydraulic resistance, and, therefore, the pores of the skin ultrafiltration layer did not become blocked by the electrospun material with only a slight decrease in permeability from irradiated membranes, PSU(0), to the composite specimens PAA-PVA[5-8]@PSU prepared using irradiated supports. This result suggests that the pore structure of the skin layer was not affected by the electrospun material. The enhancement of membrane permeability obtained by the use of polymeric mixtures or blending additives is due to the more hydrophilic pores that interact with water molecules and facilitate water flux [49]. Accordingly, significant changes in water permeability were not expected.

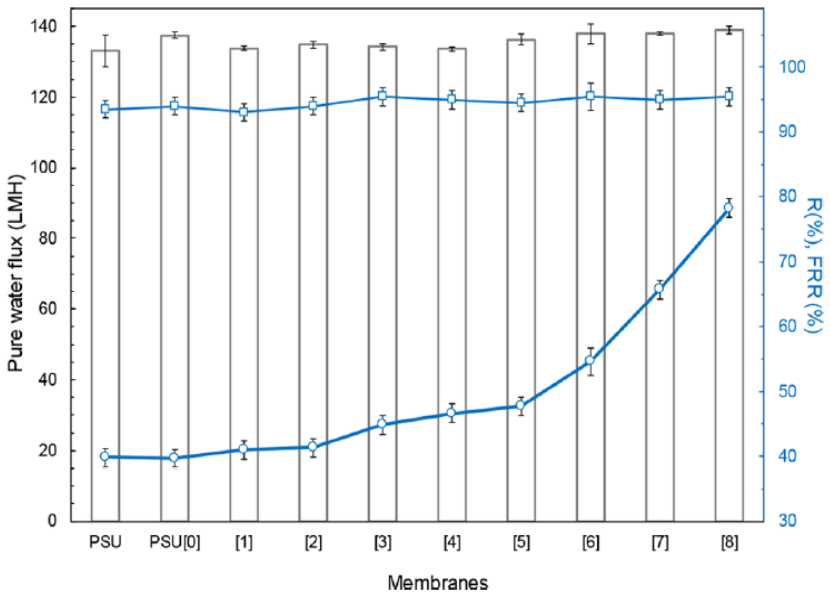

Figure 5.6. Pure water flux (bars), BSA rejection ratio (R, □), and flux recovery ratio (FRR, ○) for the tested membranes. The numbers refer to the nomenclature explained in Table 5.1. Error bars represent standard deviation.

Membrane fouling was studied in cross-flow mode by filtering 1 g L^{-1} BSA aqueous solution in rejection experiments conducted at 2 bar TMP. The rejection was studied for neat PSU and composites membranes covered with different amount of PAA-PVA nanofibers. The results were very similar (>90%) for protein rejection in all the tested specimens ranging from 93.5 ± 0.7% (PSU) to 95.5 ± 0.6% for the highest PAA-PVA coverage (Figure 5.6). Consequently, the incorporation of the electrospun top layer of PAA-PVA did not affect protein retention as expected considering the base PSU membrane bearing the ultrafiltration layer was the same. The fact that membranes prepared from irradiated supports did not show significant deviations with pristine PSU is an additional proof of the lack of degradation upon UV exposure.

The antifouling performance was determined by measuring the water flux decline before and after filtration of BSA solution (eq 1). The results, also shown in Figure 5.6, indicated that the presence of the electrospun layer increased the flux recovery ratio with the amount of PAA-PVA nanofibers. The

maximum loading of the electrospun layer resulted in flux recovery ratio of 78.3 ± 0.3% contrasting with 39.8 ± 0.2% for neat PSU membranes. The reduction of organic fouling (irreversible plus cake layer) by 38.4% can be exclusively attributed to the incorporation of the layer of electrospun PAA−PVA fibres onto the PSU base membranes. The increase of membrane hydrophilicity is a well-known way of reducing membrane fouling due to a lower interaction with colloidal and biological species [50, 51]. Another effect contributing to the antifouling performance of composite membranes is the electrostatic repulsion between top layer membrane and negatively charged substrates, which is the case of BSA, negatively charged at pH 7 (ζ-potential −15 ± 3 mV) and with isoelectric point 4.7−4.9 [52]. Surface roughness could result in the retention of particles that could fit into the microsized pores of the electrospun material. This would be the case for bacteria and other colloids. However, the negative charge of the top layer would contribute to exclude negatively charged solutes, which are by far the most commonly found in wastewater.

5.4.3 Antimicrobial Performance.

Figure 5.7 shows the results of microbial growth tests, Figure 5.7a for membranes kept in contact with *E. coli* and Figure 5.7b for *S. aureus.* In all cases, the initial microbial load was 6.7×10^4 cells/mg, and the incubation took place for 20 h at 36 °C. After the incubation period the cells attached to membranes were removed as explained before, and the resulting liquid plated in serial dilutions for viable cell counting.

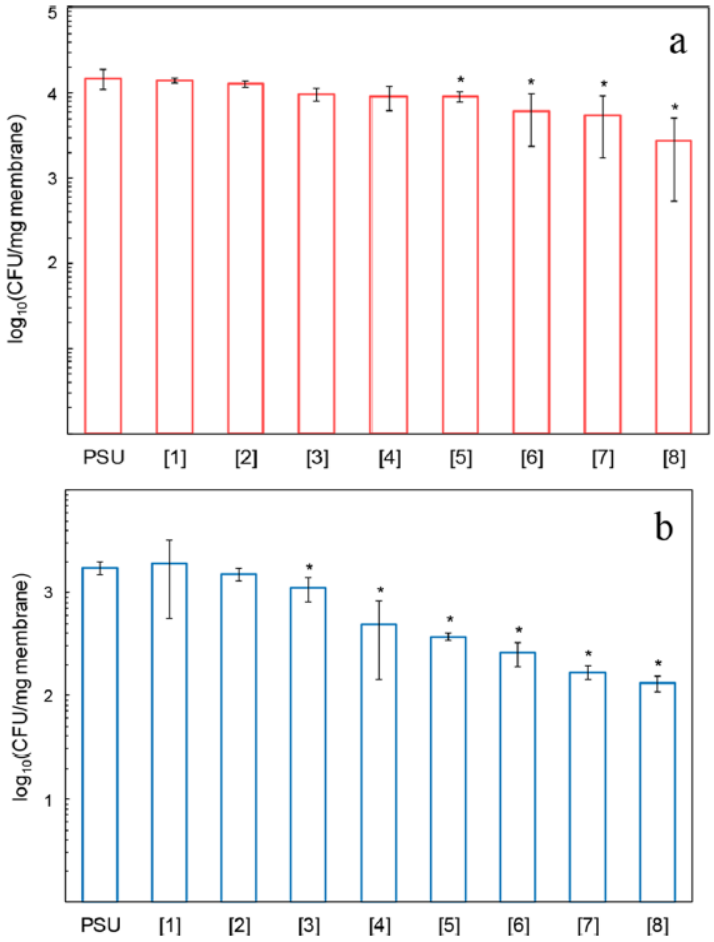

Figure 5.7. Colony-forming units (CFU) for microorganisms detached from membranes exposed to (a) *E. coli* and (b) *S. aureus*. The cultures were kept in contact with bacteria for 20 h at 36 °C. The numbers refer to the nomenclature explained in Table 5.1. Error bars represent standard deviation.

CFU counting for the culture liquid in contact with membranes after separating it from membranes at the end of the exposure experiment is shown in Figure 5.8. The results revealed a considerable impairment for both bacteria, with >1-log reduction (1-log represents 90% reduction) for *S. aureus* growth on membrane surface and 2.5-log reduction in the medium in contact with membranes. The corresponding figures for *E. coli* were <1-log for cells detached from the surface and 1.8-log reduction for the liquid culture medium.

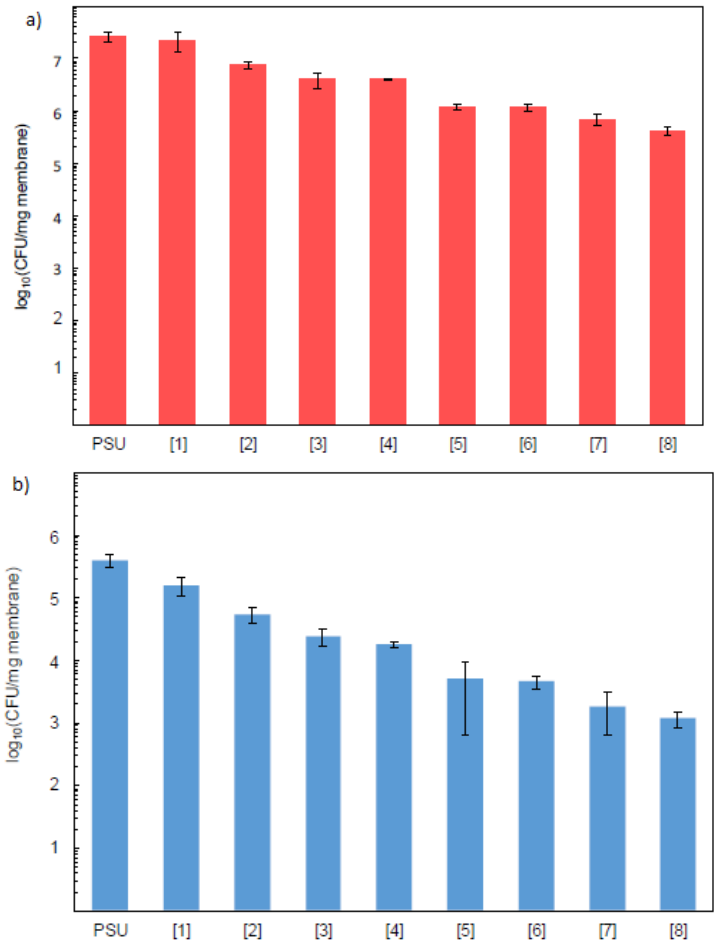

Figure 5.8. Colony-forming units (CFU) in the liquid media in contact with membranes for (a) *E. coli* and (b) *S. aureus*. The data correspond to the membrane compositions shown in Table 1. The cultures were kept in contact with bacteria for 20 h at 36 °C.

The antimicrobial effect of PAA containing polymers has been attributed to the chelation of the cations stabilizing bacterial envelopes, based on measurements of bacterial surface charge and intracellular calcium [35, 53]. The role of PAA as calcium chelator is also explained by theoretical findings showing that the sequestration process is spontaneous due to the increase in entropy rather than to electrostatic forces [54]. Further experimental evidence demonstrated that the binding constant of calcium to the bacterial cell wall was high enough to allow the removal of calcium as Ca-PAA

complexes [55]. Figure 5.7 also shows that *S. aureus* was considerably more impaired than *E. coli* after exposure to PAA-PVA@PSU composites. For the case of *S. aureus*, the specimens with 0.05 mg/cm^2 electrospun layer already displayed a significant antimicrobial effect, whereas for *E. coli* the effect was only clear at loadings of 0.46 mg/cm^2 or higher. (The asterisks in Figure 5.7 indicate results significantly different from PSU controls.) For *S.aureus,* the decrease of CFU in the liquid in contact with membranes was over 2-log compared to PSU controls, a result that can be attributed to the tendency of both strains to form biofilms.

The external differences between *S.aureus* and *E. coli* explain the different effect based on their cell wall structures. The outer membrane of *E. coli* is a lipid bilayer that includes a complex lipopolysaccharide leaflet, which includes phosphate groups electrostatically balanced with divalent cations that stabilize the assembly [56]. The removal of such cations from the outer envelope of Gram-negative bacteria by PAA affects membrane integrity by breaking the interlocking of lipopolysaccharide molecules. *S. aureus*, however, is a Gram-positive bacterium, which instead of an outer membrane possesses a thick peptidoglycan layer [57]. The phosphate groups of teichoic acid and the negatively charged moieties of peptidoglycan provide a net negative charged surface that requires cationic counterions to provide membrane integrity. It was shown that calcium is the preferred cation for stabilizing the cell wall of Gram-positive bacteria [58]. Later, it has been reported that the binding affinity of calcium for peptidoglycan was lower than that for PAA, this being the probable cause for the damage observed upon exposure of bacterial cells to the composite membranes containing PAA [59].

Representative SEM images of composite membranes after exposure to *E. coli* and *S. aureus* are shown in Figure 5.9 and Figure 5.10, respectively.

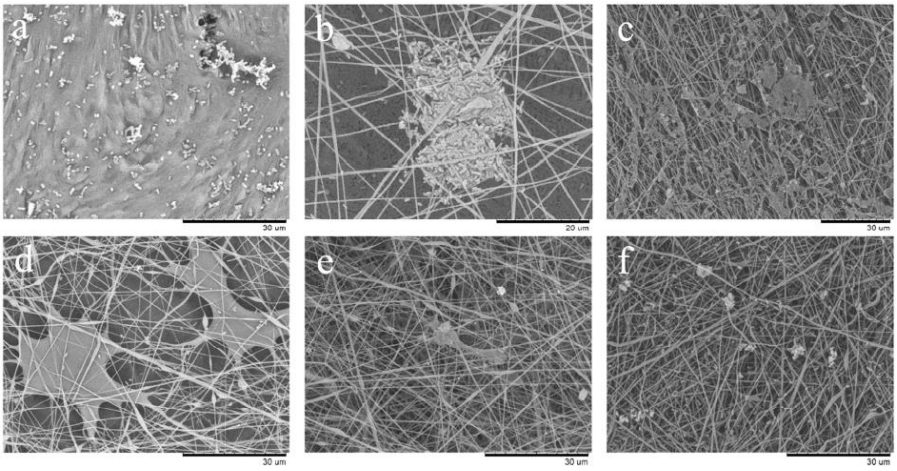

Figure 5.9. SEM images of the upper surface of composite membranes after 20 h contact with *E. coli* cultures at 36 °C. (a) PSU, (b) PAA-PVA[1]@PSU, (c) PAA-PVA[3]@PSU, (d) PAA-PVA[5]@PSU, (e) PAA-PVA[7]@PSU and (f) PAA-PVA[8]@PSU.

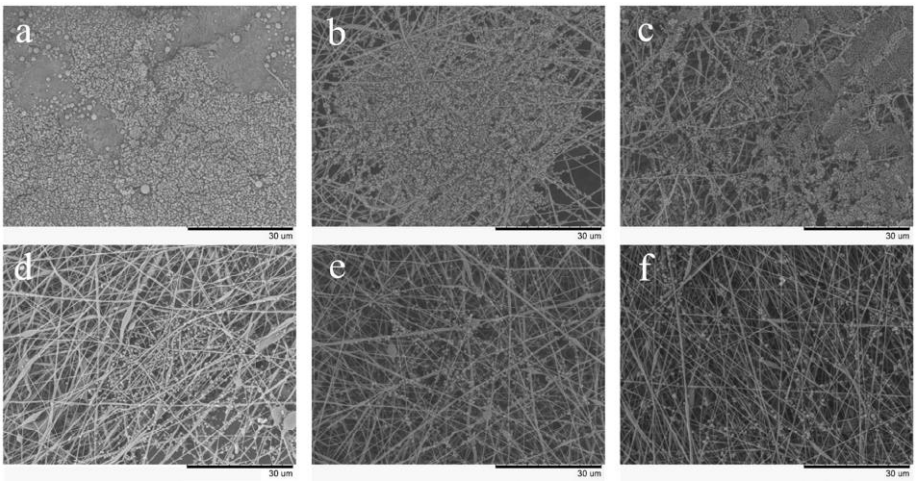

Figure 5.10. SEM images of the upper surface of composite membranes after 20 h contact with *S. aureus* cultures at 36 °C. (a) PSU, (b) PAA-PVA[1]@PSU, (c) PAA-PVA[3]@PSU, (d) PAA-PVA[5]@PSU, (e) PAA-PVA[7]@PSU and (f) PAA-PVA[8]@PSU.

The SEM images of PSU controls showed large bacterial colonization which in the case of *S. aureus* led to membranes covered with bacterial cells (Figure 5.10a). The presence of adhesion structures and extracellular matrix was clear also for the composite membranes with lower PAA-PVA loadings (Figures 5.9 b-d and Figures 5.10 b-d). However, for the specimens with higher amount of

PAA−PVA, the surfaces were almost free from bacteria, with dispersed colonization areas probably benefiting from the higher surface roughness of composites [60]. The effect of PAA-PVA loadings would be the destabilization of the bacterial wall due to the removal of divalent cations or impairment of lipopolysaccharide interlocking. The effect is also clear for planktonic cells as shown by the lower CFU counts in the liquid in contact with membranes.

Further insight into the colonization of composite membranes was provided by the visualization of biofilm formation by means of FilmTracer FM 1-43. Figure 5.11 shows representative confocal micrographs of membranes exposed to *S. aureus* cultures for 20 h at 36 °C. FM 1-43 is a nonfluorescent water-soluble lipophilic compound that inserts into the bacterial membrane where it becomes fluorescent revealing cell bodies even in complex biofilms in which other stains do not reveal cells as they are surrounded by large amounts of exopolymeric substances.

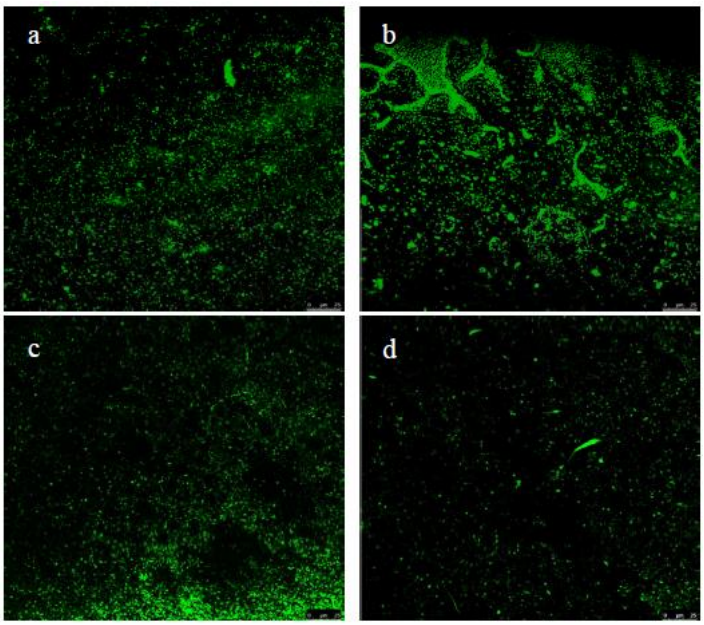

Figure 5.11. FilmTracer FM 1-43 Green Biofilm Cell Stain confocal micrographs of the surface of membranes exposed to *S. aureus* cultures at 36 °C for 20 h. (a) PSU, (b) PAA-PVA[1]@PSU, (c) PAA-PVA[7]@PSU and (d) PAA-PVA[8]@PSU.

Figure 5.11 shows that composite membrane with low PAA-PVA loadings suffered bacterial colonization and biofilm formation, whereas for higher loadings, particularly for PAA-PVA[8]@PSU, the membrane with 1.85 ± 0.32 mg PAA-PVA/cm^2, the surface was considerably more clean than PSU controls.

Control PSU and PAA-PVA[8]@PSU composites were also assayed in 48 h cross-flow runs with full filtrate and retentate recirculation at 2 bar TMP and an average linear velocity of 0.80 m s^{-1} along the membrane surface. The temperature of the assay was reduced from the 36°C of the previous antimicrobial tests to 25°C in search for more realistic conditions and due to the operational limitations of keeping a constant temperature in a circulating crossflow system over a prolonged period of time. The results are shown in Figures 5.12 and 5.13.

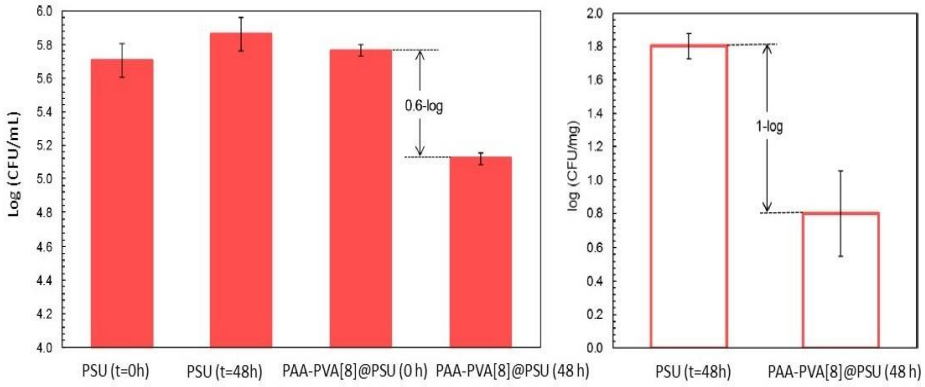

Figure 5.12. Microbial growth in cross-flow operation for 48 h at 25 °C. Left, CFU in the retentate; right, CFU detached from membrane surface at the end of the exposure period per unit mass of membrane. TMP 2 bar; linear velocity 0.80 m s^{-1}. Error bars represent standard deviation.

Figure 5.12 shows that CFU increased in the circulating liquid when using a PSU membrane, which became colonized by 63 ± 12 CFU/mg. Instead, the composite membrane with PAA-PVA, PAA-PVA[8]@PSU, was essentially free of bacterial colonization, 1-log less than PSU accompanied by lower CFU in the circulating liquid (0.6-log reduction).

SEM and confocal images of colonized membranes, PSU and PAA−PVA[8]@PSU, after 48 h runs in cross-flow at 25 °C are shown in Figure 5.13. SEM images clearly showed extensive biofilm formation in the case of PSU (Figure 5.13a). On the contrary, membranes with the PAA−PVA electrospun layer were mostly free of bacteria, with certain colonization but without evidence of the biofilm matrix produced with extracellular substances in the final stages of bacterial colonization (Figure 5.13b). The electrostatic repulsion between the outer surface of bacteria and the top layer of composite membranes could at least partially explain the lower colonization observed [61]. However, the damage observed in bacterial envelopes supports the quelation mechanism as the main driver of the antimicrobial activity of the top layer.

Cell damage is revealed by the confocal Live/Dead images shown in Figure 5.13 c-d. Using the Live/Dead staining, SYTO9 green-labelled cells correspond to non-damaged bacteria, while PI reveals as red-marked membrane-damaged bacteria. PSU membranes were covered by a considerable amount of viable green-labelled *S.aureus* cells as shown by Figure 5.13c. However, Live/Dead confocal images of PAA-PVA[8]@PSU composites under the same conditions showed extensive cell impairment with essentially all cells becoming red-stained Figure 5.13d. Red-marked cells were those internalizing PI and damaged in cell membrane integrity. The results are in good agreement with the antimicrobial assays performed in static conditions and show the advantages of using electrospun antimicrobial layers on ultrafiltration membranes to control microbial growth and biofilm formation even under flow conditions.

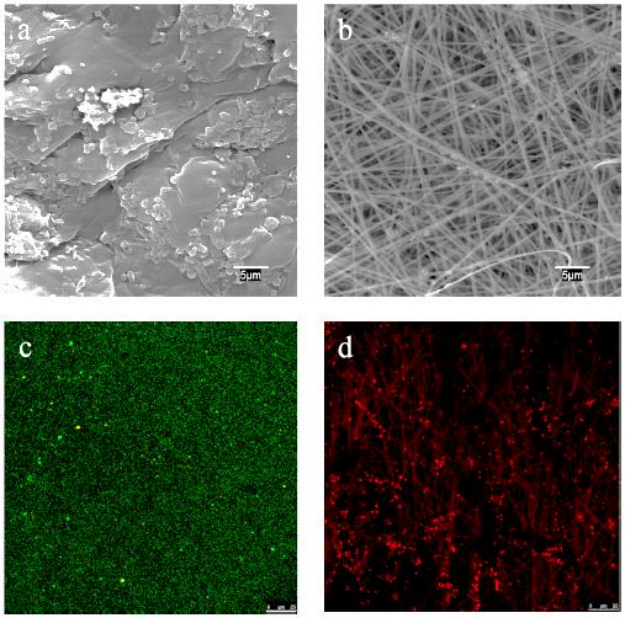

Figure 5.13. SEM and Live/Dead confocal micrographs of PSU and PAA-PVA[8]@PSU membranes after 48 h in cross-flow at 25 °C. Initial bacterial load in circulating feed: 10^6 cells/mL of *S. aureus* in NB 1/500 medium. SEM micrographs of (a) PSU and (b) PAA-PVA[8]@PSU and Live/Dead confocal micrographs of the surface of (c) PSU and (d) PAA-PVA[8]@PSU.

5.5 Conclusions

We report the preparation and properties of composite membranes consisting of electrospun layers of poly(acrylic acid)-poly(vinyl alcohol) (PAA-PVA) as top coating of a PSU ultrafiltration membrane. The electrospun layer formed a continuous coating consisting of well-formed fibres that kept their fibrous structure after heat curing and water immersion and did not detach from support.

The composite membranes displayed negative surface charge with more negative values for increasing amounts of the PAA-PVA electrospun layer up to a value of -41.2 ± 0.13 mV for the higher loading for a weight density of 1.85 ± 0.32 mg/cm^2.

PAA-PVA composite membranes showed improved resistance to organic fouling with flux recovery ratio up to 80.2% over the value of 29.4% for PSU membranes.

Composite membranes showed considerable antimicrobial activity. The effect was larger for *S. aureus* than for *E. coli*, which was attributed to the chelating effect of PAA on the divalent cations stabilizing bacterial envelopes. Viability studies showed that bacterial cells in contact with composite membranes displayed a high number of membrane-damaged bacteria.

The results demonstrated the feasibility of using electrospun layers directly created onto filtration supports as top coatings for ultrafiltration membranes with the aim of improving fouling behaviour and imparting antimicrobial functionality.

5.6 References

1. Elimelech, M. and W.A. Phillip, *The future of seawater desalination: energy, technology, and the environment.* Science, 2011. **333**(6043): p. 712-7.
2. Rajasulochana, P. and P. V, *Comparison on efficiency of various techniques in treatment of waste and sewage water - A comprehensive review*. Vol. 2. 2016.
3. Liu, P., et al., *Hollow-fiber ultrafiltration for simultaneous recovery of viruses, bacteria and parasites from reclaimed water.* J Microbiol Methods, 2012. **88**(1): p. 155-61.
4. Löwenberg, J., et al., *Comparison of pre-treatment technologies towards improving reverse osmosis desalination of cooling tower blow down*. Vol. 357. 2015. 140-149.
5. Committee, T.A.S.o.P.P.o.t.M.P., *Microfiltration and ultrafiltration membranes for drinking water.* Journal - American Water Works Association, 2008. **100**(12): p. 84-97.
6. Choo, K.H. and C.H. Lee, *Understanding Membrane Fouling in Terms of Surface Free Energy Changes*. Vol. 226. 2000. 367-370.
7. Le-Clech, P., V. Chen, and A.G. Fane, *Fouling in membrane bioreactors used in wastewater treatment*. Vol. 284. 2006. 17-53.
8. Prince, J.A., et al., *Synthesis and characterization of PEG-Ag immobilized PES hollow fiber ultrafiltration membranes with long lasting antifouling properties.* Journal of Membrane Science, 2014. **454**: p. 538-548.
9. Taniguchi, M. and G. Belfort, *Low protein fouling synthetic membranes by UV-assisted surface grafting modification: varying monomer type.* Journal of Membrane Science, 2004. **231**(1): p. 147-157.
10. Sotto, A., et al., *Effect of nanoparticle aggregation at low concentrations of TiO_2 on the hydrophilicity, morphology, and fouling resistance of PES-TiO_2 membranes*. Vol. 363. 2011. 540-50.
11. Zhao, Y.F., et al., *Improving the hydrophilicity and fouling-resistance of polysulfone ultrafiltration membranes via surface zwitterionicalization mediated by polysulfone-based triblock copolymer additive.* Journal of Membrane Science, 2013. **440**: p. 40-47.
12. Gao, H., X. Sun, and C. Gao, *Antifouling polysulfone ultrafiltration membranes with sulfobetaine polyimides as novel additive for the enhancement of both water flux and protein rejection.* Journal of Membrane Science, 2017. **542**: p. 81-90.
13. Flemming, H.C., D.G. Schaule, and R. McDonogh, *Biofouling on Membranes - A Short Review*. 1992. p. 487-497.
14. Flemming, H.C., *Biofouling in water systems-cases, causes and countermeasures.* Appl Microbiol Biotechnol, 2002. **59**(6): p. 629-40.

15. de la Fuente-Nunez, C., et al., *Bacterial biofilm development as a multicellular adaptation: antibiotic resistance and new therapeutic strategies.* Curr Opin Microbiol, 2013. **16**(5): p. 580-9.
16. Giaouris, E., et al., *Attachment and biofilm formation by foodborne bacteria in meat processing environments: causes, implications, role of bacterial interactions and control by alternative novel methods.* Meat Sci, 2014. **97**(3): p. 298-309.
17. Matin, A., et al., *Biofouling in reverse osmosis membranes for seawater desalination: Phenomena and prevention.* Desalination, 2011. **281**: p. 1-16.
18. Kochkodan, V. and N. Hilal, *A comprehensive review on surface modified polymer membranes for biofouling mitigation*. Vol. 356. 2015.
19. Zodrow, K., et al., *Polysulfone ultrafiltration membranes impregnated with silver nanoparticles show improved biofouling resistance and virus removal.* Water Research, 2009. **43**(3): p. 715-723.
20. Yu, H., et al., *Development of a hydrophilic PES ultrafiltration membrane containing SiO_2@N-Halamine nanoparticles with both organic antifouling and antibacterial properties.* Desalination, 2013. **326**: p. 69-76.
21. Díez, B., et al., *Fouling and biofouling resistance of metal-doped mesostructured silica/polyethersulfone ultrafiltration membranes.* Journal of Membrane Science, 2017. **526**: p. 252-263.
22. Reneker, D.H. and A.L. Yarin, *Electrospinning jets and polymer nanofibers.* Polymer, 2008. **49**(10): p. 2387-2425.
23. Bhattacharjee, P. and G.C. Rutledge, *Electrospinning and Polymer Nanofibers: Process Fundamentals*. 2011. p. 497-512.
24. Greiner, A. and J.H. Wendorff, *Electrospinning: A Fascinating Method for the Preparation of Ultrathin Fibers.* Angewandte Chemie International Edition, 2007. **46**(30): p. 5670-5703.
25. Quirós, J., K. Boltes, and R. Rosal, *Bioactive Applications for Electrospun Fibers.* Polymer Reviews, 2016. **56**(4): p. 631-667.
26. Patil, J.V., et al., *Electrospinning: A versatile technique for making of 1D growth of nanostructured nanofibers and its applications: An experimental approach.* Applied Surface Science, 2017. **423**: p. 641-674.
27. Dobosz, K.M., et al., *Ultrafiltration Membranes Enhanced with Electrospun Nanofibers Exhibit Improved Flux and Fouling Resistance.* Industrial & Engineering Chemistry Research, 2017. **56**(19): p. 5724-5733.
28. Wang, X., et al., *High performance ultrafiltration composite membranes based on poly(vinyl alcohol) hydrogel coating on*

crosslinked nanofibrous poly(vinyl alcohol) scaffold. Journal of Membrane Science, 2006. **278**(1): p. 261-268.
29. Yoon, K., et al., *High flux ultrafiltration membranes based on electrospun nanofibrous PAN scaffolds and chitosan coating.* Polymer, 2006. **47**(7): p. 2434-2441.
30. Hoover, L.A., J.D. Schiffman, and M. Elimelech, *Nanofibers in thin-film composite membrane support layers: Enabling expanded application of forward and pressure retarded osmosis.* Desalination, 2013. **308**: p. 73-81.
31. Sundarrajan, S., et al., *Potential of Engineered Electrospun Nanofiber Membranes for Nanofiltration Applications.* Drying Technology, 2013. **31**(2): p. 163-169.
32. Lu, T.D., et al., *Electrospun nanofiber substrates that enhance polar solvent separation from organic compounds in thin-film composites.* Journal of Materials Chemistry A, 2018. **6**(31): p. 15047-15056.
33. Kumeta, K., et al., *Crosslinking reaction of poly(vinyl alcohol) with poly(acrylic acid) (PAA) by heat treatment: Effect of neutralization of PAA.* Journal of Applied Polymer Science, 2003. **90**(9): p. 2420-2427.
34. Gratzl, G., et al., *Antimicrobial activity of poly(acrylic acid) block copolymers.* Materials Science and Engineering: C, 2014. **38**: p. 94-100.
35. Santiago-Morales, J., et al., *Antimicrobial activity of poly(vinyl alcohol)-poly(acrylic acid) electrospun nanofibers.* Colloids and Surfaces B: Biointerfaces, 2016. **146**: p. 144-151.
36. Nyström, M. and P. Järvinen, *Modification of polysulfone ultrafiltration membranes with UV irradiation and hydrophilicity increasing agents.* Journal of Membrane Science, 1991. **60**(2): p. 275-296.
37. Amariei, G., et al., *Dendrimer-functionalized electrospun nanofibres as dual-action water treatment membranes.* Sci Total Environ, 2017. **601-602**: p. 732-740.
38. Jeong, S., et al., *Biofouling potential reductions using a membrane hybrid system as a pre-treatment to seawater reverse osmosis.* Appl Biochem Biotechnol, 2012. **167**(6): p. 1716-27.
39. Herzberg, M. and M. Elimelech, *Biofouling of reverse osmosis membranes: Role of biofilm-enhanced osmotic pressure.* Journal of Membrane Science, 2007. **295**(1): p. 11-20.
40. Kessler, F., et al., *Controlling the surface wettability of poly(sulfone) films by UV-assisted treatment: benefits in relation to plasma treatment.* Polymer International, 2013. **62**(2): p. 310-318.
41. Kasemset, S., et al., *Effect of polydopamine deposition conditions on polysulfone ultrafiltration membrane properties and threshold flux during oil/water emulsion filtration.* Polymer, 2016. **97**: p. 247-257.

42. Bildyukevich, A.V., et al., *Hydrophilization of polysulfone hollow fiber membranes via addition of polyvinylpyrrolidone to the bore fluid.* Journal of Membrane Science, 2017. **524**: p. 537-549.
43. Kirwan, L.J., P.D. Fawell, and W. van Bronswijk, *In Situ FTIR-ATR Examination of Poly(acrylic acid) Adsorbed onto Hematite at Low pH.* Langmuir, 2003. **19**(14): p. 5802-5807.
44. Arndt, K.F., et al., *Poly(vinyl alcohol)/poly(acrylic acid) hydrogels: FT-IR spectroscopic characterization of crosslinking reaction and work at transition point.* Acta Polymerica, 1999. **50**(11-12): p. 383-390.
45. Rivaton, A. and J.L. Gardette, *Photodegradation of polyethersulfone and polysulfone.* Polymer Degradation and Stability, 1999. **66**(3): p. 385-403.
46. Yamashita, T., et al., *Degradation of sulfur-containing aromatic polymers: Photodegradation of polyethersulfone and polysulfone.* Polymer Degradation and Stability, 1993. **39**(1): p. 47-54.
47. Rupiasih, N.N., et al., *Study of Effects of Low Doses UV Radiation on Microporous Polysulfone Membranes in Sterilization Process*. Vol. 3. 2013. 12-18.
48. Jin, X. and Y.L. Hsieh, *pH-responsive swelling behavior of poly(vinyl alcohol)/poly(acrylic acid) bi-component fibrous hydrogel membranes.* Polymer, 2005. **46**(14): p. 5149-5160.
49. Zhang, J., et al., *Improved hydrophilicity, permeability, antifouling and mechanical performance of PVDF composite ultrafiltration membranes tailored by oxidized low-dimensional carbon nanomaterials*. Vol. 1. 2013. 3101-3111.
50. Habimana, O., A.J.C. Semião, and E. Casey, *The role of cell-surface interactions in bacterial initial adhesion and consequent biofilm formation on nanofiltration/reverse osmosis membranes.* Journal of Membrane Science, 2014. **454**: p. 82-96.
51. Yu, W., M. Brown, and N.J.D. Graham, *Prevention of PVDF ultrafiltration membrane fouling by coating MnO_2 nanoparticles with ozonation.* Scientific Reports, 2016. **6**: p. 30144.
52. Rezwan, K., et al., *Change of zeta potential of biocompatible colloidal oxide particles upon adsorption of bovine serum albumin and lysozyme.* J Phys Chem B, 2005. **109**(30): p. 14469-74.
53. Gratzl, G., et al., *Mechanistic approaches on the antibacterial activity of poly(acrylic acid) copolymers.* Colloids Surf B Biointerfaces, 2015. **126**: p. 98-105.
54. Sinn, C.G., R. Dimova, and M. Antonietti, *Isothermal Titration Calorimetry of the Polyelectrolyte/Water Interaction and Binding of Ca_2^+: Effects Determining the Quality of Polymeric Scale Inhibitors.* Macromolecules, 2004. **37**(9): p. 3444-3450.

55. Doyle, R.J., T.H. Matthews, and U.N. Streips, *Chemical basis for selectivity of metal ions by the Bacillus subtilis cell wall.* Journal of bacteriology, 1980. **143**(1): p. 471-480.
56. Clifton, L.A., et al., *Effect of divalent cation removal on the structure of gram-negative bacterial outer membrane models.* Langmuir, 2015. **31**(1): p. 404-12.
57. Domingues, M.M., et al., *Antimicrobial protein rBPI21-induced surface changes on Gram-negative and Gram-positive bacteria.* Nanomedicine, 2014. **10**(3): p. 543-51.
58. Rose, R.K., S.P. Matthews, and R.C. Hall, *Investigation of calcium-binding sites on the surfaces of selected Gram-positive oral organisms.* Archives of Oral Biology, 1997. **42**(9): p. 595-599.
59. Thomas, K.J., 3rd and C.V. Rice, *Revised model of calcium and magnesium binding to the bacterial cell wall.* Biometals, 2014. **27**(6): p. 1361-70.
60. Ammar, Y., et al., *Influence of surface roughness on the initial formation of biofilm.* Surface and Coatings Technology, 2015. **284**: p. 410-416.
61. Zhao, D.L., S. Das, and T.-S. Chung, *Carbon Quantum Dots Grafted Antifouling Membranes for Osmotic Power Generation via Pressure-Retarded Osmosis Process.* Environmental Science & Technology, 2017. **51**(23): p. 14016-14023.

CHAPTER 6

GENERAL DISCUSSION

Chapter 6. GENERAL DISCUSSION

Membrane technology plays a significant role in water and wastewater treatment due to the growing global population and increased water demand. Among all membrane processes, ultrafiltration is considered a very promising technique to be used in water purification processes due to its high removal rate of organic matter and microorganisms. However, most commercial membranes are made from hydrophobic polymers due to their excellent thermal stability as well as mechanical strength and chemical stability [1]. Though, their vulnerability to fouling owing to their inherent hydrophobic nature compromises their long-term performance [2]. Foulants are typically adsorbed to the membrane surface by hydrophobic interactions, hydrogen bonding, Van der Waals attraction or electrostatic interactions [3]. Numerous studies have shown that increasing the surface hydrophilicity, varying the membrane roughness or incorporating charged groups on the surface through different modification strategies, reduces fouling [4].

Blending hydrophilic additives into the polymeric matrix is considered an attractive and simple method to modify membranes without affecting their main polymer structure [5]. Generally, hydrophilic surfaces easily form a thin layer of bounded water -known as hydration layer- due to the formation of hydrogen bonds, which prevents the adsorption and deposition of undesirable hydrophobic foulants via repulsive hydration forces [6]. In the present work, a common hydrophilic additive was used to minimize attractive interactions between membrane surface and feed components, namely poly(vinyl pyrrolidone) (PVP). PVP has several advantageous properties such as low toxicity, good chemical stability and low cost [7]. It has a high affinity for water molecules due to its highly polar pendant amide groups conferring a highly hydrophilic character [8, 9]. PVP is also used as a pore-forming agent during membrane preparation. Nevertheless, it was demonstrated in this work that

PVP concentration has considerable influence on the properties and morphology of membranes in the sense that there is an optimum value beyond which the size and number of finger-like pores decreases and turns to a sponge-like structure. Chapter 2 showed that the pure water flux of polysulfone membranes reached the maximum value with up to 10 wt % PVP. Its role in accelerating de-mixing during the phase inversion process contributes to the enlargement of membrane surface pores. However, a decrease in permeability can be observed when adding higher amount of PVP (above 10 wt %) due to the increase of viscosity that delays the de-mixing of casting solution yielding a sponge-like structure of closed pores.

Alternatively, embedding inorganic nanoparticles into the matrix is a promising alternative to improve the thermal stability, permeability, hydrophilicity, strength and stiffness of membranes [10]. Nevertheless, homogeneous dispersion of nanoforms in the casting solution is a difficult task due to the tendency of nanoparticles to agglomerate [11]. It was demonstrated throughout the assays carried out in this work that a wide variety of porous materials with interconnected nanochannels, can be used as support for embedding metal nanoparticles. In Chapter 2 sepiolite, a porous hydrated magnesium silica, was used as a host for different metallic cations. Chapter 3 shows that metal-loaded mesoporous silica can act as a vehicle for introducing nanometals into the polymeric matrix. Silica-supported nanomaterials are stable and avoid nanoparticle aggregation and their release to the environment. Further, this work analyses the influence of nanocarriers in altering membrane properties and their role in improving filtration performance. Membranes containing sepiolite materials showed higher porosity compared to neat polysulfone membranes. The increase of membrane porosity with hydrophilic fillers is a well-known fact explained by the faster interdiffusion process resulting from their addition to the ternary thermodynamic system [12]. The modification of membranes by embedding

metal-doped SBA-15 nanoparticles resulted in an increase in water permeability, because of the morphological changes observed in membrane structure, namely enhanced porosity, thinner skin layer, and better pore interconnectivity. Moreover, the addition of hydrophilic fillers mitigated the severity of organic fouling, indicating that blended polymeric membranes can be effectively used in water treatment. In both cases, the changes of structure and properties due to the presence of metal-loaded nanoparticles rely on the good dispersion of nanomaterials in casting solution and, hence, in the polymer matrix.

Hyperbranched polymers (HBPs) have attracted considerable interest in recent years due to their highly branched structure, large number of terminal functional groups, and easy one-step synthesis [13]. However, not previous studies proposed using HBPs or dendritic structures as additive in porous membrane preparation [14]. In this work, Hellux-3316, a hyperbranched polyamidoamine polymer was directly added into the casting solution to create functionalized membranes with the additive uniformly dispersed in the polymer matrix. Chapter 4 shows that the incorporation of amino groups increased the membrane hydrophilicity, which resulted in enhanced water permeability. Functionalized membranes displayed significant antifouling behaviour revealed upon filtering bovine serum albumin (BSA) solutions and lower irreversible fouling than neat membranes, indicating that the incorporation of Hellux-3316 in the casting solution provides significant benefits to the membrane performance in terms of permeability and antifouling potential.

UV irradiation constitutes another strategy to increase the hydrophilicity of membrane surface. It was established in Chapter 2 that UV-irradiated polysulfone membranes displayed higher permeabilities than non-irradiated specimens. It has been reported that polyarylsulfone membranes are

intrinsically photosensitive due to the phenoxyphenyl chromophores present in their structure. Consequently, UV-light absorption takes place in the backbone of their polymeric chains leading to the formation of polar functional groups such as carbonyl (-C=O) and hydroxyl (-OH) groups, resulting in an increase of the hydrophilic character of membranes [15]. Moreover, the formation of carboxylic and sulfonic acid groups on membranes is supposed to create internal repulsion forces within the pores. This repulsion causes pore enlargement, which results in permeability increase [16].

Chapter 5 describes a functionalization process of polysulfone membranes starting with their treatment with UV light, which leads to the formation of anchoring points due to the oxidative photolysis of aromatic moieties. Accordingly, irradiated membranes can interact with the carboxyl or hydroxyl groups of an outer layer formed by electrospun fibres made of polymer containing such functional groups, namely poly(acrylic acid) (PAA) and poly(vinyl alcohol) (PVA). Surface coating by the electrospun nanofibers is the last modification technique used in the work. It has been previously reported that the incorporation of a highly porous layer of nanofibers directly onto the surface of conventional membranes can enhance their permeability and fouling resistance without adversely impacting base membrane properties [17]. Additionally, it has been proposed that randomly coated nanofibers can induce shear stresses that prevents the attachment of BSA and other foulants to membrane surface [18]. The results showed that the higher surface polarity of coated membranes provides certain increase in water permeability. The increase in membrane hydrophilicity is a well-known way to reduce the fouling formation over membrane surface due to lower interaction with colloidal compounds. This work demonstrated that electrospun nanofibers is an effective surface coating method to improve the performance of polysulfone ultrafiltration membranes.

The work conducted during this thesis has not only focused on obtaining membranes with antifouling capacities but also have sought to incorporate antimicrobial activity to avoid biofilm formation over their surface.

Biofouling increases energy costs, decreases membrane permeability and compromises permeate quality during water filtration processes [19]. Developing antimicrobial membranes is an important issue to increase membrane efficiency and to expand the application of membrane processes [20].

In this work, several bacterial strains including, *Escherichia coli* (CECT 516) and *Staphylococcus aureus* (CECT 240) were used to assess the anti-biofouling behaviour of the newly developed membranes. *Escherichia coli* is a gram-negative, rod-shaped, coliform bacterium commonly found in the intestines of healthy animals and humans. Although most strains of *E. coli* are harmless, including the one used in this work, some are able to cause severe diseases such as bloody diarrhoea, urinary tract infections, meningitis and septicaemia [21]. *S. aureus* is a gram-positive, cocci-shaped bacterium that tends to form grape-like clusters. It is usually found in the skin and mucous membranes of healthy humans and animals and is considered one of the most common pathogens. The symptomatology varies depending on the strains involved and the site of infection due to these bacteria can produce invasive infections and/or toxin-mediated diseases [22]. Biofilm formation is a two-stage process that involves reversible bacterial attachment to a surface, followed by the microcolony formation and biofilm maturation [23]. Bacterial adhesion is known to be influenced by the physicochemical properties of the solid surface. Generally, hydrophobic surfaces with larger roughness and coated by a conditioning film – adsorption of molecules on the substrate – increase of cell attachment and biofilm development [24, 25].

The antibiofilm activity involves the ability of some molecules to prevent the biofilm formation processes, avoiding cells adhesion, exerting an antibacterial action or inhibiting quorum sensing signals [23]. Chapter 2 and 3, exploit the well-known oligodynamic effect of some metals, using silver and copper-loaded membranes which strongly inhibit bacterial attachment and reduce biofilm formation. The antimicrobial action of silver and copper has been extensively debated in the literature with the general agreement that they 1) increase ROS (reactive oxygen species) production by attacking antioxidant enzymes, 2) impart protein dysfunction and loss of enzyme activity, 3) interfere with nutrient assimilation and 4) produce genotoxicity [26, 27]. It was also shown that the release of soluble metal ions, under aerobic conditions, is an important factor leading to the toxicity to biofilm forming microorganisms [28]. Chapter 4 shows that the antimicrobial behaviour of composite PVC membranes can be attributed to the presence of positively charged domains associated with Hellux, a hyperbranched polymeric nanomaterial.

Positively charged amino groups are able to interact with the negatively charged bacterial wall, replacing divalent cations which are essential to maintain the membrane structure. Hellux-PVC membranes in contact with bacteria revealed a considerable number of membrane-damaged cells, indicating a disruption of the bacterial envelope for gram-negative and gram-positive bacteria.

The functionalization of membrane surface is another strategy to achieve antimicrobial activity that was demonstrated in Chapter 5. Nanofibers are a suitable coating method to enhanced antimicrobial performance of membranes due to its extraordinary properties such as high surface area, small dimensions and multi-scale porosity [29]. It is known that calcium is an essential ion to maintain the structure and integrity of the cell membrane [30]. The results showed that PAA containing nanofibers can destabilize bacterial

envelopes due to the chelation of intracellular calcium, forming PAA-Ca complexes. Thus, the absence of calcium in cell membrane leads to bacterial impairment and death.

Overall, this Doctoral thesis develops several modification techniques for ultrafiltration membranes in order to avoid or reduce the unsought accumulation of foulants and microorganisms over their surface or inside their pore structure. The interaction between membrane surface and molecules plays an important role in explaining the extent of membrane fouling. It is generally accepted that fouling is enhanced by an increase in membrane hydrophobicity and surface roughness, and if it exposed to a conditioning film, the surface also tends to be easily colonized by bacteria. The adsorption of (macro)molecules on the substrate, often changes its physicochemical properties and surface topography, favouring the bacterial adhesion. Considering the remarkable diversity of microorganisms existing in the earth and different compounds present in the water, it is difficult to visualize a universal set of guidelines for designing materials with anti(bio)fouling capacities. However, the rules mentioned before provide general principles for developing bio(fouling)-resistant surfaces. Further investigations and evaluations would be needed to better understand the complex interplay between bacteria and surface topography and to evaluate membrane-colloid interactions at the polymer interface. Specifically, this work focuses on membrane functionalization strategies to design materials with enhanced antifouling and antimicrobial capacities that could improve membrane performance, long-term stability and durability.

6.1 References.

1. Drioli.E., G.L., F.E., *Comprehensive Membrane Science and Engineering.* Oxford, United Kingdom. Elsevier, 2017.
2. Pal, A., et al., *Mixed-matrix membranes with enhanced antifouling activity: probing the surface-tailoring potential of Tiron and chromotropic acid for nano-TiO_2.* 2017. **4**(9): p. 170368.
3. Zaidi, S., K. Mauritz, and M. Hassan, *Membrane Surface Modification and Functionalization*. 2019. p. 391-416.
4. Rana, D. and T. Matsuura, *Surface Modifications for Antifouling Membranes.* Chemical Reviews, 2010. **110**(4): p. 2448-2471.
5. Miller, D., et al., *Surface Modification of Water Purification Membranes: a Review.* Angewandte Chemie, 2016. **129**.
6. Gu, L., et al., *Construction of Antifouling Membrane Surfaces through Layer-by-Layer Self-Assembly of Lignosulfonate and Polyethyleneimine.* Polymers, 2019. **11**(11).
7. Wu, J., et al., *Improving the hydrophilicity and fouling resistance of RO membranes by surface immobilization of PVP based on a metal-polyphenol precursor layer.* Journal of Membrane Science, 2015. **496**: p. 58-69.
8. Cai, C., et al., *Using polyvinylpyrrolidone to enhance the enzymatic hydrolysis of lignocelluloses by reducing the cellulase non-productive adsorption on lignin.* Bioresource Technology, 2017. **227**: p. 74-81.
9. Malina, D., et al., *Silver nanoparticles synthesis with different concentrations of Polyvinylpyrrolidone.* Digest Journal of Nanomaterials and Biostructures, 2012. **7**: p. 1527-1534.
10. Garcia, J., et al., *Enhancement in hydrophilicity of different polymer phase-inversion ultrafiltration membranes by introducing PEG/Al2O3 nanoparticles.* Separation and Purification Technology, 2014. **128**: p. 45–57.
11. Garcia-Ivars, J., et al., *Enhancement in hydrophilicity of different polymer phase-inversion ultrafiltration membranes by introducing PEG/Al2O3 nanoparticles.* Separation and Purification Technology, 2014. **128**: p. 45-57.
12. Díez, B., et al., *Antimicrobial organic-inorganic composite membranes including sepiolite-supported nanometals.* RSC Advances, 2017. **7**(4): p. 2323-2332.
13. Zhao, Y.H., et al., *Porous membranes modified by hyperbranched polymers: I. Preparation and characterization of PVDF membrane using hyperbranched polyglycerol as additive.* Journal of Membrane Science, 2007. **290**(1): p. 222-229.
14. Schulze, A., M. Went, and A. Prager, *Membrane Functionalization with Hyperbranched Polymers.* Materials (Basel), 2016. **9**(8).

15. Konruang, S., T. Chittrakarn, and S. Sirijarukula, *Surface Modification of Asymmetric Polysulfone Membrane by UV Irradiation.* Jurnal Teknologi, 2014. **70**.
16. Nyström, M. and P. Järvinen, *Modification of polysulfone ultrafiltration membranes with UV irradiation and hydrophilicity increasing agents.* Journal of Membrane Science, 1991. **60**(2): p. 275-296.
17. Vanangamudi, A., et al., *Nanofiber Composite Membrane with Intrinsic Janus Surface for Reversed-Protein-Fouling Ultrafiltration.* ACS Applied Materials & Interfaces, 2017. **9**(21): p. 18328-18337.
18. Dobosz, K.M., et al., *Ultrafiltration Membranes Enhanced with Electrospun Nanofibers Exhibit Improved Flux and Fouling Resistance.* Industrial & Engineering Chemistry Research, 2017. **56**(19): p. 5724-5733.
19. Yin, J. and B. Deng, *Polymer-matrix nanocomposite membranes for water treatment.* Journal of Membrane Science, 2015. **479**: p. 256-275.
20. Nguyen, T., F.A. Roddick, and L. Fan, *Biofouling of water treatment membranes: a review of the underlying causes, monitoring techniques and control measures.* Membranes (Basel), 2012. **2**(4): p. 804-40.
21. Belanger, L., et al., *Escherichia coli from animal reservoirs as a potential source of human extraintestinal pathogenic E. coli.* FEMS Immunol Med Microbiol, 2011. **62**(1): p. 1-10.
22. Unakal., T.A.T.C.G., *Staphylococcus Aureus.* StatPearls publishing 2019.
23. Moura, M., et al., *Bacterial biofilms: The structure, development and potential of plant compounds for alternative control*. 2017. p. 1-34.
24. Tuson, H.H. and D.B. Weibel, *Bacteria-surface interactions.* Soft Matter, 2013. **9**(17): p. 4368-4380.
25. Lorite, G.S., et al., *The role of conditioning film formation and surface chemical changes on Xylella fastidiosa adhesion and biofilm evolution.* Journal of Colloid and Interface Science, 2011. **359**(1): p. 289-295.
26. Lemire, J., J. Harrison, and R. Turner, *Antimicrobial activity of metals: Mechanisms, molecular targets and applications.* Nature reviews. Microbiology, 2013. **11**.
27. Slavin, Y.N., et al., *Metal nanoparticles: understanding the mechanisms behind antibacterial activity.* Journal of Nanobiotechnology, 2017. **15**(1): p. 65.
28. Dong, F. and Y. Zhou, *Differential transformation and antibacterial effects of silver nanoparticles in aerobic and anaerobic environment.* Nanotoxicology, 2019. **13**(3): p. 339-353.
29. Afshari, M., *Electrospun nanofibers* Elsevier, Cambridge USA, 2017.

30. Ballen, K.G., et al., *Acidity and calcium interaction affecting cell envelope stability in Rhizobium.* Canadian Journal of Microbiology, 1998. **44**(6): p. 582-587.

GENERAL CONCLUSIONS

&

CONCLUSIONES GENERALES

GENERAL CONCLUSIONS

- New (bio)fouling-resistant ultrafiltration membranes were successfully prepared by phase inversion. Several surface modification techniques were developed that reduced the accumulation of molecules and microorganisms on membrane surface.

- Nanoparticles embedded in sepiolite fibres or silica particles displayed a good dispersion in casting solutions and hence, in the polymer matrix. Membranes functionalized with metal nanoparticles showed higher porosity and pore interconnectivity, providing higher flux and better antifouling performances. Biofilm formation was completely inhibited by the strong antimicrobial activity of silver and copper ions.

- The addition of hyperbranched polyamidoamine polymer into the casting solution increased membrane hydrophilicity maintaining their porous structure. Functionalized membranes displayed higher permeability, resistance against irreversible organic fouling as well as protection against bacterial growth. The antimicrobial effect was attributed to the interaction of polyamidoamine positively charged groups with bacterial cell envelopes.

- Composite ultrafiltration membranes could be created adding a highly porous layer of nanofibers directly onto the surface of polysulfone membranes. The electrospun hydrophilic coating made by a blend of poly(acrylic acid) and poly(vinyl alcohol) improved membrane performance reducing protein adsorption and displayed an antimicrobial activity, avoiding biofilm formation. The antibacterial action was due to the chelating effect of poly(acrylic acid) on the divalent cations stabilizing bacterial cell wall.

CONCLUSIONES GENERALES

- Nuevas membranas de ultrafiltración resistentes al ensuciamiento orgánico y biológico fueron preparadas con éxito utilizando el método por inversión de fase. Se desarrollaron varias técnicas de modificación de las membranas, para reducir la acumulación de moléculas y microorganismos sobre su superficie.

- Las nanopartículas incrustadas en fibras de sepiolita o partículas de sílice mostraron una buena dispersión en las soluciones poliméricas y, por tanto, en la matriz de la membrana. Las membranas funcionalizadas con nanopartículas metálicas mostraron una mayor porosidad e interconectividad de los poros, proporcionando un mayor flujo y mejores prestaciones contra el ensuciamiento. La formación de biopelículas se vio completamente inhibida por la fuerte actividad antimicrobiana de los iones de plata y cobre.

- La incorporación del polímerico hiperramificado de poliamidoamina en la solución polimérica aumentó la hidrofilicidad de membrana, manteniendo su estructura porosa. Las membranas funcionalizadas mostraron una mayor permeabilidad, resistencia contra la suciedad orgánica irreversible, así como protección contra el crecimiento bacteriano. El efecto antimicrobiano se atribuyó a la interacción de los grupos cargados positivamente de la poliamidoamina con la pared celular bacteriana.

- Se crearon membranas compuestas de ultrafiltración añadiendo una capa altamente porosa de nanofibras electrohiladas, compuestas por una mezcla de ácido poliacrílico y alcohol polivinílico, directamente sobre la superficie de las membranas de polisulfona. El recubrimiento hidrófilo de las nanofibras mejoró el rendimiento de la membrana,

reduciendo la adsorción de proteínas y evitando la formación de biopelículas. La actividad antimicrobiana se debió al efecto quelante del ácido poliacrílico con los cationes divalentes que estabilizan la pared celular bacteriana.

ABBREVIATIONS

ATR-FTIR	Attenuated total reflectance Fourier transform infrared
BSA	Bovine Serum Albumin
CA	Cellulose acetate
CF6	Fluorinated carbon chains
CFU	Colonies Forming Units
DLS	Dynamic light scattering
DMA	N, N-dimethylacetamide
DMSO	Dimethyl sulfoxide
EC	Epoxy-containing coumarin moieties
EDS	Energy Dispersive X-rays spectroscopy
EIPS	Evaporation-induced phase separation
EO	Ethylene oxide
EPS	Extracellular polymeric substance
FE-SEM	Field Emission Scanning Electron Microscope
FRR	Flux recovery ratio
GO	Graphene oxide
HBPs	Hyperbranched polymers
HNTs	Halloysite nanotubes
ICP-MS	Inductively Coupled Plasma Mass Spectrometry

IFR	Irreversible Fouling Ratio
LPS	Polyanionic lipopolysaccharides
MF	Microfiltration
MOFs	Metal-organic frameworks
MSPs	Mesoporous silica particles
NB	Nutrient broth
NF	Nanofiltration
NIPS	Non-solvent induced phase separation
NMP	1-methyl-2-pyrrolidone
NPs	Nanoparticles
OD	Optical density
OM	Outer membrane
PA	Polyamides
PAA	Poly(acrylic acid)
PAMAM	Poly(amido amine)
PAN	Polyacrylonitrile
PBS	Phosphate buffered saline
PD	Polydopamine
PEA	Poly(ether amine)
PEG	Poly(ethylene glycol)
PEI	Poly(ether imide)

PES	Poly(ethersulfone)
PET	Poly(ethylene terephtlate)
PI	Propidium iodide
PO	Propylene oxide
PP	Polypropylene
PSF	Polysulfone
PVA	Poly(vinyl alcohol)
PVC	Poly(vinyl chloride)
PVDF	Poly(vinylidene fluoride)
PVP	Poly(vinyl pyrrolidone)
PWF	Pure water flux
QS	Quorum sensing
R	Rejection
RFR	Reversible Fouling Ratio
RO	Reverse osmosis
SCDLP	Soybean casein digest broth with lecithin and polysorbate
SEM	Scanning Electron Microscopy
TEM	Transmission electron microscopy
TEOS	Tetraethyl orthosilicate
TFN	Thin-film nanocomposite
TFR	Total Fouling Ratio

TIPS	Thermally induced phase separation
TMP	Transmembrane pressure
UF	Ultrafiltration
UV	Ultraviolet
VIPS	Vapor-induced phase separation
WCA	Water contact angles
XRD	X-ray powder diffraction